UNIVERSITY OF OKLAHOMA

GRADUATE COLLEGE

# INTEGRATED GEOPHYSICAL INVESTIGATIONS OF LINKAGES BETWEEN PRECAMBRIAN BASEMENT AND SEDIMENTARY STRUCTURES IN THE UCAYALI BASIN, PERU; FORT WORTH BASIN, TEXAS; AND OSAGE COUNTY, OKLAHOMA

A DISSERTATION

SUBMITTED TO THE GRADUATE FACULTY

in partial fulfillment of the requirements for the

Degree of

DOCTOR OF PHILOSOPHY

By

OLUBUNMI OLUMIDE ELEBIJU
Norman, Oklahoma
2009

INTEGRATED GEOPHYSICAL INVESTIGATIONS OF LINKAGES BETWEEN PRECAMBRIAN BASEMENT AND SEDIMENTARY STRUCTURES IN THE UCAYALI BASIN, PERU; FORT WORTH BASIN, TEXAS; AND OSAGE COUNTY, OKLAHOMA

A DISSERTATION APPROVED FOR THE
CONOCOPHILIPS SCHOOL OF GEOLOGY AND GEOPHYSICS

BY

Dr. G. Randy Keller, Co-Chair

Dr. Kurt J. Marfurt, Co-Chair

Dr. Roger A. Young

Dr. Carl H. Sondergeld

Dr. Kevin Mickus

## Dedication

This dissertation is dedicated to the Almighty God for his continued grace, strength, and love over my life. It is in him I live, move, and have my being.

## Acknowledgments

I will like to thank my advisor and my co-advisor, Dr. Randy Keller and Dr. Marfurt for their dedicated help and support all through these years. Galileo once said, "You cannot teach a man anything. You can only help him to find it within himself". Thus, you have helped me discover and improve upon my research abilities. You keep pushing me to get better at scientific writings and I thank you for all your support and constructive criticism. You have proved to be more than just an advisors but also great friends. I am indebted to Randy for his financial support and payment of my school fee during my program here at the University of Oklahoma. I will also like to express my sincere appreciation to my other committee members: Dr. Roger Young, Dr Carl Sondergeld, and Dr. Kevin Mickus for their commitment to serve on my committee, their insightful comments during my oral exam, and reading through this dissertation.

We express sincere thanks to the Hess Corporation, Devon Energy, Osage Nation and Spyglass Energy LLC for the use of their datasets that includes seismic, gravity and magnetic data, and well information for research and education. I also want to thank Charles Wickstrom and Shane Matson for access to more recently acquired proprietary seismic surveys, and more importantly, for their geologic insight into the complexities of the Osage County region.

The Geophysical Society of Houston/ Charlie and Jean Smith Scholarship of the Society of Exploration Geophysicists (SEG) supported me for two year, and I thank them for the award.

My sincere thanks goes to the entire staffs at the ConocoPhillips School of Geology and Geophysics at the University of Oklahoma: Adrianne Fox, Donna Mullins

(Blonde), Nancy Leonard, and Niki Chapin. What a wonderful and kind people you all are. You all go beyond your call duties to answer all my questions and made my stay here in the sooner land worthwhile. In time of registration, clarification of bursar bills, holds removal, booking of airline, and my favorite: getting paid or reimbursed, you been so fantastic. My special thanks to Adrianne Fox for taking the time and energy to make me a quilt, which has OU and UTEP logo on it, that is my graduation gift.

I would also like to thank Rodger Denison for sharing his Oklahoma and Texas basement rocks experience with me. I thank you for taking the time to share your thoughts. I have received a great deal of software, networking, and computer help from Ha Mai. T- (Mighty Ha), Grant Mouser, Steve Holloway, and Brad Wallet, to you guys I say thank you.

In addition, my appreciation the help of Faith Okpotor, Chinedu Agbalaka, Joyce Keller, and Linda Ibodje for proof reading and correcting part of my dissertation. I thank you for making your time available.

I must admit that one thing only I know, and that is that I know nothing (Socrates), however, it is not that I am so smart, it is just that I stay with problems longer (Albert Einstein), thus my quest for knowledge is not going to end here  it is just the beginning.

Last and most importantly, my utmost and sincere appreciation goes to my parents; Mr and Mrs M.O. Elebiju and siblings. Thank you for all your prayers, phone calls, and encouragement.

## Table of Contents

## List of Tables

## List of Figures

## Abstracts

I conducted integrated geophysical studies within the Fort Worth basin, Texas; Osage County, Oklahoma, and the Ucayali basin, Peru. My studies are directed at understanding the relationships or links between Precambrian basement structures and sedimentary structures using these three areas as case studies. Links between basement structure, hydrocarbon reservoirs, and sedimentary sequences are not a new concept. Such relationships have been documented in the Paradox, Hardeman, Anadarko, Arkoma, Ardmore and Williston basins among others. Structures such as fault zones that can influence the formation of sedimentary basins and mineral deposits are often formed by intraplate tectonism.

In order to compare the relationship between the Precambrian basement structures and sedimentary structures, I analyzed series of derivative and filtered maps of aeromagnetic and gravity data, which enhance basement structures, that were integrated with seismic data and seismic attribute data that enhance structures within the sedimentary sections. Other information such as well data and geologic information etc were also integrated. This integrated workflow facilitates the comparison of the links or relationships between the two structures.

The results of the Fort Worth basin are presented in Chapter 3. The results of this integrated study show that the sedimentary structures within the study area are mainly related to basement structures because these structures are aligned parallel to anomalies identified on the high-resolution aeromagnetic (HRAM) data. The northeast-southwest and northwest-southeast orientations of sedimentary features are consistently parallel with Precambrian structural fabrics that are associated with structures such as the

northeast trending Ouachita orogenic belt and the northwest trending Muenster Arch, which reactivated a late Cambrian/Late Precambrian faults. The knowledge gained in this study will impact oil and gas exploration and development within the study area because, the orientation of the natural and induced fractures can be predicted even if seismic data is limited or unavailable.

In Chapter 4, the results of an integrated analysis that includes the use of 3D seismic data, seismic attributes, and derivative maps from potential field data to study the basement, Mississippi Chert and the Arbuckle Group of Osage County, Oklahoma are presented. The workflow employed in this study was effective in studying and identifying polygonal, highly coherent, and high amplitude lineaments that strike northwesterly and northeasterly within these reservoirs. Basement structure lineaments are found to be parallel in orientation with the trend of lineaments seen within the Mississippian Chert and the Arbuckle Group. The northwest-striking lineaments may be related to the late-Paleozoic tectonism that affected both the Precambrian and Paleozoic section of Osage County. Another part of this research investigated the large gravity and magnetic anomalies and their association with the Mid-Continent Rift System (MCRS). Results of this analysis revealed prominent northeast trending anomalies that suggest that the MCRS extends into northern Oklahoma. However, geochronological data for basement rocks suggest that this extension would have to be limited to intrusive bodies that have little or no subcrops.

The integrated study conducted in the Ucayali basin of Peru revealed that the northwest-southeast trending lineaments interpreted as Precambrian basement structures are sub-parallel to the late Paleozoic fold and thrust belts that resulted from the

shortening associated with the formation of the Andes. These fold and thrust belts are reactivated along the zones of weaknesses that already existed in the Precambrian basement. The east-northeast lineaments are located beneath the Fitzcarrald Arch locate above the buoyant Nazca ridge. I interpret these east-northeast lineaments as part of the Ene Pisco – Abancay Fitzcarrald tectonic lineaments, which is one of the five tectonic domains in these region. Gravity modeling suggests that the crustal thickness and the subduction slab-dip beneath Peru increase from the north of the Ucayali basin towards the south. My 2-dimensional gravity model suggests that the crust thickness and Nazca plate dip increase southward within the Ucayali basin. These results also establish a correlation between known geologic features and the regional gravity anomalies

# Chapter 1: Introduction

## 1.0 Background, Motivations and Problem Addressed

Basement structures due to intraplate tectonism often form structures such as fault zones that control sedimentary basins and mineral deposits formation (Barosh, 1995). Examples of basins in the United States that exhibit structural relationships between Paleozoic features and Precambrian basement fault patterns includes the Paradox, Hardeman, Anadarko, Arkoma, Ardmore basins, Fort Worth basin (Thomas and Baars, 1992; Elebiju et al., 2008) and the Williston basins among others (Gerhard and Anderson, 1998). The structural fabric of the Precambrian basement that underlies Phanerozoic basins is highly complex, and many scientists believe that an understanding of Phanerozoic geology hinges on adequate knowledge of the underlying basement structure. Gay (1995), through aeromagnetic techniques, documented how basement fault block pattern and basement fracture reactivation (Wilson and Berendsen, 1998) control structural and stratigraphic features that are important to petroleum exploration. Basement features can also prove insight into reservoirs, sources, traps and hydrocarbon migration (Carlson, 2005).

Until relatively recently, Precambrian basement rocks had received little attention in the oil and gas exploration world. However, the role of basement rock as a viable element in an exploration strategy has changed because of a broader appreciation of Precambrian tectonic processes controlling the distribution of petroleum resources (Carlson, 2005). Production of hydrocarbons directly from the basement has also heightened an awareness of the need for understanding the basement (Dickas, 1992).

The main objective of my dissertation is to investigate and understand how Precambrian basement structures are influencing geologic phenomena in the younger Paleozoic strata such as faults, fractures, karst, collapse features, and dolomitization. This dissertation consists of three main chapters or paper-styled format. Each paper will be submitted to various leading geophysics and geology journal for publication. Paper in Chapter 3, which has initially been submitted to the GEOPHYSICS journal, is currently undergoing revisions. Chapter 4 and 5 are currently in preparation stage for submission.

The studies in this dissertation includes an integrated geophysical analyses of basement structure in the Ucayali basin in Peru, the Fort Worth basin in Texas, and Osage County in northeast Oklahoma. Figure 1.1 shows the location of the three study areas. The ability to map basement features is very important to exploration because natural and induced fractures, like those associated with the Fort Worth basin for example, are believed to be related to basement structures. Consequently, understanding of this interaction between these structures is very important because it will influence prospecting in these basins.

I develop and employ integrated geophysical and geological methodologies in order to address some of the issues associated with the influence of basement structures on Paleozoic and younger structures. This integrated approach based on several three-dimensional (3D) seismic data supplemented by gravity, aeromagnetic high-resolution aeromagnetic (HRAM) and high-resolution gravity where available, drilling, and outcrop data provides a means to study the regional structural framework of the three study areas (Figure 1.1).

Chapter 2 reviews some of the gravity and magnetic background principles and recent advances in potential field enhancement and filtering techniques designed to highlight anomalies of interest not directly evident in the original data but potentially related to geologic features of interest.

Chapter 3 present the results of using integrated seismic attributes and new enhancement and filtering techniques associated with HRAM data to establish links between Precambrian basement structures and sedimentary basin structures in the Fort Worth basin. The Fort Worth integrated studies was able to establish a link between basement structures and Paleozoic features. We also evaluate whether the HRAM data can be used to predict structures within the sedimentary rock in frontier areas or area where seismic data is limited or unavailable.

Chapter 4 presents the results of seismic data analysis of several 3D seismic surveys acquired in Osage County, Oklahoma. The objective of this study is to understand the interaction between Precambrian basement structures and the overlying fractured controlled Ordovician Arbuckle dolomite, Mississippian limestone, and Chert reservoirs. A regional section of this study utilizes regional gravity and aeromagnetic data to investigate the extent of the 1100 Ma Mid-Continent Rift System (MCRS) through Oklahoma, toward Texas. Authors such as Jones and Lyons (1964), Nixon and Ahern (1988), Robbins and Keller (1990), and Adams and Keller (1994) have used gravity and magnetic information to suggest a possible extension of the MCRS into west Texas and New Mexico. We also investigated the conspicuous large Bouguer gravity anomaly, which is centered within the Osage County. 2). Density variation (Cook, 1956), deeper crustal source (Denison, 1981), thinned crust, and Moho bumps or anti-root (Roark,

1962) have been suggested as the cause of this anomaly because of its lack of correlation with regional structural geology. Could this anomaly be related to the MCRS?

Chapter 5 focuses on improving the understanding of the structure and geometry of the Ucayali basin, Peru as well as the underlying basement structure and its interaction with Paleozoic or younger sediments. This project is an integrated geophysical and geological study conducted in a sparsely explored area of Peru that is occupied by foreland basins east of the Andes. I attempt to develop a regional geophysical cross-section across the western Andes toward to the sub-Andean basin using all available resources and published information (e.g., Sobolev and Babeyko, 2005; Tassara et al., 2006; Mamani et al., 2008). Our goal is to construct a 2D gravity model across the Peruvian Andes describing the major structural features and regional architecture within the region. I also hope to investigate the type of lithospheric-slab plate type beneath the study area.

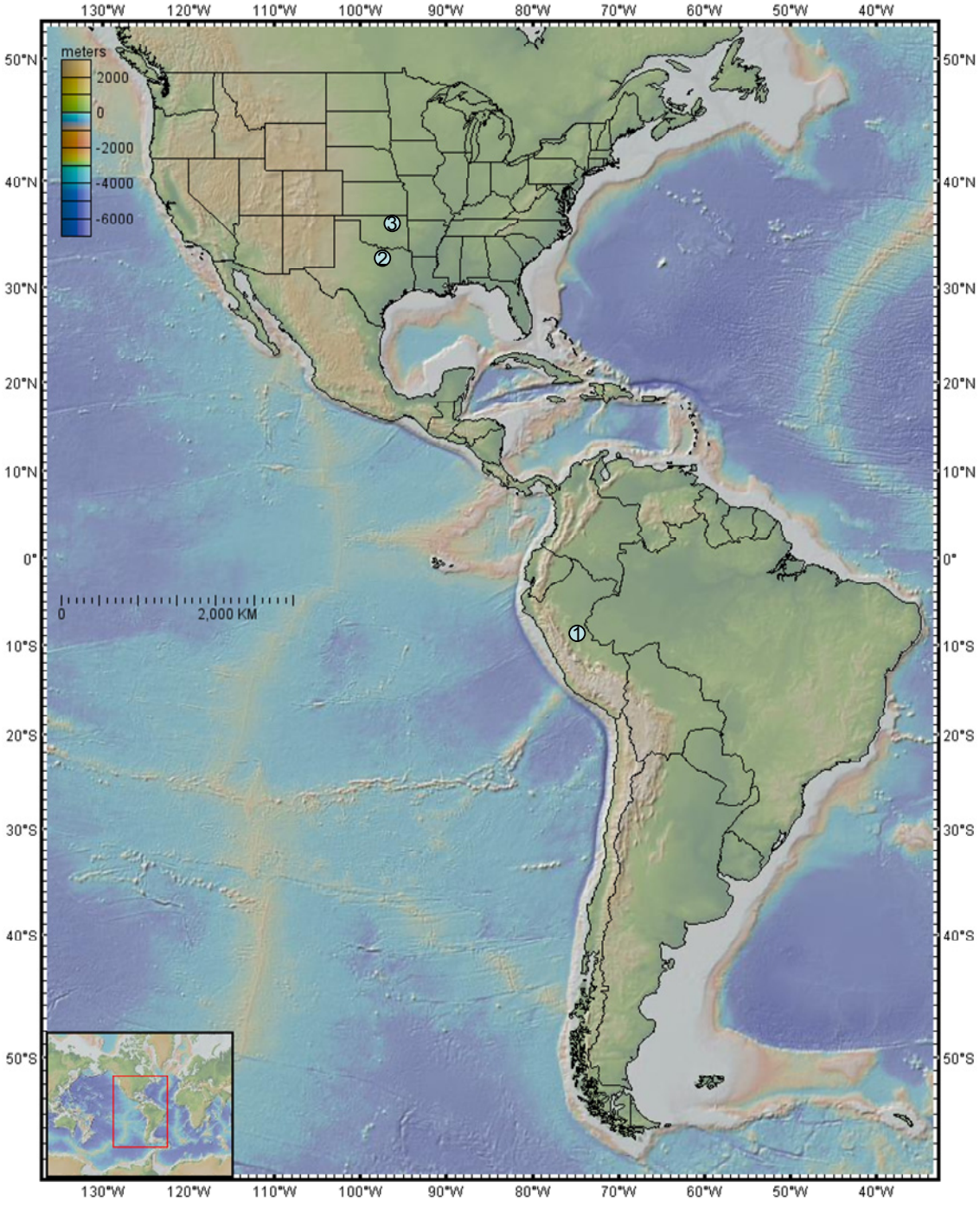


Figure 1.1. Map showing the location of the three study areas that constitutes this dissertation. (1) Ucayali and Maranon Basin in Peru, (2) Fort Worth basin in Texas, and (3) Osage County in Oklahoma.

# Chapter 2: Background and Methodology

Gravity and magnetic methods have proven to be an effective method for studying the Precambrian basement rocks beneath sedimentary basins (Cordell and Grauch, 1985; Keller et al., 1985; Gay, 1995; Adams and Keller, 1996; Lyatsky et al., 2004). Interpretation of potential field data generally lacks uniqueness. However, the integration of potential field data with other available geophysical or geological information can reduce the interpretation risk that usually plaque utilization of potential field data alone. This approach can overcome the non-uniqueness problem.

## 2.1 Introduction to Gravity and Magnetic Anomaly

Gravity and magnetic anomalies reflect lateral change in density and magnetic susceptibility caused by structures or changes in lithology. Gravity anomalies reflect the difference between the observed and predicted gravity value and usually contain a regional effect (Dobrin, 1988; Telford et al, 1990). Such anomalies can occur below or above the Precambrian basement crust (Lyatsky and Dietrich, 1998). Generally, igneous and metamorphic rocks are denser and magnetic than sedimentary rocks but overlap does occur.

According to Sims et al. (2005), aeromagnetic anomalies consist of a complex integration of crustal magnetic sources, mostly originating from the Precambrian basement. These kinds of anomalies are devoid of large-scale regional features (Telford et al., 1990) and are generally associated with features from the upper crust above the Curie depth. The Curie depth is the depth (~ 30 km) below, which the temperature of rocks is above the Curie temperature, making rocks too hot to possess or retain

magnetization. Thus, magnetic anomalies are an indicator of the structure and distribution of magnetization in the basement, and variations in magnetization are usually more important than structures (Dobrin and Savit, 1988). As a rule-of-thumb, magnetic minerals, mainly magnetite, are generally more abundant in mafic igneous rocks than in felsic igneous rocks. A magnetic anomaly is a reflection of a susceptibility contrast, which is a measure of the magnetic minerals present. However, magnetite is not the only magnetic mineral that can produce a magnetic anomaly other minerals include those described in Reynolds et al. (1990) and Clark (1997). Likewise, igneous and metamorphic rocks are more magnetic than sedimentary rocks but metamorphism often reduces magnetism in rocks.

## 2.2 Methodology

The integrated nature of the three research projects presented in this dissertation requires similar datasets and methods of investigation. Combined public domain aeromagnetic, propriety high-resolution aeromagnetic and gravity data, 3D seismic data, well information, and geologic information were utilized to effectively characterize the Precambrian structures and conduct research in the three areas.

The ability to integrate all these datasets makes this approach a viable option. Each dataset provide constraints on the overall solution. For example, the structural configuration and features of the sedimentary section can be easily mapped using seismic data and its attributes. The ability to map basement features on seismic data can be challenging because of the incoherent nature of reflectors. However, utilizing gravity and aeromagnetic data and their respective derivatives can compensate for such shortcomings.

The integrated approach in this study began with seismic interpretation using commercial available software such as IESX GEOQUEST and PETREL, which are Schlumberger's interpretation tools. With the aid of the seismic data, various sedimentary structures were identified. Seismic attribute data enhances some of these sedimentary structures. Codes supplied by the Attribute-Assisted Seismic Processing and Interpretation (AASPI) group in the ConocoPhillips School of Geology and Geophysics at the University of Oklahoma, were used to compute the various seismic attributes.

Seismic attributes visually enhance or quantitatively measure features of interest in a seismic data and provide an interpreter with a unique view of the data. Thus, physical and geometrical features, which are not easily seen in seismic data, become visible on images of attribute data (Chopra and Marfurt, 2005). However, it is still the interpreter's job to intuitively extract geological information from these attributes data. Using a combined physical model such as dip and azimuth, waveform similarity or frequency content from adjacent seismic samples, attribute data classifies subtle features into a display, which is then enhanced for the human or computers interpretation (Chopra and Marfurt, 2007).

Examples of geometric attributes used in this study include coherence, volumetric curvatures, dip, and azimuth. These attributes are sensitive to lateral changes in the physical model and are generally calculated using a vertical window (Chopra and Marfurt, 2007). Their sensitivity to lateral changes makes them suitable to map sedimentary features like faults (Lawrence, 1998; Gersztenkorn et al., 1999) and fractures effectively (Neves et al., 2004). The application of seismic attributes to fault mapping has been mostly limited to sedimentary basins because basement rock lacks stratified and

coherent reflectors. However, some of the attributes used such as curvature, can be effective even with limited stratified and coherent basement reflectors. A full detailed description of the physics, mathematical foundation, and application of these attributes can be found in Chopra and Marfurt (2007).

## 2.3 Potential Field Data Enhancement and Filtering Techniques

Potential field anomalies generally contain a wide range of signals from various sources and depths. Short wavelength anomalies typically reflect shallow features while larger and broader anomalies are often indicative of deeper, regional sources. Therefore, anomalies of interest must be separated. Potential field enhancement and filtering techniques are designed to better image and delineate both regional scale anomalies associated with Precambrian structures and local anomalies of interest, which cannot be easily seen in raw data. Thus, the potential field enhancement and filtering products derived are similar to seismic attributes (Verduzco et al., 2004) and can often help with geological interpretation. However, both may target different ranges of anomaly wavelengths. These products facilitate the ability to relate physical properties associated with potential field data with geological features of interest.

The 2-D Fourier transform allows us to easily apply most anomaly separation and enhancement techniques because it maps a spatial domain function, *f (x, y)*, into a 2-D function of wavenumber (the reciprocal of wavelength); *($k_x$, $k_y$)*. This transformation allows for easy computation in the Fourier domain and yields.

$$F\left(k_x k_y\right) = \int_{-\infty}^{\infty}\int_{-\infty}^{\infty} f\left(x,y\right) e^{-i2\pi(k_x x + k_y y)}\, dxdy \,, \tag{2.1}$$

where $|\boldsymbol{k}| = \left(k^2 + k^2\right)^{1/2} = 2\pi/\lambda$

A few of the techniques that will be discussed herewith are applicable to both gravity and magnetic data. Others are applicable only to individual datasets. Those discussed below include, residual anomaly separation, upward continuation, derivatives, horizontal gradients, reduction-to-the pole of magnetic data, band-pass and directional filters; these can be used to isolate linear anomalies of interest with tectonic implication.

### 2.3.1 Residual anomaly separation

Potential field anomalies can be due to both regional and local features. Thus, residual anomaly separation is a mathematically stable way of highlighting anomalies that are caused by upper crustal geology and subdue the effects of deeper features. For the purpose of this dissertation, the term 'regional anomaly' would refer to anomaly with a deep source origin, such as the deep root of the Andes Mountains. On the other hand, the term 'residual anomaly' will refer to an anomaly created by shallow to intermediate sources (Jacobsen 1987).

To create a residual anomaly map, a simple subtraction method of a low-pass anomaly map, which highlights the regional anomaly, from the complete anomaly map worked effectively for our applications. More importantly, we computed the low-pass anomaly map from a upward continuation operator and not from a low-pass filter selected by trial-and-error. The upward continuation filter technique, which is a form of a low-pass filter, is preferable to an ordinary low-pass filter because the upward continuation map is usually devoid of the ringing artifact or Gibbs phenomena, which is often characteristic of a broadband low-pass filtered map (Figure 2.1 and 2.2). The Gibbs phenomenon occurs on the anomaly map where the amplitude of the data is rapidly changing. In the frequency domain, the truncation of the frequency spectrum with a

rectangular window (Step function window) causes the Gibb's effect, which is expressed as short wavelength ringing in the space domain data (Paoulis, 1962; Ku et al., 1971). Because most band-pass filters suffer from this phenomenon, smaller amplitude signals can be perturbed. Thus, I adopted a more stable approach of applying a low-pass filter without using the rectangular window.

The anomaly separation workflow employed is discussed below using a sample of complete Bouguer data covering part of Texas, Oklahoma, and Kansa. At various upward continuation heights ranging from 10 km – 100 km, several regional anomalies or upward continuation maps were generated (Figure 2.3). The selection of the upward continuation height was geologically constrained but this can be subjective, depending on the geologic features that will be eventually removed when the residual is calculated.

In the examples shown in (Figure 2.2), deep anomalies related to the northwest trending Southern Oklahoma aulacogen (SOA) and northeast trending Mid-Continent Rift System (MCRS) are the two obvious regional trend anomalies that were highlighted. I visually examined and compared all the upward continuation maps until there were no longer any noticeable changes among the subsequent upward continuation results (Figure 2.3). At this point, an upward continuation height is defined, and the grid is selected. An upward continuation height of about 20 km or 30 km seemed to be appropriate in this case.

Afterwards, the preferred upward continuation grid is subtracted from the original anomaly grid containing the regional anomaly in order to generate the residual anomaly grid (Figure 2.4). The subtraction of the regional anomaly map from the original anomaly grid is a form of high pass filter, but without the ringing effect associated with Gibb's

effect. Residual grids can be generated from both gravity and magnetic grids. It also has the advantage of having the physical basis of the representation of the regional anomaly being very clear.

### 2.3.2 Upward continuation

Upward continuation of potential field data is not a new concept to potential field data processing. It provides the luxury of viewing a magnetic or gravity field at a different higher levels or lower levels (downward continuation) over an anomaly source and can act as a standard separation filter for potential field maps (Jacobsen, 1987). This method transforms anomalies measured at a particular surface into what they would have been if the measurement were taken at a higher surface (Blakely, 1996) provided there is no disturbing of mass or magnetized body (Nettleton, 1976).

Dating back to the 1940's, authors such as Hughes et al. (1947), Henderson and Zietz (1949), and Robinson (1970) have applied this method effectively to attenuate short wave-number noise and also to remove regional large-scale fluctuations from potential field grids. Robinson (1970) used upward continuation as an aid in interpreting surface anomaly sources. This process is a form of low pass filter that enhances long wavelength anomalies (regional anomalies) and attenuates short wavelength anomalies (noise or shallow sources) (Figure 2.3). The smoothening is done with respect to wavenumber and the greater the upward continuation height, the greater the smoothing (Blakely, 1996). A simple upward continuation filter in the Fourier domain is described mathematically as:

$$F\left(x, y, \Delta z\right) = e^{\Delta z|\mathbf{k}|} \tag{2.2}$$

where $\Delta z(>0)$, is the upward continuation distance and k is the wavenumber.

The upward continuation operator shown above has an easily comprehensible physical term with explicit term expressed in both space and wavenumber domain. Thus, upward continuation operator is numerically and physically stable (Jacobsen, 1987).

### 2.3.3 Reduction-to-the-pole and/or reduction-to-the-equator

This operation is peculiar to a magnetic anomaly because of the dependence of the total magnetic intensity anomaly on magnetization direction and the direction of the measure field. The distortion will cause anomaly to be directly centered on it causative source on a magnetic anomaly map. A profile-view across a total magnetic intensity anomaly map that has not been reduced-to-the-pole, will display an asymmetric anomaly whose magnetization inclination is not vertical (Figure 2.5a).

Reduction-to-pole removes the distortion caused by the varying magnetization inclination and azimuth, thus, making the actual inclination vertical. It causes a phase shift or removes the asymmetry associated with the anomaly and centers the magnetic anomaly over the anomaly causative source by applying a Hilbert transform to the raw data (Blakely, 1996). Reduction-to-pole operation is a linear transformation that transforms a anomaly that would be measured at the north pole with induced magnetization and ambient field to be vertically pointing downward (Kis, 1990; Blakely, 1996) (Figure 2.5b). The Reduction-to-pole filter (Grant and Dodds, 1972) is:

$$R_{TP}(\theta) = \frac{1}{\left[\sin(I) + i\cos(I)\cos(D-\theta)\right]^2} \tag{2.3}$$

where $i$, $\theta$, $I$, and $D$ are the imaginary unit, wavenumber direction, magnetic inclination and magnetic declination of the magnetic anomaly respectively. Remanent

magnetization is assumed to be present and its direction is assumed to be consistent with the ambient field.

In low-latitude areas, such as Peru, a magnetic anomaly grid needs to be reduced-to-the-equator (RTE) in order to ameliorate problems that are associated with low-latitude magnetic data. Reduction-to-the-equator in low-latitude areas is a substitute where two-dimension reduction-to-the-pole (RTP) would have been unstable due to its transfer function that has an infinite discontinuity. Reduction-to-the-pole becomes unstable at latitudes that are less than 15 degrees (Kis, 1990).

The caveat of the RTE transformation is that it has the tendency to change anomaly sign so that a maximum will appear as a minimum. However, this typically occurs at 0-degree latitude. An example of a magnetic intensity map that has been reduced-to-the-pole is shown in Figure 2.6

### 2.3.4 Pseudogravity transformation

Pseudogravity transformation converts a magnetic anomaly into a gravity anomaly using a Poisson relation (Baranov, 1957) that shows a relationship between an anomaly caused by a uniformly dense and a uniformly magnetized body. The magnetic anomaly is converted to a gravity anomaly that would be observed if the magnetic source were replaced with an exact density source (Blakely, 1996).

Mathematically, a pseudogravity anomaly is proportional to the reduced-to-the-pole magnetic potential of an equivalent source (Blakely, 1996). After a pseudogravity transformation, broad wavelength anomalies (i.e. regional anomalies) are amplified while short wavelengths are attenuated (Figure 2.7).

Pseudogravity transformation facilitates a way of comparing magnetic and gravity interpretation considering that a gravity map is easy to interpret without much concern about the inclination and remanent magnetization problems associated with magnetic data. It can thus act as a quality control for both maps.

### 2.3.5 Horizontal gradient magnitude

A horizontal gradient magnitude operator estimates the location of lateral changes or abruptness in magnetization or density source (Blakely and Simpson, 1986). Density and magnetic susceptibility changes caused by features such as faults can be highlighted by the horizontal gradient magnitude.

Blakely (1996) used a different terminology for the horizontal gradient while Grauch and Cordell (1987) referred to horizontal gradient magnitude as horizontal gradient maxima respectively.

Horizontal gradient magnitude can be computed on both gravity and reduced-to-pole magnetic data or on pseudogravity data. Horizontal gradient magnitude computed on pseudogravity data will reflect a magnetization boundary.

According to Blakely (1996), the horizontal gradient magnitude of potential field data $h(x, y)$ can be calculated via a simple finite-difference relationship:

$$h(x,y) = \left\{ \left[ \frac{\partial M(x,y)}{\partial x} \right]^2 + \left[ \frac{\partial M(x,y)}{\partial y} \right]^2 \right\}^{1/2} \tag{2.4}$$

where $M(x,y)$ is the potential field anomaly in the $x$ and $y$ direction

A gravity anomaly from a near vertical or fault-like boundary produces a horizontal gradient magnitude maxima reflecting the steepest horizontal gradient directly over or

near the top edge of a tabular body (Grauch and Cordell, 1987; Blakely, 1996 ) and zero over gradual varying gradient (Miller and Singh, 1994) (Figure 2.8). Horizontal gradient magnitude has been applied in mineral exploration (Verduzco et al., 2004), Precambrian basement structure mapping in the Williston basin of Canada (Lyatsky and Dietrich, 1998), and in the Caldera boundary definition south of Italy (Florio et al., 1999).

A word of caution, horizontal gradient magnitude and other derivatives are pretty much an interpretation aid tool however, the gradient maxima seen on a gradient map could mean different things, and therefore, it is still interpreter's responsibility to find a meaningful interpretation. Another caveat of this technique is that, a non- near vertical boundary or when two source boundaries occur in close proximity to each other, the gradient maxima are offset from a position directly over the source boundary and this could lead to two peaks maxima, which could be interpreted as two edges (Grauch and Cordell, 1987).

### 2.3.6 Tilt derivative and horizontal derivative of the tilt derivative

Tilt derivative and horizontal derivative of the tilt derivative of a reduced-to-pole magnetic data can help determine magnetic source shape, continuity, and geologic edges. Both techniques excel in their ability to map subtle basement features.

These techniques are more effective than their contemporary vertical derivatives because they can effectively discriminate between signal and noise in the data and normalize magnetic anomaly amplitude. Tilt derivative acts like an automatic-gain-control (AGC) because, unlike other magnetic derivatives whose amplitude responses are linked to the total magnetic intensity amplitude (amplitude fall-off with depth), tilt derivative is independent of the total magnetic intensity's amplitude. It depends on the

ratio between vertical derivative and the absolute value of the horizontal derivative, and the reciprocal of the source depth. Thus, it does not depend on its amplitude for resolution (Miller and Singh, 1994; Verduzco et al., 2004). That means that subtle basement features will have amplified amplitude and therefore will be enhanced as much as already amplified features. Tilt derivative also has an advantage of responding well to both shallow and deep sources, and the zero value of the tilt derivative is near the edges of the anomaly body (Figure 2.9a).

On the other hand, the horizontal derivative of the tilt derivative preserves the amplified amplitude; thus, horizontal derivative magnitude has a well-defined maximum along the edges. For mineral exploration where remanent magnetization is not assumed, horizontal derivative of the tilt derivative is also very useful because it is independent of inclination (Verduzco et al., 2004). (See figure 2.9b)

Tilt derivative is the arctangent of the ratio of the vertical derivative to the absolute value of the horizontal derivatives:

$$\theta(x,y) = \tan^{-1}\left\{\frac{\left(\frac{\partial M_{(x,y)}}{\partial z}\right)}{\left[\left(\frac{\partial M_{(x,y)}}{\partial x}\right)^2 + \left(\frac{\partial M_{(x,y)}}{\partial y}\right)^2\right]^{1/2}}\right\}$$

(2.5)

Where M is the reduced-to-poles total magnetic intensity data. $\theta_{(x,y)}$ ranges between $+90^{o}$ *and* $-90^{o}$.

Horizontal derivative of the tilt derivative is given as

$$\delta\theta(x,y)=\left\{\left[\frac{\partial\theta(x,y)}{\partial x}\right]^2+\left[\frac{\partial\theta(x,y)}{\partial y}\right]^2\right\}^{1/2} \quad (2.6)$$

### 2.3.7 Analytical signal

An analytical signal can indicate where magnetization contrast occurs. It can also outline a magnetic source because it centers the maxima over or near where the magnetic susceptibility contrast occurs (Roest et al., 1992) (see Figure 2.9c and d). The analytical signal and horizontal derivative of the tilt derivative are independent of inclination, and this is one of the advantages of using these approaches to define edges of a body. It assumes the anomaly causative source has a vertical contact and that there is no remanent magnetization (Salem et al., 2007).

Among its recent application in the potential field community, analytical signal and tilt-derivative have been used to compute depth-to-source, using the simple amplitude half-width rule to estimate source characteristics (Roest et al., 1992; Salem et al., 2007).

Mathematically, analytical signal is defined as the sum of the square horizontal derivative in the *x* and *y* direction and the vertical derivative:

$$\left|AS(x,y)\right|=\left[\left(\frac{\partial M(x,y)}{\partial x}\right)^2+\left(\frac{\partial M(x,y)}{\partial y}\right)^2+\left(\frac{\partial M(x,y)}{\partial z}\right)^2\right]^{1/2}$$

(2.7)

The absolute value of the analytical signal enables the determination of source characteristic without necessarily making an assumption about the direction of source body magnetization.

### 2.3.8 First and second vertical derivatives

First and second vertical derivatives are a type of high-pass filter that quantifies gradients in the vertical direction. Vertical derivatives applied to a magnetic data are similar to measuring the magnetic field between two-vertically separated magnetometers and dividing the field strength by the distance of separation (Hood, 1965). Derivatives of these types enhance local short wavelength anomalies at the expense of the regional long-wavelength anomalies (Dobrin and Savit, 1988). The first and second vertical derivatives enhance and sharpen shallow sources (Figure 2.10a). However, the second vertical derivative can help resolve the edges of a potential field source, but with noise amplification (Blakely, 1996). As shown in (Figure 2.10b), second derivatives amplify edges where individual aeromagnetic grids have been patched together. More often than not, a low-pass filter is applied to remove noise related signals. The first vertical derivative is positive over a source body, zero near its edges and negative outside them (Miller and Singh, 1994).

The $n^{th}$ order of vertical derivative with respect to $x$ and $y$ is given by

$$F\left[\frac{\partial M(x,y)}{\partial z}\right] = |\mathbf{k}|^n, \tag{2.8}$$

### 2.3.9 Directional filtering

Directional filtering allows interpreters to isolate a linear anomaly that might have geological or tectonic implications. This filtering technique applies a fan-like filter to the data in the frequency domain (2D frequency spectrum) and only rejects or passes the linear anomaly of interest without perturbing the location of the spatial amplitude peak (Thorarinsson et al., 1988). The anomalies within the pass band consist of anomalies

within a selected azimuth. The filtered anomaly map displays the passed lineament in the space domain based on specified azimuth. Such filtering must be done with proper attention to the geology. An example of the use of this filter is shown in Figure 2.11. The anomaly of interest was the northeast trending Mid-Continent Rift System (MCRS).

## 2.4 Depth Estimation – Euler Deconvolution Method

Estimation of the depth of the Precambrian basement top from seismic data can be difficult due to poor data quality and is often further complicated by the lack of wells penetrating the Precambrian basement. For this reason, estimation of Precambrian depth from HRAM data is beneficial. Knowledge gained from such analysis can then be transferred to areas where seismic data are unavailable or limited. The Euler deconvolution method is an automated depth estimation method (Thompson, 1982) that can help determine the location or depth to the shallowest or deepest reasonable magnetic source or edges for various geological sources such as, dikes, faults, magnetic contacts, and extrusives (Phillips, 2007). It utilizes the structural index (SI), which is used to describe the geometry of the desired geologic structure, as a geological constraint (Reid et al., 1990; Barbosa et al., 1999). In addition to estimating source depth, Euler deconvolution can delineate source type and magnetic boundary or fault trends (Reid et al., 1990).

Euler deconvolution links orthogonal horizontal and vertical gradients of the total magnetic field to source depth using (SI) which is directly related to the nature and geometry of the magnetic source (Thompson, 1982; Barbosa et al., 1999). Euler deconvolution is based on the work of Thompson (1982) and Reid et al. (1990), and can be written as:

$$(x-x_0)\frac{\partial M}{\partial x}+(y-y_0)\frac{\partial M}{\partial y}+(z-z_0)\frac{\partial M}{\partial z}=N(R-M), \qquad (2.9)$$

where $(x_0, y_0, z_0)$ is the magnetic source (point, magnetic dipole, etc) position observed at point $(x, y, z)$ with total magnetic intensity field $M$, whose regional background value is $R$. The right-hand-side of equation 2.9 accounts for strike, dip and amplitude (Reid et al., 1990). The degree of homogeneity, N, represents the type of source which best represents the anomaly. N is related to the structural index described by Thompson (1982) and Reid et al. (1990) and is a measure of anomaly gradient fall-off with distance of a field relative to its depth. An N of 1.0 can best be used to delineate structures such as dikes, edges, sills or low-displacement faults. Faults with large throw and irregular contacts can be delineated with an N of 0.0. An N of 0.5 is appropriate for intermediate cases (Thompson, 1982; Reid et al., 1990).

Three-dimensional Euler depth estimation on a magnetic grid data will include selecting a desired range of structural indices (i.e. N = 0.0, 0.5, and 1.0) and an analysis square window size within the grids. Window size should be determined based on the grid size and anomaly length (Phillips, 2007). It should be large enough to contain the curvature of the anomaly of interest without compromising lateral resolution yet small enough to reduce interference from an adjacent anomaly without yielding poor results (Reid et al., 1999). High-frequency magnetic anomaly which reflect shallow source will be better imaged with small size window and vice versa for low-frequency anomalies. For each selected structural index, all points within the window will be used to solve the Euler equation (Reid et al, 1990). As this window is moved across the entire grid, several solutions, from which the four unknowns, are computed.

All the solutions from the different structural indices can be plotted effectively, using a circle cluster with depth proportionality indicated with the circle diameter. A plot of this kind can be used to delineate magnetic source boundary trends (Reid et al., 1990). An example of Precambrian depth estimates plotted using the circle cluster is shown in Figure 2.12. These plots indicate how Euler estimates can be used as a source boundary or type delineator. Figure 2.13 shows when the solutions are gridded to represent the shallowest or deepest reasonable depth to the top a magnetic edge or contacts.

The choice of structural index controls the accuracy of depth estimation. If the selected structural index is too low, the depth estimation will be underestimated and vice versa. From the cluster plots, an incorrect structural index will produce a scattered solution cluster, but the general trend of boundaries can still be deciphered from the scattered plot (Reid et al., 1990). A detailed Euler depth analysis is provided in Phillips (2007).

If the structural index is set at zero, the computed solution is the shallowest possible magnetic basement surface. An advantage of using a zero structural index is that the minimum possible depth to the top of the magnetic source is estimated (Phillips, 2007). A common practice we adopted was to estimate the minimum, intermediate, and maximum possible depth to the tops of the magnetic source and then compare all the plots for the best clusters.

## 2.5 Seismic Data and Seismic Attribute Data

Seismic attribute data measures a characteristic of interest in the seismic data and can be a powerful arsenal in an interpreter's hands. Subtle physical and geometrical

features that are not easily seen in conventional seismic data often become visible in attribute data (Chopra and Marfurt, 2005).

Geometric attributes used in this study that we found most useful include coherence, volumetric curvatures, and dip and azimuth. These attributes are sensitive to lateral changes in amplitude and phase and are measured within a vertical window (Chopra and Marfurt, 2007). Their sensitivity to lateral changes makes them suitable to effectively map faults (Lawrence, 1998; Gersztenkorn et al., 1999) and fractures (Neves et al., 2004). A full detailed description of the physics, mathematical foundation, and application of these attributes can be found in Chopra and Marfurt (2007).

### 2.5.1 Coherence

The coherence attribute is a similarity measurement between waveforms. Thus, a highly coherent seismic waveform indicates a laterally continuous rock formation. In contrast, discontinuous or abrupt changes (low coherence) on seismic waveform might reflect faults, fractures or channels. Structural and stratigraphic information not readily seen in ordinary seismic data are enhanced in a coherence volume because coherence integrates information from adjacent traces and samples in a non –linear fashion (Chopra and Marfurt, 2007). Coherence volumes are more effective to view faults and fractures either in vertical coherence section or spatially on a time slice. Correlation of shallower sedimentary features to deeper basement features can be facilitated by animating through the coherency volume. Representative coherence slice from the Fort Worth basin is shown in Figure 2.14a. Trends of lineaments seen within the sedimentary features can then be compared with lineament seen within the crystalline basement and revealed by potential field derivatives and filter products.

### 2.5.2 Volumetric curvature

This attribute measures the shape of a reflector. In 2D, synclinal reflectors will have a negative curvature, while anticlinal reflectors will have a positive curvature. Planar reflectors have zero curvature. In 3D, we have two components of curvatures. In this dissertation, I use the most-positive curvature $K_{pos}$ and most-negative curvature, $K_{neg}$, where $K_{pos} \geq K_{neg}$. Formal definitions can be found in Roberts (2001) and Chopra and Marfurt (2007). Most-positive and most-negative curvatures can be effective in highlighting faults, fractures, folds, and flexures. The zone of high curvature is tied to the flexure area because it is believed that fractures occur when rock is flexed or bent. Lisle (1994) correlated reflector curvature with fractures. Interpretation of curvature data needs to be constrained with available geologic or production data. An example of a most-negative curvature sliced at the same time on the coherence cube shown in Figure 2.14a is shown on Figure 2.14b.

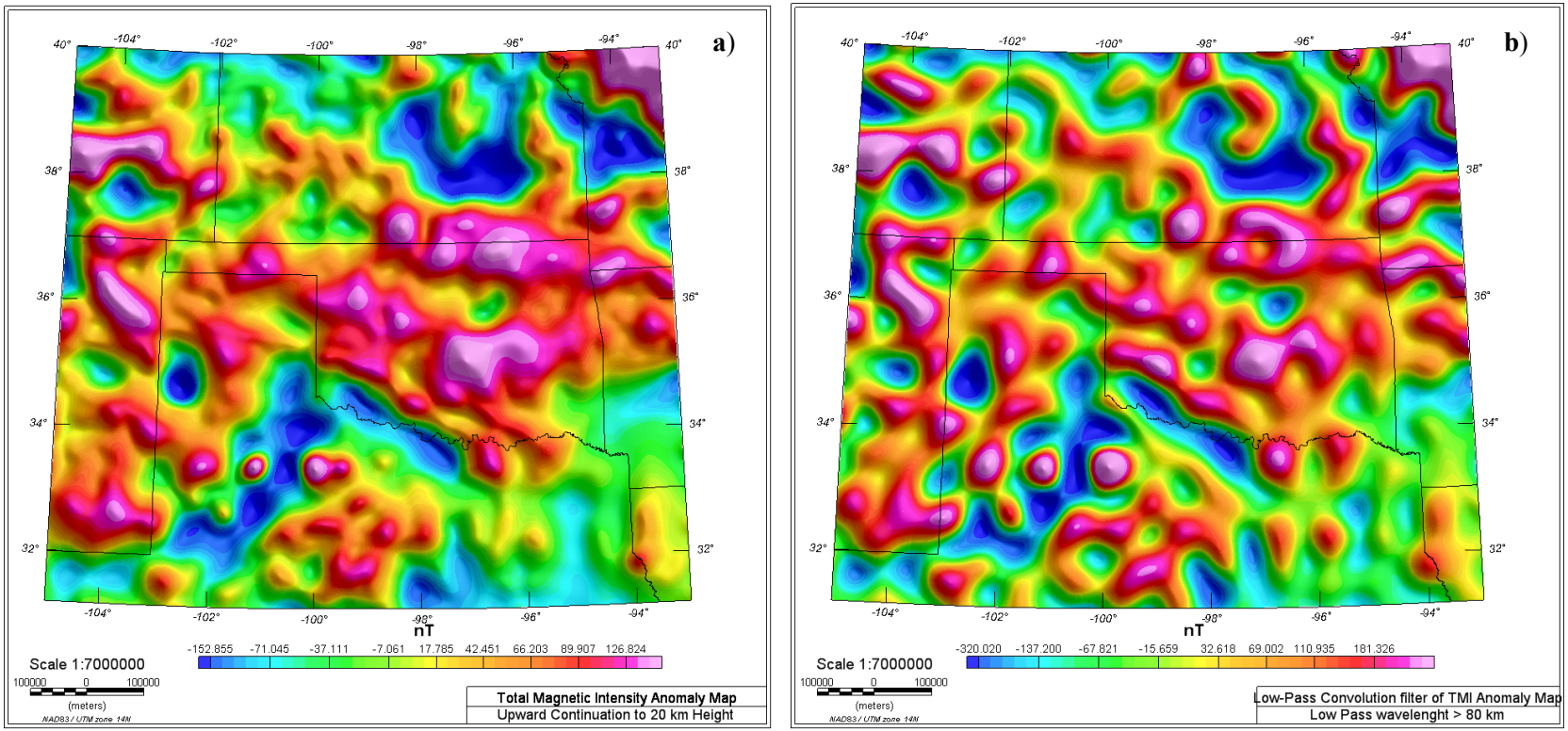


Figure 2.1. (a) Upwards continuation anomaly map of the TMI. (b) TMI low pass filter map with wavelength cut-off less than 80 km. Upwards continuation filter techniques which is a form of a low pass is preferable because it is not plagued with noise and effect such as the Gibbs phenomena manifested in the low pass map as ringing artifacts.

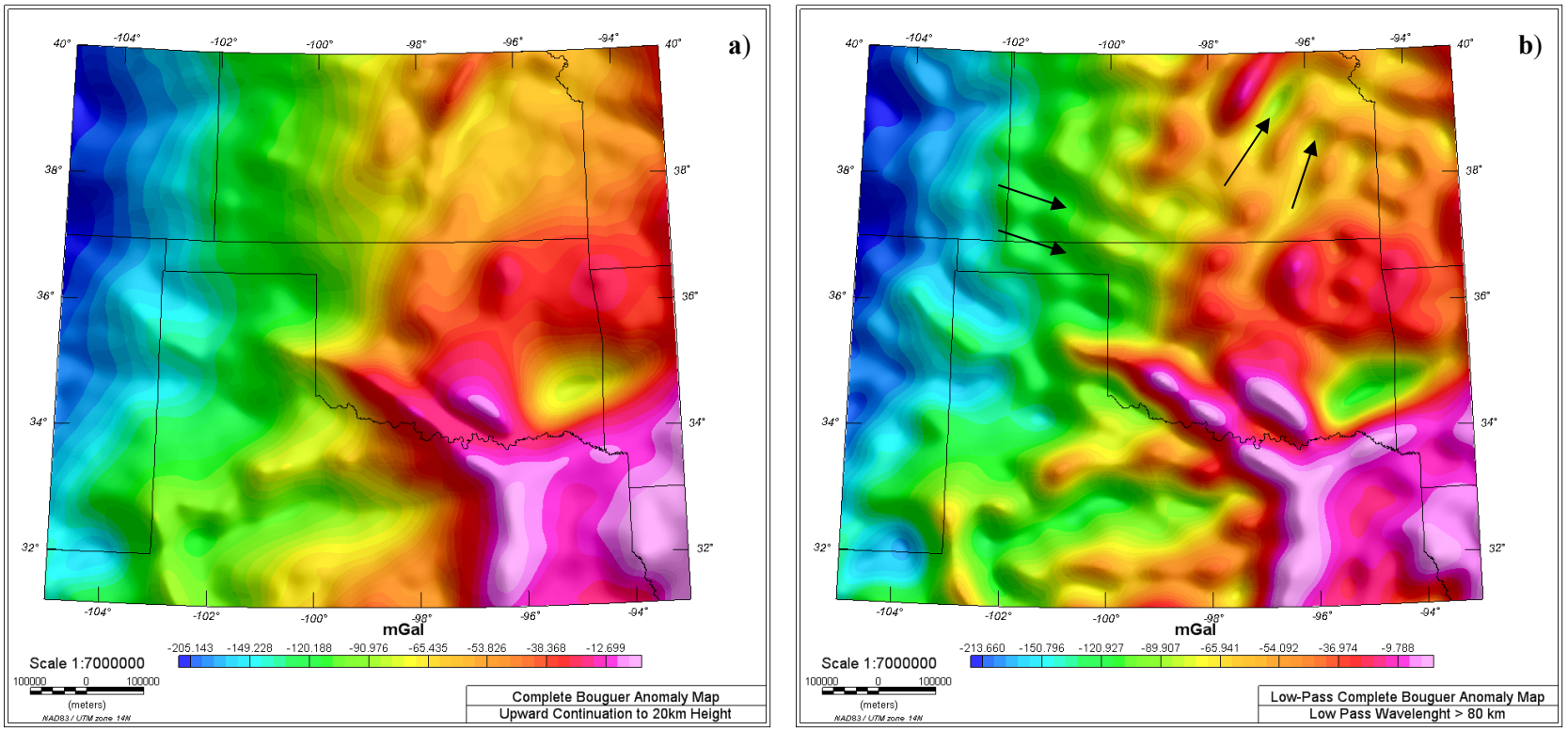


Figure 2.2. (a) Upwards continuation anomaly map of the Bouguer gravity (b) Bouguer low pass filter map with wavelength cut-off less than 80 km. Upwards continuation filter techniques which is a form of a low pass is preferable because it is not plaque with noise and effect such as the Gibbs phenomena (black arrow on Figure 2.2b) manifested in the low pass map as ringing artifacts.

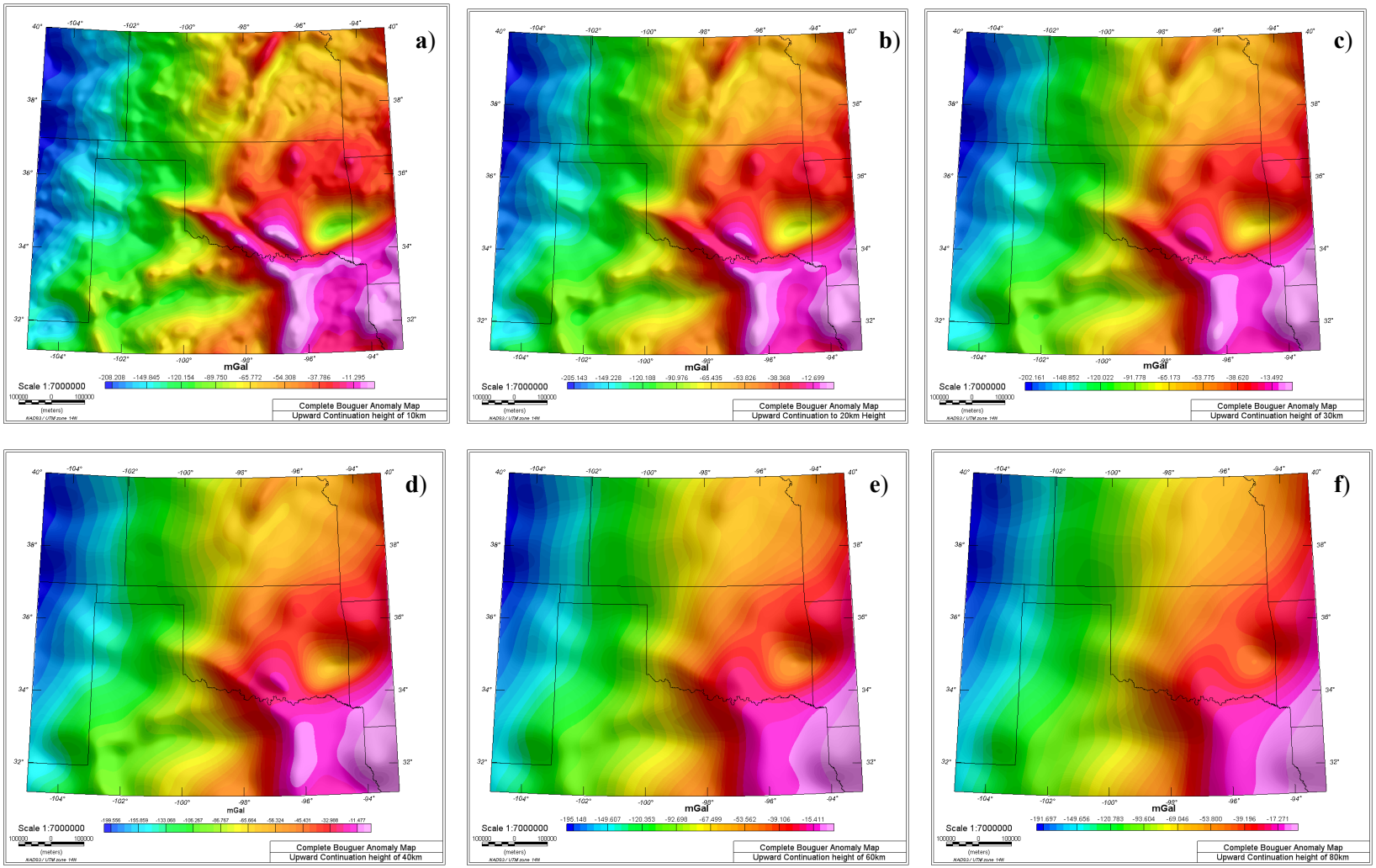


Figure 2.3. Various upward continuation anomaly maps of the Bouguer gravity upward continued to (a) 10 km (b) 20 km (c) 30 km (d) 40 km (e) 60 km (f) 80 km. Maps are not plagued with noise related to Gibbs phenomena manifested as ringing in the low pass map (See Figure 2.2b).

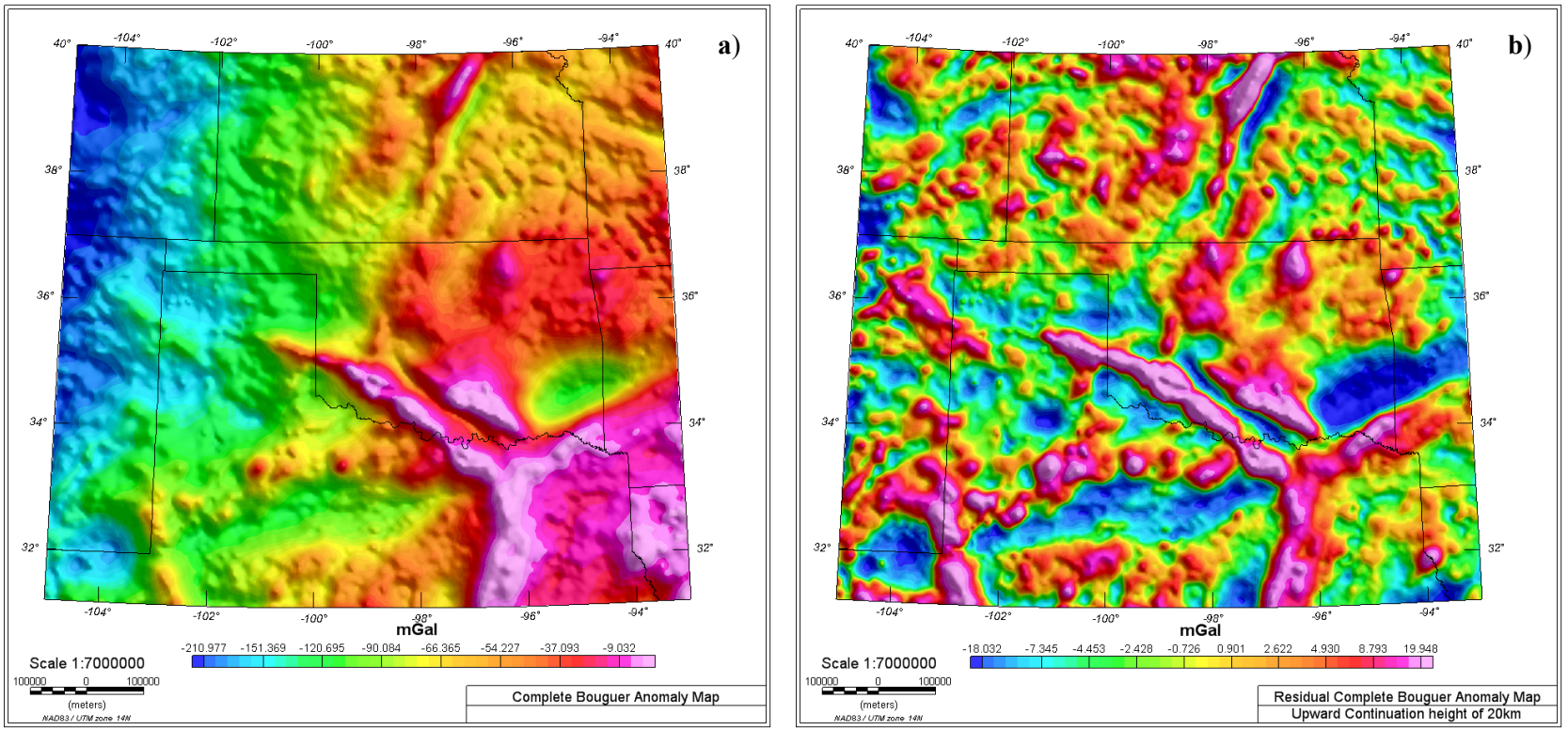


Figure 2.4. (a) Complete Bouguer anomaly map over most of Texas, Oklahoma, and Kansas. (b) Residual Bouguer anomaly map generated by subtracting an upward continued map of 20 km height from the complete Bouguer map shown in (a). The residual map is a form of a high pass filtered map because it enhances local features removing the regional features.

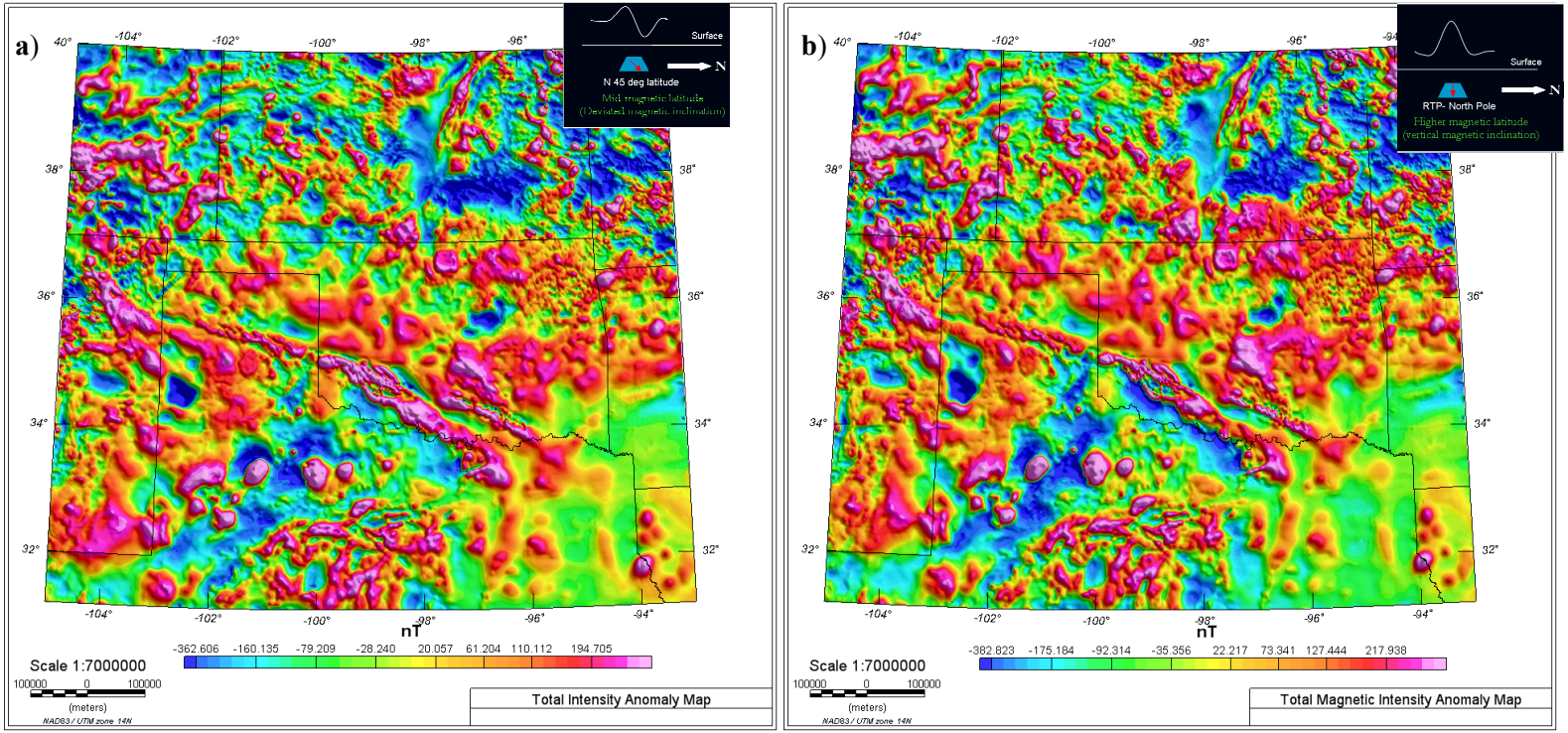


Figure 2.5. (a) Total magnetic intensity anomaly map that has not been reduced-to-the-pole. (b) Reduce-to-the-pole total magnetic intensity anomaly map. Inset box show the profile illustration of how RTP centers anomaly over its causative source, transforming the anomaly into what would be measure at the north-pole with induce magnetization and ambient field vertically pointing downward.

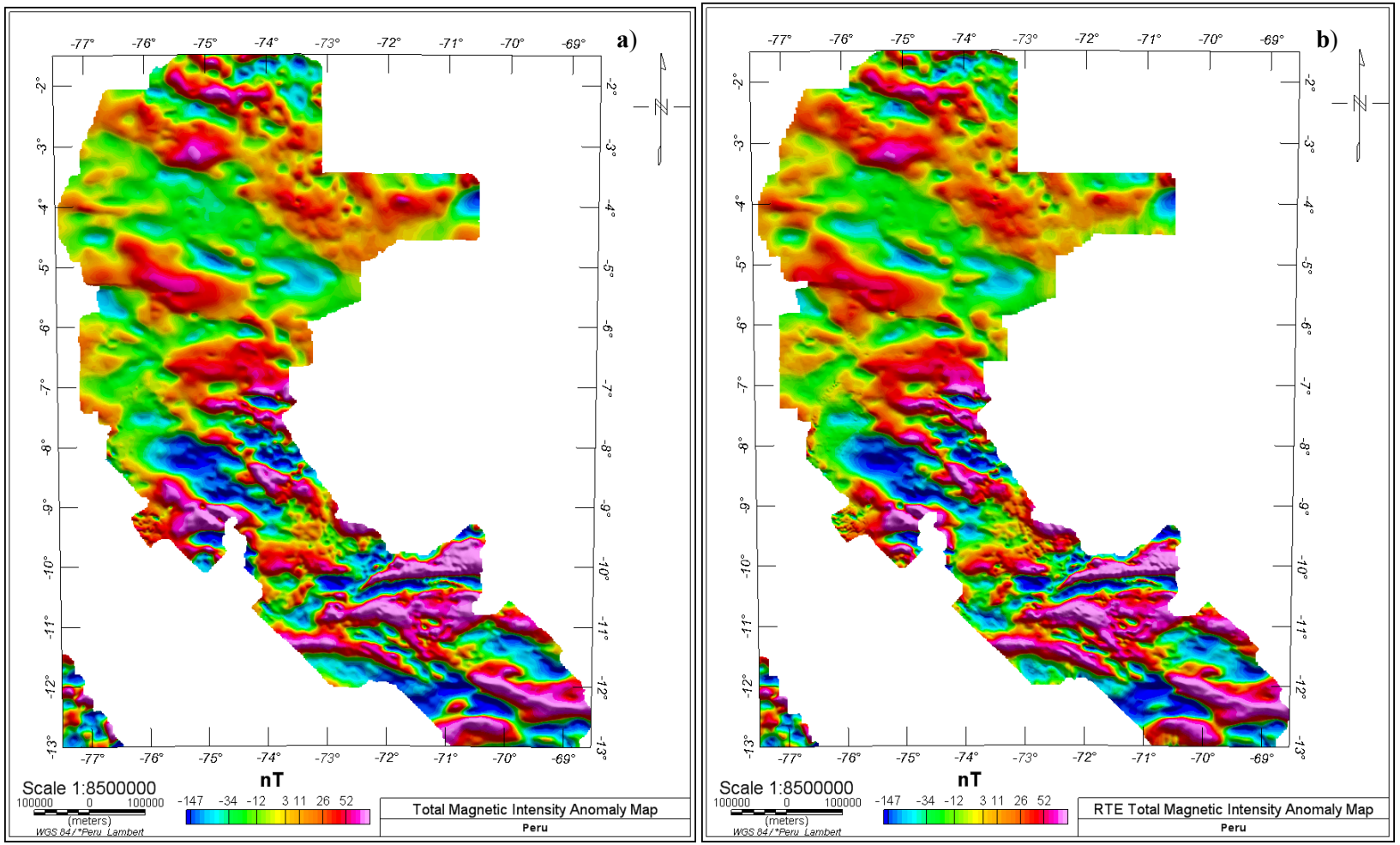


Figure 2.6. (a) Total magnetic intensity anomaly map over Peru that has not been reduced-to-the-equator. (b) Reduce-to-the-equator total magnetic intensity anomaly map.

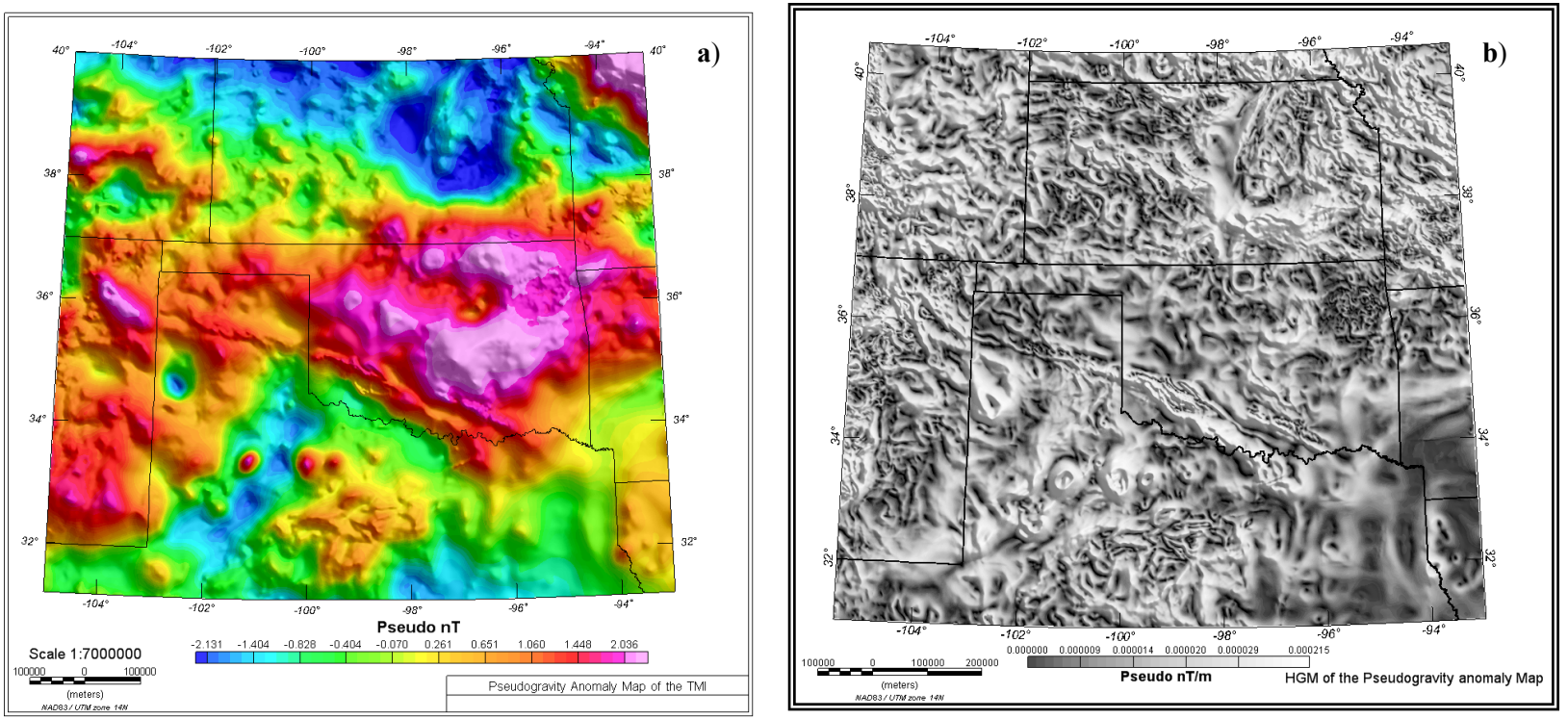


Figure 2.7. (a) Pseudogravity anomaly map of the TMI enhances broad wavelength anomalies attenuating short wavelength. (b) Horizontal gradient magnitude of the pseudogravity anomaly map, which locate lateral changes in anomaly and enhances source edges or anomaly trend directions that may correspond to faults.

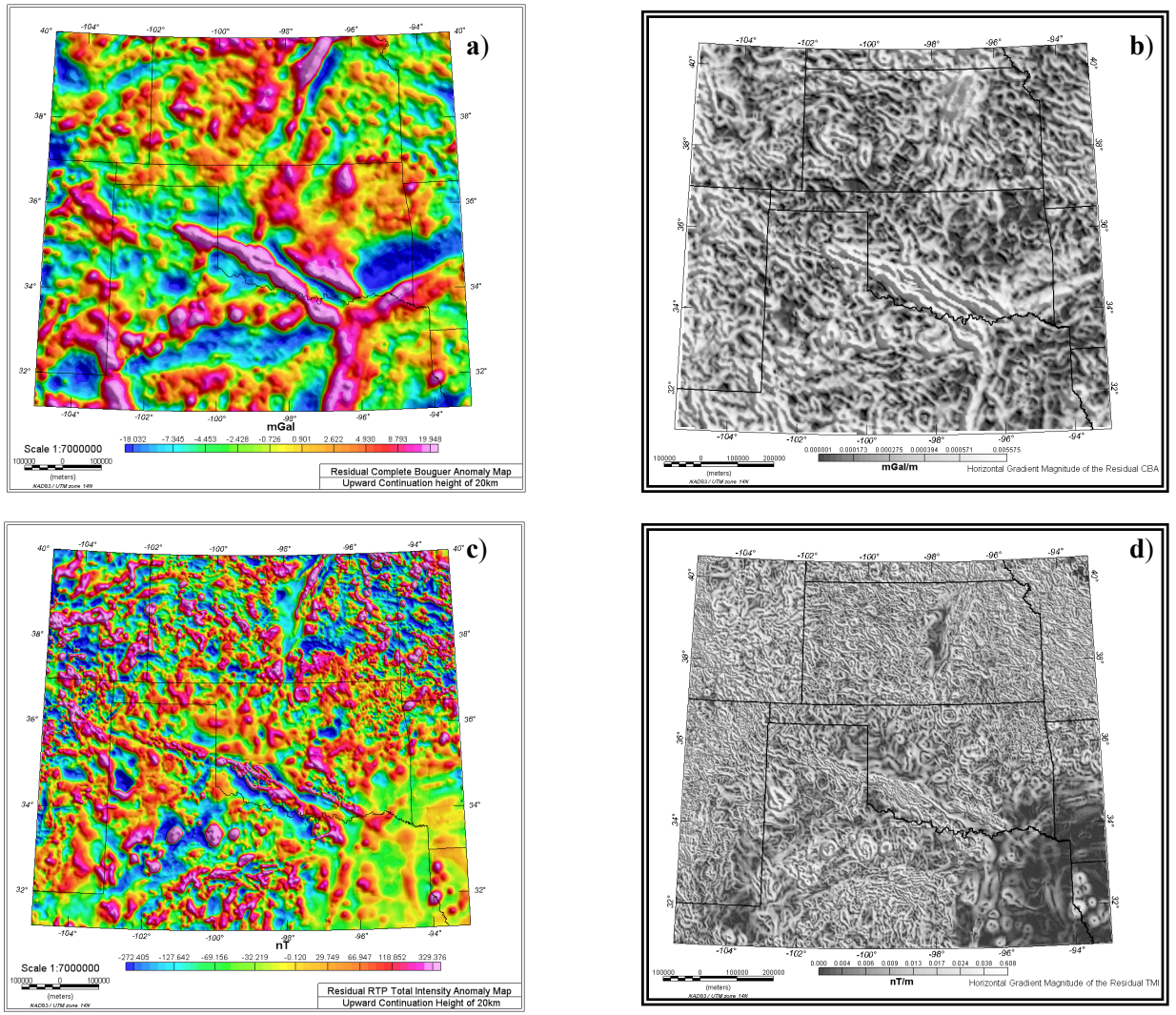


Figure 2.8. (a) Residual Bouguer anomaly map with (b) its equivalent horizontal gradient magnitude plotted on a grey scale color. (C) Residual TMI anomaly map with (d) its equivalent horizontal gradient magnitude plotted on a grey scale color.

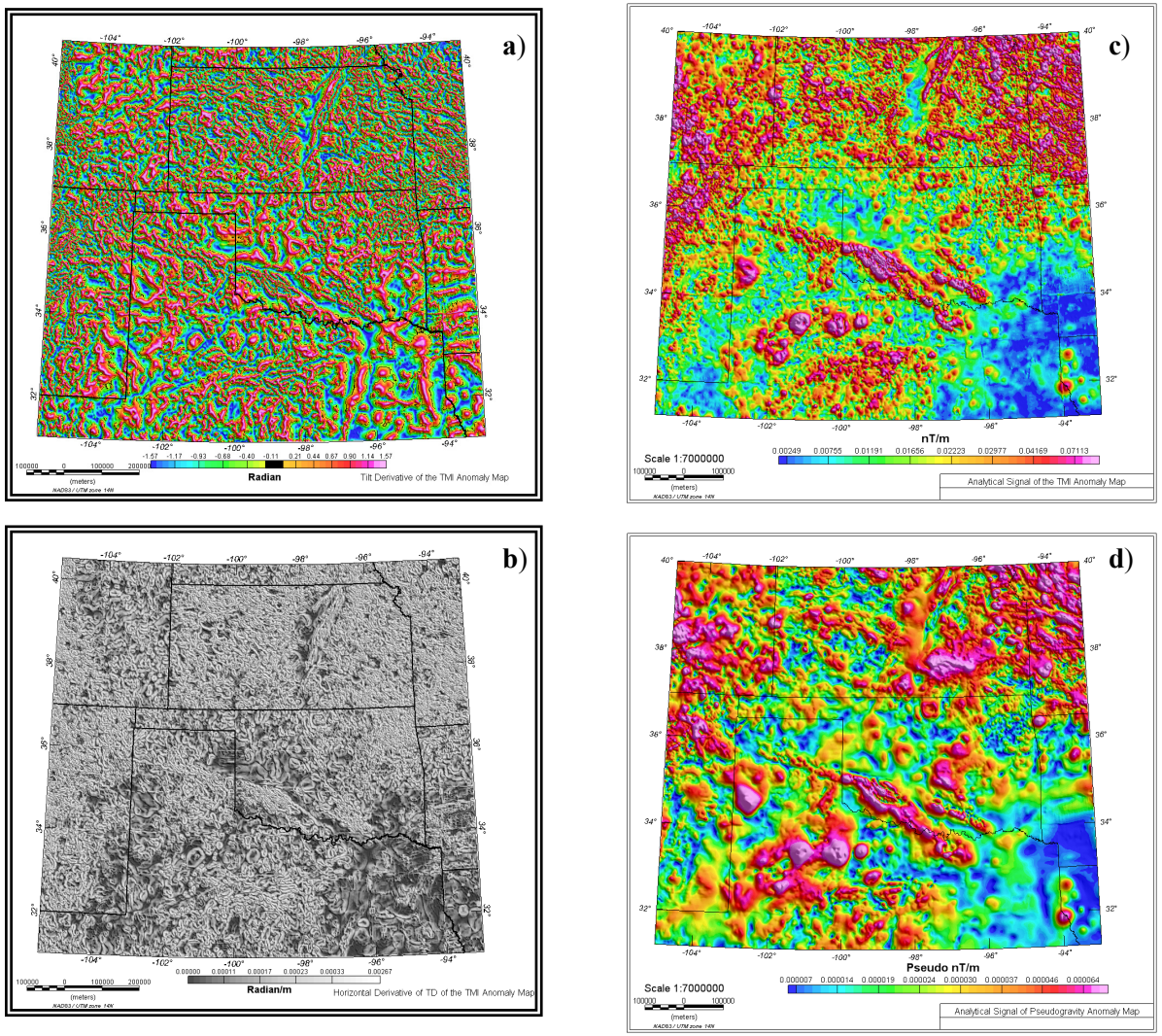


Figure 2.9. (a) Tilt derivative of the TMI anomaly map. (b) Horizontal derivative of the tilt derivative anomaly map. (c) Analytical signal of the TMI anomaly map. (d) Analytical signal of the pseudogravity anomaly map.

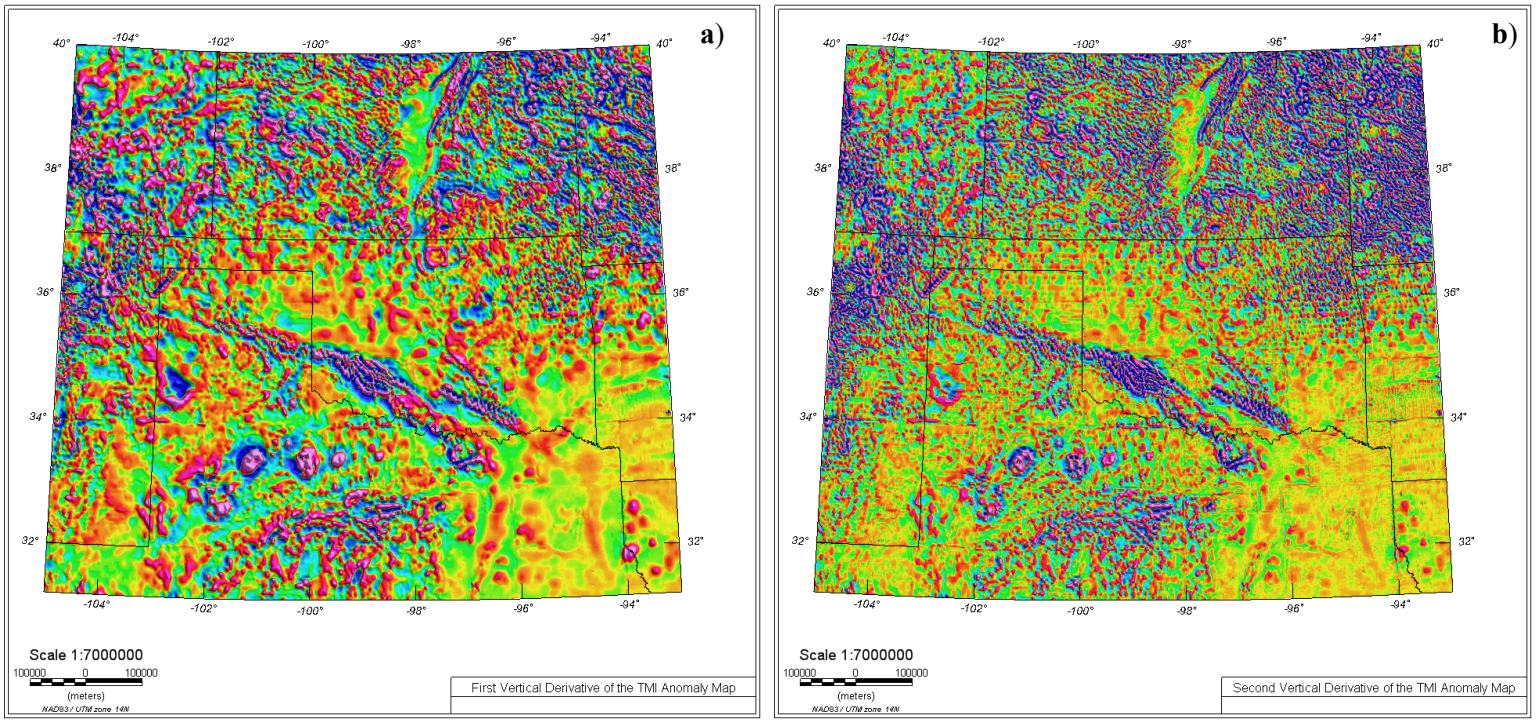


Figure 2.10. (a) First vertical derivative anomaly map enhances and sharpens anomalies. (b) Second vertical derivative anomaly map sharpens anomalies and amplifies noise.

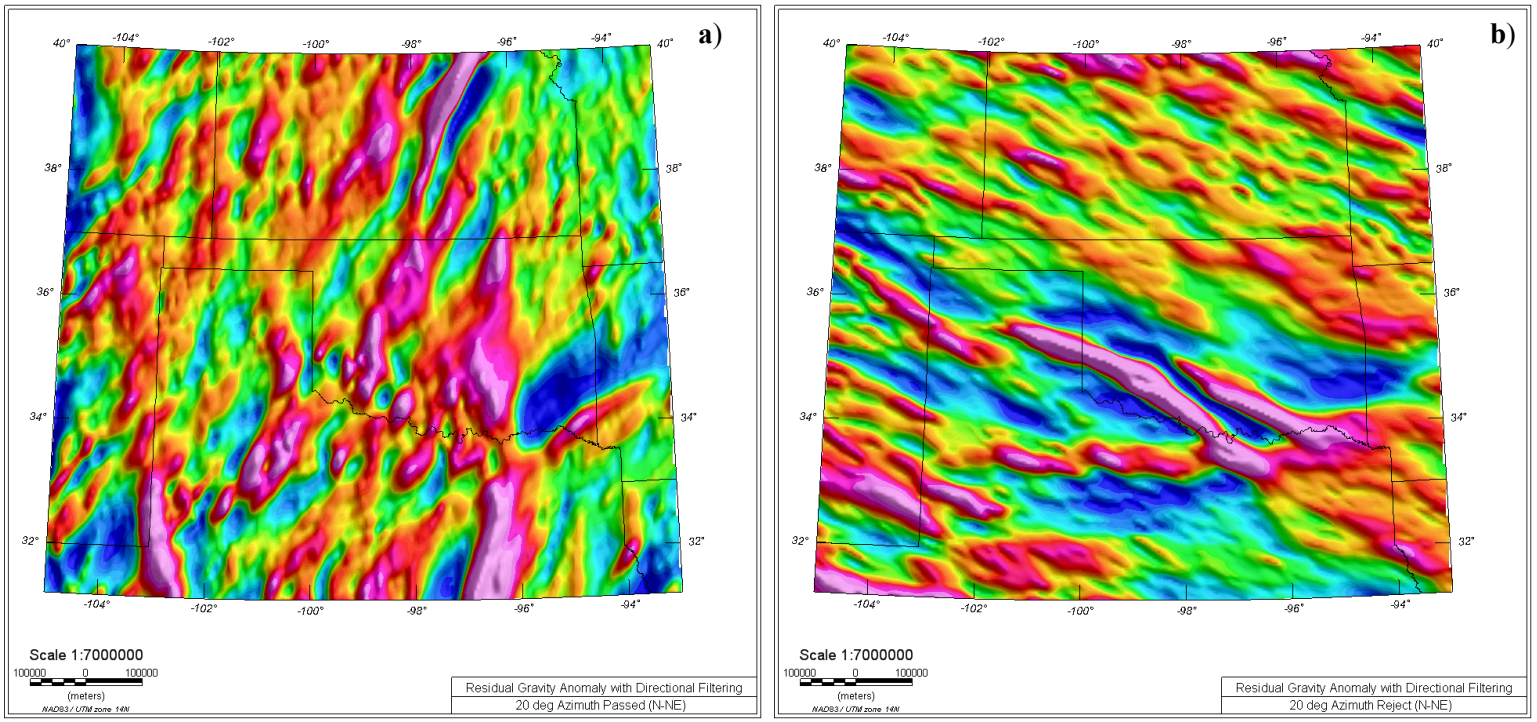


Figure 2.11. (a) Directional filter anomaly map enhances northeast features related to the Mid-Continent Rift System, Ouachita Orogeny, and Central Basin platform. (b) Directional filter anomaly map enhances northwest features related to the Southern Oklahoma aulacogen (SOA).

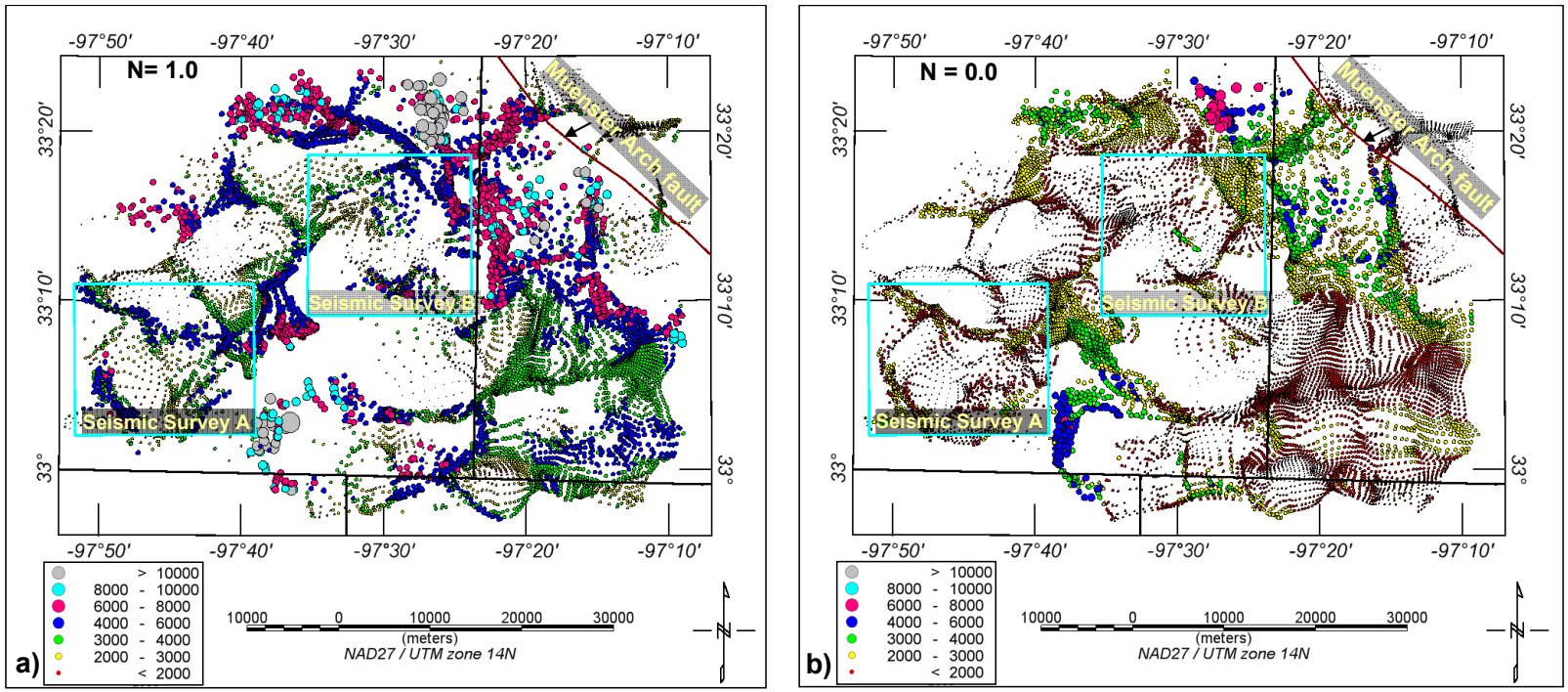


Figure 2.12. (a) Euler deconvolution cluster plots computed using a structural index, N, of (a) 1.0 and (b) 0.0.

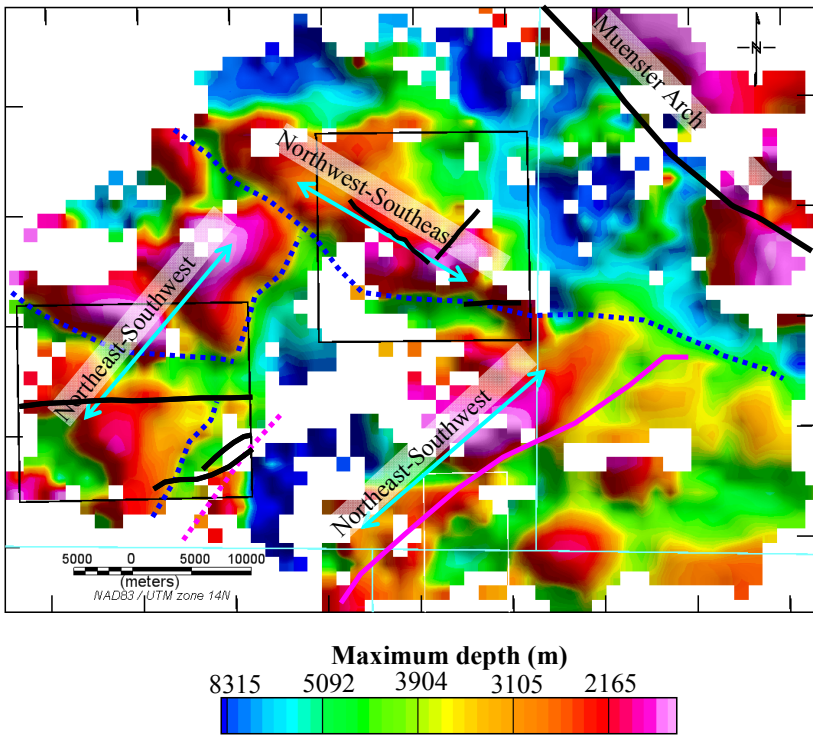


Figure 2.13. (a) Precambrian depth estimates map gridded from the cluster plots showing the structural complexity associated with the basement of Fort Worth basin. The result shows the deepest reasonable magnetic source depth of various geological sources such as dikes, faults, and magnetic contacts. Cyan arrows indicate the complex northeast-southwest and northwest-southeast structural grain of Precambrian basement beneath the Fort Worth basin.

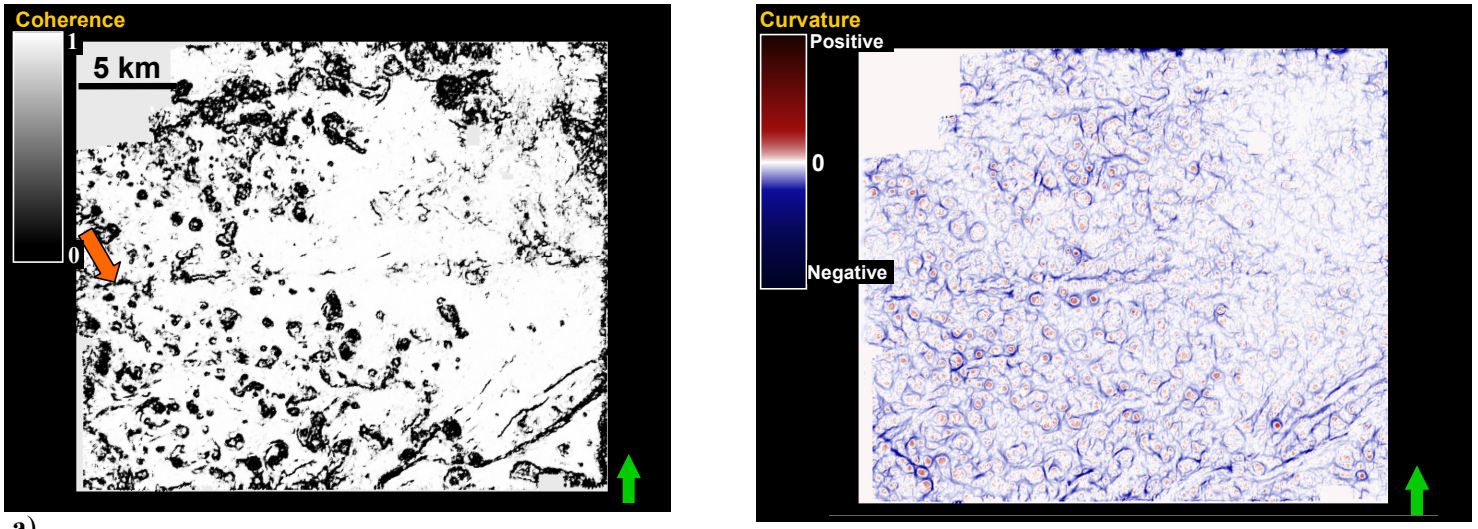


a)

b)

Figure 2.14. (a) Coherency slice seismic attributes that measures similarities between seismic waveforms. This attribute is sensitive to faults, fractures, and incoherent karst. (b) Most-negative curvature seismic attributes that measures seismic reflector shapes. Attribute is sensitive to folds, flexures, differential compaction, and collapse features.

## 2.6. References


Adams, D. C., and G.R. Keller, 1994, Possible extension of the Midcontinent Rift in west Texas and eastern New Mexico: Canadian Journal of Earth Science, **31**, 709-720.

Adams, D. C., and G.R. Keller, 1996, Precambrian basement geology of the Permian basin region of west Texas and eastern New Mexico: a geophysical perspective: American Association of Petroleum Geologist Bulletin, **80**, 410-431.

Baranov, V., 1957, A new method for interpretation of aeromagnetic maps: Pseudo-gravimetric anomalies: Geophysics, **22**, 359-383.

Barbosa, V. C. F., J.B.C. Silva, and W.E. Medeiros, 1999, Stability analysis and improvement of structural index estimation in Euler deconvolution: Geophysics, **64**, 48-60.

Barosh, P. J., 1995, A brief history of basement tectonics and the international basement tectonics conferences, *in* R. W. Ojakangas, A.B. Dickas, and J.C. Green, ed., Basement Tectonic **10**: Kluwer Academic Publisher, xvii-xxi.

Blakely, R. J., and R.W. Simpson, 1986, Approximating edges of source bodies from magnetic or gravity anomalies - Short Note: Geophysics, **51**, 1494-1498.

Blakely, R. J., 1996, Potential theory in gravity and magnetic applications: Cambridge University Press.

Carlson, M. P., 2005, The application of basement tectonic research to the development of natural resources - Example Midcontinent North America: Natural Resources Research, **14**, 125-128.

Chopra, S., and K.J. Marfurt, 2005, Seismic attributes - A historical perspective: Geophysics, **70**, 3SO-28SO.

Chopra, S., and K.J. Marfurt, 2007, Seismic Attributes for Prospect Identification and Reservoir Characterization, Society of Exploration Geophysicists Geophysical Development Series No. **11**.

Clark, D. A., 1997, Magnetic petrophyiscs and magnetic petrology: aids to geological interpretation of magnetic surveys: AGSO Journal of Australian Geology and Geophysics, **17**, 83-103.

Cook, K. I., 1956, Regional gravity survey in northeastern Oklahoma and southeastern Kansas: Geophysics, **21**, 88-106.

Cordell, L., V.J.S. Grauch, 1985, Mapping basement magnetization zones from aeromagnetic data in the San Juan basin, New Mexico, *in* W. J. Hinze, ed., The Utility of Regional Gravity and Magnetic Anomaly Maps: Society of Exploration Geophysicists, 181-191.

Denison, R. E., 1981, Basement rocks in northeastern Oklahoma: Oklahoma Geological Survey Circular, **84**, 1-84.

Dickas, A. B., 1992, The association of hydrocarbon with basement rock of Pre-Phanerozoic age, *in* R. W. Ojakangas, A.B. Dickas, and J.C. Green, ed., Basement Tectonics 10: Kluwer Academic Publishers, **10**, 283-295.

Dobrin, M. B., C.H. Savit, 1988, Introduction to Geophysical Prospecting: McGraw-Hill Book Company.

Elebiju, O. O., G.R. Keller, and K.J. Marfurt, 2008, New Structural mapping of basement features in Fort Worth Basin, Texas, using high-resolution aeromagnetic derivatives and Euler depth estimates: 78th Annual international meeting, SEG, Expanded Abstracts, **27**, 844.

Florio, G., M. Fedi, F. Cella, and A. Rapolla, 1999, The Campanian plain and Phlegrean Fields: Structural setting from potential field data: Journal of Volcanology and Geothermal Research, **91**, 361-379.

Gay Jr., S. P., 1995, The basement fault block pattern: its importance in petroleum exploaration, and its delineation with residual aeromagnetic techniques, *in* R. W. Ojakangas, A.B. Dickas, and J.C. Green, ed., Basement Tectonics **10**: Kluwer Academic Publisher, 159-207.

Gerhard, L. C., and S.B. Anderson, 1988, Geology of the Williston Basin (United States portion), *in* L. L. Sloss, ed., Sedimentary cover - North American Craton, U.S.: Boulder, Geological Society of America, The Geology of North America, **D-2**, 221-241.

Gersztenkorn, A., J.A. Sharp, and K.J. Marfurt, 1999, Delineation of tectonic features offshore Trinidad using 3D seismic coherence: The Leading Edge, **18**, 1000-1008.

Grauch, V. J. S., and L. Cordell, 1987, Limitation of determining density or magnetic boundaries from the horizontal gradient of gravity or pseudogravity data: Geophysics, **52**, 118-121.

Grant, F.S., and Dodds, J., 1972, MAGMAP FFT processing system development notes, Peterson Grant and Watson Limited.

Henderson, R. G., and I. Zietz, 1949, The upward continuation of anomalies in total magnetic intensity fields: Geophysics, **14**, 517-534.

Hood, P. J., 1965, Gradient measurements in aeromagnetic survey: Geophysics, **30**, 891-902.

Hughes, D. S., and W.L. Pondrom, 1947, Computation of vertical magnetic anomalies from total magnetic measurements: Trans American Geophysical Union, **28**, 193-197.

Jacobsen, B. H., 1987, A Case for upward continuation as a standard separation filter for potential-field maps: Geophysics, **52**, 1138-1987.

Jones, V. L., and P.L. Lyons, 1964, Vertical-intensity magnetic map of Oklahoma. Oklahoma Geological Survey Map GM-6 Scale 1:750,000

Keller, G. R., R.A. Smith, W.J. Hinze, and C.L.V. Aiken, 1985, Regional gravity and magnetic study of west Texas, *in* W. J. Hinze, ed., The Utility of Regional Gravity and Magnetic Anomaly Maps, **198**-212.

Kis, K. I., 1990, Transfer properties of the reduction of magnetic anomalies to the pole and to the equator: Geophysics, **55**, 1141-1147.

Ku, C. C., W.M. Telford, and S.H. Lim, 1971, The use of linear filtering in gravity problems: Geophysics, **36**, 1174-1203.

Lawrence, P., 1998, Seismic attributes in the characterization of small-scale reservoir faults in Abqaid field: The Leading Edge, **17**, 521-525.

Lisle, R. J., 1994, Detection of zones of abnormal strains in structures using Gaussian curvature analysis: AAPG Bulletin, **78**.

Lyatsky, H. V., and J.R. Dietrich, 1998, Mapping Precambrian basement structure beneath the Williston Basin in Canada: Insights from horizontal-gradient vector processing of regional gravity and magnetic data: Canadian Journal of Exploration Geophysics, **34**, 40-48.

Lyatsky, H. V., D. Pana, R. Olson, and L. Godwin, 2004, Detection of subtle basement faults with gravity and magnetic data in the Alberta Basin, Canada: A data-use tutorial: The Leading Edge, **23**, 1282-1288.

Mamani, M., A. Tassara, and G. Wörner, 2008, Composition and structural control of crustal domains in the central Andes: Geochemistry Geophysics Geosystems, **9**, 1-13.

Miller, H. G., and V. Singh, 1994, Potential field tilt - a new concept for location of potential field sources: Journal of Applied Geophysics, **32**, 213-217.

Nettleton, L. L., 1976, Gravity and magnetic in oil prospecting: McGraw-Hill Book Company.

Nettleton, L. L., 1976, Gravity and magnetic in oil prospecting: McGraw-Hill Book Company.

Neves, F., M.S. Zahrani, and S.W. Bremkamp, 2004, Detection of potential fractures and small faults using seismic attributes: The Leading Edge, **23**, 903-908.

Nixon, G. A., and J.L. Ahern, 1988, Southern extension of the Midcontinent geophysical anomaly; evidence for Keweenawan rifting in north-central Oklahoma: geological Society of America Abstract with Programs, **20**, A234.

Papoulis, A., 1962, The Fourier integral and its applications: McGraw Hill Book Company.

Phillips, J. D., 2007, Geosoft executables (GX's) developed by the U.S. Geological Survey, version 2.0 with notes on GX development from Fortran code: U.S. Department of Interior, U.S. Geological Survey.

Reid, A. B., J.M. Allsop, H. Granser, A.J. Millett, and I.W. Somerton, 1990, Magnetic interpretation in three dimensions using Euler deconvolution: Geophysics, **55**, 80-91.

Reynolds, R.L., J.G., M.R. Hudson, and N.S. Fishman, 1990, Rock magnetism, the distribution of magnetic minerals in the earth's crust, and aeromagnetic anomalies, *in* W. F. Hanna, ed., Geologic Application of Modern Aeromagnetic Survey: U.S. Geological Survey Bulletin, **1924**, 24-46.

Roark, J. J., 1962, Earth crust measurements by seismograph in Oklahoma - An interim report Geophysical Society of Tulsa Proceedings, 1959-1961: Presented at the 30th Annual meeting of the Society of Exploration Geophysicists.

Roberts, A., 2001, Curvature attributes and their application to 3D interpreted horizons. First Break, 19, 85-99

Robinson, E. S., 1970, The upward continuation of anomalies in total magnetic intensity fields: Geophysics, **35**, 920-926.

Roest, W.R., J. Verhoef, and M. Pilkington, 1992, Magnetic interpretation using 3-D analytical signal: Geophysics, **57**, 116-125.

Salem, A., S. William, J.D. Fairhead, D. Ravat, and R. Smith, 2007, The meter reader - Tilt-depth method: A simple depth estimation method using first-order derivatives: The Leading Edge, **26**, 1502-1505.

Sims, P. K., R.W. Saltus, and E.D. Anderson, 2005, Preliminary Precambrian basement structure map of the continental United State - an interpretation of geologic and aeromagnetic data: U.S. Geological Survey Open-File Report 2005-1029.

Sobolev, S.V., and A.Y. Babeyko, 2005, What drives orogeny in the Andes?: Geology, **33**, 617-620.

Tassara, A., H. Götze, S. Schmidt, and R. Hackney, 2006, Three-dimensional density model of the Nazca plate model and the Andean continental margin: Journal of Geophysical Research, **111**, 1-26.

Telford, W. M., L.P. Geldart, R.E. Sheriff, 1990, Applied Geophysics: Cambridge University Press.

Thomas, W.A., and D.L. Baars, 1992, A North American continental-scale fracture zone (Abstract): Presented at the Structural styles in the Southern Midcontinent - a workshop; Abstract and Program, Oklahoma Geological Survey.

Thompson, D.T., 1982, EULDPH: A new technique for making computer-assisted depth estimates from magnetic data: Geophysics, **47**, 31-37.

Thorarinsson, F., S.G. Magnusson, and A. Bjornsson 1988, Directional spectral analysis and filtering of geophysical maps: Geophysics, **53**, 1587-1591.

Verduzco, B., D.J. Fairhead., C.M. Green, and C. MacKenzie, 2004, The meter reader - New insight into magnetic derivatives for structural mapping: The Leading Edge, **23**, 116-119.

Wilson, F. W., and P. Berendsen, 1998, The role of recurrent tectonics in the formation of the Nemaha Uplift and Cherokee-Forest City Basins and adjacent structural features in eastern Kansas and Contiguous State, USA (abstract), *in* J. P. Hogan, and M.C. Gilbert, ed., Basement Tectonics 12 Central North America and other regions: Kluwer Academic Publishers, **12**, 301-303.

**Chapter 3: Investigation of linkages between Precambrian basement structure and Paleozoic strata in the Fort Worth Basin, Texas using high-resolution aeromagnetic data and seismic attributes**

Olubunmi O. Elebiju[1], G. Randy Keller[1] and Kurt J. Marfurt[1]

[1]*ConocoPhillips School of Geology and Geophysics, The University of Oklahoma*

E-mail: ooelebiju@ou.edu; grkeller@ou.edu; kmarfurt@ou.edu

Date of Submission: 5th of May, 2009

Paper Presented at the 78th Annual Society of Exploration Geophysicists International Exposition meeting in Las Vegas, Nevada, USA

SEG Expanded Abstracts 27, 844 (2008)

INT 1: Integrated Studies session, on November 11 at 4:25 PM

This paper originally submitted to GEOHPYSIC journal is currently undergoing revision by the author.

Chapter 3: Investigation of linkages between Precambrian basement structure and Paleozoic strata in the Fort Worth Basin, Texas using high-resolution aeromagnetic data and seismic attributes

## 3.1 Abstract

We have integrated high-resolution aeromagnetic (HRAM) data and seismic attributes extracted along the Ellenburger Formation and the top of basement from the north-central portion of the Fort Worth basin (FWB) and found that this approach is effective in deciphering links between Precambrian basement structures and sedimentary structures. In the FWB, induced fracturing is a key part of hydrocarbon exploitation within the Barnett Shale. Therefore, knowledge of the nature of the induced and natural fractures, faults, and collapse features that may form conduits to the underlying Ellenburger aquifer is vital. We employed coherence and curvature seismic attributes, which are sensitive to faults, fractures and collapse features to map these features that have been suggested to be related to Precambrian basement structures. The association of these sedimentary structures with the Precambrian basement makes the understanding of the relationship between these two structures a key part of exploitation programs. To examine possible relationships, we analyzed a series of HRAM derivative maps that were designed to enhance basement structures. This allowed us to compare both individual structures and investigate the links between them. The results show that the sedimentary structures within the study area are mainly related to basement structures because these structures are aligned parallel to anomalies identified on the HRAM data. The northeast-southwest and northwest-southeast orientations of sedimentary features are consistently parallel with Precambrian structural grains that are associated with structures such as the northeast trending Ouachita Orogeny and the northwest trending Muenster Arch, which

reactivated a late Cambrian/Late Precambrian fault. The knowledge gained in this study will impact oil and gas exploration and development within the Fort Worth basin because, the orientation of the natural and induced fractures can be predicted even if seismic data is limited or unavailable.

## 3.2 Introduction

Almost all hydrocarbon production from the Barnett Shale of the Fort Worth basin (Figure 3.1) requires inducing fractures while avoiding natural fractures, faults and karst collapse features that form conduits to the underlying Ellenburger aquifer. These northwest striking natural fractures and the northeast trending present day stress field and induced fractures are sub-parallel to the Muenster Arch, which is a reactivated basement fault, and the northeast trending Ouachita thrust front respectively (Simon, 2005). Imaging the structural and stratigraphic structures or the ability to predict them has been the core objective of seismic programs within the Fort Worth basin (FWB). Some of these structural and stratigraphic features have been linked to the Precambrian basement. Recent efforts by Montgomery et al. (2005), Sullivan et al. (2006), Aktepe et al. (2008), and Elebiju et al. (2008) have suggested that the Precambrian basement structures may be controlling some of the overlying sedimentary features such as the structures within the Ellenburger Formation. Thus, it is important to understand how Precambrian basement structures are linked with geologic structures within the Paleozoic strata.

The existence of links between basement structure, hydrocarbon containers, and structures within the sedimentary section is not a new concept (e.g., Gay, 1995; Wilson and Berendsen, 1998; Plotnikova, 2006; Berger et al., 2008). Such relationships can be seen in the Paradox, Hardeman, Anadarko, Arkoma, Ardmore basins (Thomas and Baars,

1992), and the Williston basins among others (Gerhard and Anderson, 1988). Structures such as fault zone that can influence the formation of sedimentary basins and mineral deposits are often formed by intraplate tectonism (Barosh, 1995) and many of these basement structures are very difficult to determine by seismic.

The objective of this paper is to investigate the use of high-resolution aeromagnetic (HRAM) data and seismic data to map basement and sedimentary structures within the north central part of the FWB. We also explored the link and interaction between these two features. We do believe that in areas where seismic data is limited or unavailable, HRAM data can be used to predict the kinds of intra-sedimentary features that may be present.

This paper presents the results of integrating seismic attributes and enhancement and filtering techniques applied to HRAM data to establish links between Precambrian basement structures and faults in the overlying sedimentary section. The enhancement methods employed were designed to highlight anomalies of potential interest not directly observed in the original.

## 3.3 HRAM Data and Precambrian Basement

HRAM data typically consist of data acquired at flight heights of less than ~800 m, flight line spacing in the range of 145 - 150 m, and a sample spacing of about 15 m along the flight lines with an accuracy on the order of 0.1 nT (Peirce et al., 1998a). The aeromagnetic (e.g. HRAM) method has long been recognized as an effective tool for mapping structures within the Precambrian basement rocks because measured magnetic anomalies usually reflect magnetic susceptibility contrasts within the crystalline basement.

Applications of HRAM surveys in hydrocarbon exploration have significantly increased recently, and this is due to the development of magnetometers that are more accurate, improved aircraft positioning due to availability of high precision global positioning systems (GPS), and advancements in data processing (Magoon and Dow, 1994; Glenn and Badgery 1998; Peirce et al., 1998a; Spaid-Reitz and Eick, 1998). Such improvements can be seen in its application to basement structure mapping (Gibson and Millegan, 1998) and intra-sedimentary structure mapping (Goussev et al., 1998; Peirce et al., 1998; Grauch et al., 2001; Berger et al. (2008).

Many mathematical operations to extract detailed information from magnetic data have also gained wide acceptance in recent years (e.g., Grauch and Cordell, 1987; Tarlowski and Koch, 1988; Verduzco et al., 2004; Nabighian, et al., 2005; Hansen and deRidder, 2006; Salem et al., 2007). Modern processing techniques for aeromagnetic data produce a variety of derivative maps (e.g., tilt-derivative, gradients, and Euler deconvolution depth estimation) that extract important details from the data. Since interpretation of magnetic data is non-unique, interpreting HRAM data calls for an integrated interpretation approach that involves the calibration of data and derivative maps with drilling, gravity, and/or seismic data.

Such integrated approaches have been used in the FWB to establish a link between Precambrian basement structures and sedimentary basin structures and features (Elebiju et al., 2008). Other area where such links have been established include, the Jonah field in the Green River basin, the Doig Sand play in the Horn River basin, and the Bakken play from Williston basin in Canada (Stone, 2008). HRAM surveys are gradually becoming a tool of choice for imaging subtle, deep Precambrian and shallow sedimentary

structures. In these aforementioned basins, the HRAM data and its derivatives were used to image shallow structures and trends not detectable by the seismic data. This methodology has also been used to extend interpretations beyond the limits of existing seismic data coverage. The author believes that, this approach would positively impact how unconventional plays are explored and exploited.

## 3.4 General Tectonic Setting of Study Area

The Fort Worth basin (FWB) is one of the major late Paleozoic foreland basins associated with the Ouachita Orogenic belt located along the southern margin of North America (e.g. Viele, 1989). It is an asymmetric basin whose structural axis is aligned parallel to the east-bounding and advancing Ouachita structural front. The FWB is bounded on the west by the Bend Arch, to the south by the Llano Uplift, and to the north and northwest by basement uplifts of the Muenster and Red River Arches, which were created by the reactivation of Southern Oklahoma aulacogen basement faults during the Ouachita orogeny (Figure 3.1) (Walper, 1982; Kruger and Keller, 1986). Deepening northward, the deepest part of the basin is located at its northeast corner adjacent to the Muenster arch, where the sediment thickness reaches about 3700 m (Montgomery et al., 2005).

Prior to the late Paleozoic orogeny that affected the FWB, the Grenville Orogeny and the Cambrian rifting affected the basement upon which the FWB is deposited (Mosher, 1998). This classic failed rift intersects the early Paleozoic passive continental margin that was stable until Mississippian time when the Ouachita orogeny began (e.g., Thomas, 1989).

The Ouachita orogeny controlled the sedimentary history and structural setting of the FWB. The subsidence and sedimentation from the uplifted Ouachita thrust belt resulted in a westward migration of the depocenter with time and the development of the northeast-trending faulted anticlinal flexure across the Llano uplift (Walper, 1982). These northeast trending features disappear to the northeast, where the FWB intersects the Muenster Arch.

In the FWB region, late Paleozoic – Mississippian movements periodically reactivated a northeast-southwest trending Precambrian structure that was mapped across the Newark East field. This structure, termed the Mineral Wells fault, is important to exploration within the FWB because it controls sediment deposition, oil and gas distribution. Specifically, it prohibits gas accumulation in the Barnett Shale within the Newark East field, where it intercepts closed fractures (Figure 3.1). Other minor structures sub-parallel to the Mineral Wells faults and the Ouachita thrust front have been identified by Montgomery et al. (2005) and Pollastro (2007).

## 3.5 Methodology

The integrated geophysical and geological methodology employed in this study consisted of 3D seismic data analysis that was supplemented by HRAM data analysis. Figures 3.1 and 3.2 show the location of the HRAM and 3D seismic data used for the study. Within the study area of Fort Worth basin, we hypothesized that calibrating HRAM derivative images and HRAM Euler deconvolution results with scattered 3D seismic surveys would provide a means to accurately map and study the relationships between the basement structures and the overlying sedimentary structures in areas where seismic data are sparse.

### 3.5.1 HRAM and seismic data

Devon Energy, as part of their Barnett Shale exploitation program, acquired the seismic data used for this study. Pearson, deRidder and Johnson, Inc. on behalf of Mitchell Energy (Devon's Predecessor) acquired the HRAM data during January and February of 2000. The HRAM survey was flown at 152 m ground clearance, with an east-west profile separation of 402 m tied by north-south lines spaced at 805 m. Corrections applied to the HRAM data by Pearson, deRidder and Johnson, Inc. included removing the International Geomagnetic Reference Field (IGRF), leveling, and diurnal correction. Cultural noise was also removed.

*Seismic data*

Conventional workflows for most seismic interpreters involve the integration of lower vertical resolution but denser areal coverage seismic data with higher vertical resolution, but aerially sparse production, well log, and geologic outcrop data. By design, structural and stratigraphic features in the sedimentary column can be accurately mapped using seismic reflection data and seismic attributes. However, mapping Precambrian features using seismic reflection can often be a difficult task because reflections from the Precambrian basement are laterally discontinuous due to heterogeneities within the basement and poor signal strength. Wells that penetrate the Precambrian are also very limited. Therefore, potential field data can be used effectively to delineate Precambrian structures even with its lower spatial resolution.

We adopted a conventional seismic interpretation workflow to interpret sedimentary structures using seismic data and seismic attributes. The seismic attributes were generated in-house, and we extracted the desired attributes along the Ellenburger

horizons and the top of basement. We found the coherence and the most-negative curvature attributes to be very useful. Hakami et al. (2004), Sullivan et al. (2006), and Aktepe et al. (2008) have effectively utilized these kinds of attributes to study the various sedimentary features within the FWB. The physical and geometrical features in these attributes use models of dip and azimuth, amplitude, frequency content, and waveform similarity from adjacent seismic samples (Chopra and Marfurt, 2007).

Coherence is a measure of seismic waveform or trace similarities. This attribute is sensitive to lateral changes in the physical models mentioned above, and their lateral sensitivity makes them suitable to map features like faults (see Lawrence, 1998; Gersztenkorn et al., 1999) and fractures (Neves et al., 2004) effectively.

Curvature is a measure of the deviation from a planar geometry based on a calculated quadratic surface derived in three dimensions (Chopra and Marfurt, 2007). Most-negative curvature measures synclinal reflector shapes and this attribute is effective in mapping subtle lineament within fault blocks (Blumentritt et al., 2006) karst features, fractures, and faults that appears as bowls or synclines on a carbonate surface such as the Ellenburger Formation (Akpete et al., 2008).

### 3.5.2 HRAM data and derivative maps

We resampled the HRAM grid to 400 m grid spacing using a minimum curvature algorithm available in a commercial gravity and magnetic processing and interpretation software package. This grid spacing is appropriate for selecting a window size for our Euler deconvolution depth estimation. For example, an anomaly with a width length of 10000 m on a data that has a grid spacing of 400 m will require a window size of 25.

However, if a larger anomaly is the target, then the grid spacing will have to be increased (Phillips, 2007).

Before any interpretation was done on the HRAM data, the data was reduced-to-the pole (RTP) in order to remove magnetic anomaly distortion caused by varying magnetization inclination and azimuth (Kis, 1990).

To highlight local anomalies, we generated a residual total magnetic intensity (TMI) map (Figure 3.2a) by subtracting a grid values calculated by upward continuing the original RTP HRAM to 5 km that represents regional anomalies (Figure 3.2b) from the original RTP HRAM grid. Several upward continuation height (i.e., 1 km, 10 km, e.t.c.) a generated and evaluated before we choose the height that best represent the regional anomaly.

To highlight lateral or abrupt changes in magnetization, that can suggest faults or source contacts, we computed the horizontal gradient magnitude (HGM) and horizontal derivative of the tilt derivative from the HRAM data. These derivatives (Figure 3.3), are edge-detecting derivatives that enhance lateral discontinuities in a TMI grid (Grauch and Cordell, 1987; Roest et al., 1992; Miller and Singh, 1994; Blakely, 1996; Verduzco et al., 2004; Li, 2006). The interpreter still has a responsibility of providing geological meaningful interpretation of what is seen on these maps.

We also attempted to estimate the depth to the top of the Precambrian basement from the HRAM data. Depth estimates from the Euler deconvolution can be transferred to areas where seismic data are unavailable or limited to provide an indirect knowledge of overlying sediment thickness (Li, 2003).

We attempted to use the results of Euler deconvolution to delineate magnetic anomaly source type and fault trends (Reid et al., 1990). The Euler deconvolution method is an automated depth estimation method (Thompson, 1982) that can help determine the location or depth to the shallowest or deepest reasonable magnetic source or edges for various geological sources such as, dikes, faults, magnetic contacts, and extrusives (Phillips, 2007). It utilizes the structural index N, which is used to describe the geometry of the desired geologic structure, as a geological constraint (Reid et al., 1990; Barbosa et al., 1999).

## 3.6 Integrated Analysis and Integrated Interpretation

### 3.6.1 Seismic Survey A

Our integrated analysis and interpretation commenced in areas where seismic and HRAM data were both available (Figure 3.2). In Seismic Survey A, 3D visualization view of the coherence horizon slice extracted over the Ellenburger horizon and a north-south seismic section view shows two major faults systems (orange and blue arrows) (Figure 3.2a). These faults that trends east-west and northeast-southwest agree with the interpretation of Sullivan et al. (2006). These two features were interpreted as a wrench fault (blue arrows) and a possible strike-slip fault (orange arrows) that penetrate the Precambrian basement. Wrench fault is a type of basement-involved strike-slip with near-vertical fault surface. Circular collapse features (few location of collapse features indicated by yellow arrows) seen on the coherence horizon slice shows orthogonal northeast and northwest orientation (red-dashed lines in Figure 3.2a). The circular collapse features that are often associated with cockpit karst and karst collapse features

shows well on the most-negative curvature attribute. The most-negative curvature attribute enhances features with a bowl or valley shape usually exhibited by the collapse features. Faults interpreted in Figure 3.2a are also seen on the most-negative curvature (Figure 3.2b).

In an effort to compare structures seen within the sedimentary section via seismic attributes with Precambrian basement structures, we generated series of derivative magnetic maps. Within the area occupied by Seismic Survey A, the horizontal gradient magnitude and the horizontal derivative of the tilt derivative anomaly map generated from the HRAM data (Verduzco et al., 2004) show lineament trends that are parallel to the wrench fault interpreted from the seismic data. The anomalies marked with blue arrows strike northeast-southwest and black arrows mark anomalies with northwest-southeast trends (Figure 3.4). Termination of northwest trending anomaly marked by a black arrow along the east-west trending fault is the only indication of the east-west fault that we can see on the derivative maps of Figure 3.4 (See Figure 3.6a).

The result of the Euler deconvolution computation using N of 1 (Figure 3.5a) and 0 (Figure 3.5b) should be effective in delineating low-displacement and large-displacement faults respectively (Reid et al., 1990). Within the area of Seismic Survey A, we noticed linear clustering of depth solutions that trend northeast and northwest (Figure 3.6b). Lineament indicated by the blue arrow is consistent in orientation with what was observed in the seismic attribute data (Figure 3).

The collapse features and faults indentified within the sedimentary section of Seismic Survey A generally display a northeast and northwest trend. The strike-slip fault located at the southeast corner of Seismic Survey A correlates with a derivative anomaly

that is also parallel to the northeast trending anomalies located about 25 km east of Seismic Survey A (Figure 4.4). Based on our workflow, we predict that a northeast trending fault will be present within the sedimentary section above these anomalies. Although, the seismic data for that location is not available for this study, however, a northeast trending basement penetrating sedimentary fault termed the Mineral Wells fault (Montgomery et al., 2005) has been interpreted at this location (Roderick, P., E. Baruch, and O.O. Elebiju, 2009, per comm.). Thus, this interpretation suggests that HRAM can also be used to predict sedimentary features where seismic data is unavailable or limited.

### 3.6.2. Area of Seismic Survey B

Seismic Survey B (Figure 3.7) shows more diverse lineaments orientation than survey A. We identified three lineaments on the coherence and most negative curvature horizon slices at the Ellenburger horizon. Two orthogonal lineaments trend northeast (blue arrows) and northwest (black arrows) in addition to an east-west (orange arrow) lineament (Figure 3.7). Circular collapse features were also indentified (yellow arrow). However, we did not notice any preferred orientation of these circular features. We suggest that the three lineaments we identified are faults that penetrate the Precambrian basement (See Figure 3.8).

A rose diagram plot was derived from manually picking the trends of anomalies on the horizontal gradient magnitude map and we identify anomalies with orientations similar to fault orientations interpreted from seismic data in Figure 3.7 (Figure 3.9a). Similarly, the linear clustering of Euler depth solutions are parallel to fault interpreted on seismic data (Figure 3.9b). These similarities in orientations between sedimentary and

Precambrian basement structures are common to both survey areas (Figures 3.6a and 3.9a).

Based on the analysis of all the available datasets, we indentified three trends of lineaments within the study area. The lineaments within the sedimentary section strike northeast, northwest and an east-west. Precambrian basement lineaments are predominantly northeasterly and northwesterly.

We relate the northeast-southwest trending sedimentary faults to the current maximum stress (Soebrits et al., 2000). The Mineral-Wells fault system and induced fractures have been documented to be associated with the northeast trending present day stress (Simon, 2005). Regionally, the northeast trend of these structures is also similar to the northeast trending Paleozoic Ouachita orogenic belt located east of the study area.

Similarly, the northeast-southwest directed Ouachita orogenic compression controlled the depositional history and the types of structures found within the FWB. For example, northeast trending normal faults and anticlinal flexures of Atokan age that offset the basement developed across the exposed Llano uplift, which is located south of the FWB. According to Ewing (1991), these northeast trending features disappear to the northeast toward the Muenster Arch.

In contrast, the natural fractures have orientations parallel to the northwest trending lineaments that are parallel to the Muenster Arch fault, which is a reactivated basement fault. Another lineament study conducted east of the FWB near the Ouachita thrust front subcrop, indicates that faults and surface lineaments trends are sub-parallel to the Ouachita basement structural grain (see Caran et al., 1981). Pre-existing basement faults associated with formation of the Cambrian rifted southern edge of the North

American craton may be related to both the Muenster Arch and the Ouachita thrust (Hale-Erlich and Coleman, 1993). Thus, these lineaments within the study area are suggested to be mimicking the zones of weakness within the basement that may have formed during the reactivation and propagation of these structures through the sedimentary section. On a regional scale, strains generally are related to deep crustal movements during reactivation and may be directly expressed as faults and shear zones in the overlying sedimentary cover (Jauques, 2003).

The structures identified within the sedimentary section in this study are suggested to be related to the basement structures because lineaments indentified with the aid of a seismic attributes are aligned parallel to basement features indentified with the aid of HRAM data.

## 3.7 Conclusions

Our integration of seismic data that is effective in mapping sedimentary structures with high-resolution aeromagnetic data that is effective in mapping Precambrian basement structures was used to compare the interaction and links between Precambrian and sedimentary structures within the northern part of the Fort Worth basin. Sedimentary features such as faults and collapse features mapped on seismic attribute display orientations that are parallel with trends of anomalies displayed on the HRAM data. The northeast-southwest and northwest-southeast orientation of these features are consistently parallel with Precambrian structural grains that form structures such as the northeast trending Ouachita orogenic belt and the northwest trending Muenster Arch, which is a reactivated Precambrian fault. We suggest that propagation of the Precambrian structural

grain through the sedimentary section via zones of weakness is responsible for creating the linear sedimentary features that we interpreted as fault in the seismic data

Based on the analysis of the HRAM data we can predict the occurrence of the northeast fault systems that occur beneath the Mineral Wells even if seismic data is unavailable. We confirm this prediction with an independent seismic study, which identified a northeast trending fault system that is part of the Mineral Wells fault. This is a classic example of how the integration of HRAM data and seismic data can help for reconnaissance purposes where seismic data is unavailable or limited. This can improve or extend hydrocarbon exploration objectives in frontier areas before an expensive seismic survey is undertaken. In frontiers areas where seismic data is limited, HRAM data can be cheaply used to expand on the structures interpreted on the seismic data. Acquisition of HRAM data is also relatively faster than seismic data, thus exploration cycle-time can be significantly reduced.

Our results have shown that that the integration of derivative images from high resolution aeromagnetic data with scattered 3D seismic surveys can provide a means of effectively mapping basement features and establishing a links between the basement and sedimentary structures within the north central part of the FWB. The knowledge gained here will positively impact oil and gas exploration and development within the study area because the orientation of the natural and induced fractures can be predicted even if seismic data is limited or unavailable.

## 3.8 Acknowledgments

Thanks to Devon Energy for providing us with the high-resolution aeromagnetic (HRAM) data, the 3D-seismic data, and most of all, the encouragement to pursue this

study. The regional gravity and magnetic data were obtained from an online community database maintained at the University of Texas at El Paso (http://research.utep.edu/paces).

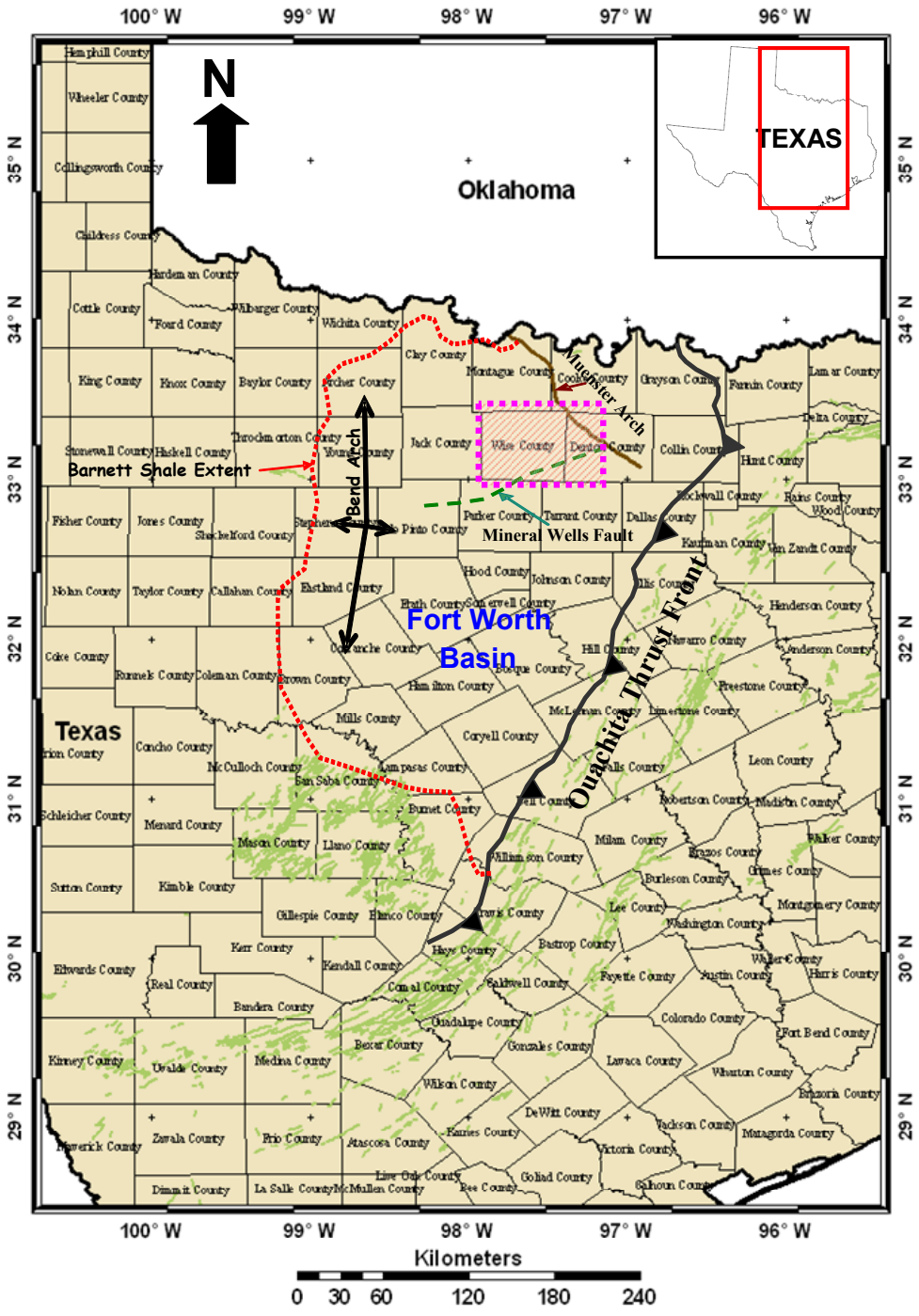


Figure 3.1. Map showing the Fort Worth Basin province and its major surrounding structural features (e.g., Mineral Wells fault, Bend Arch, Muenster Arch, etc). The thick shaded magenta-dash rectangle shows the location of the seismic and high-resolution aeromagnetic (HRAM) data used for part of this study. (Adapted after Pollastro et al., 2007).

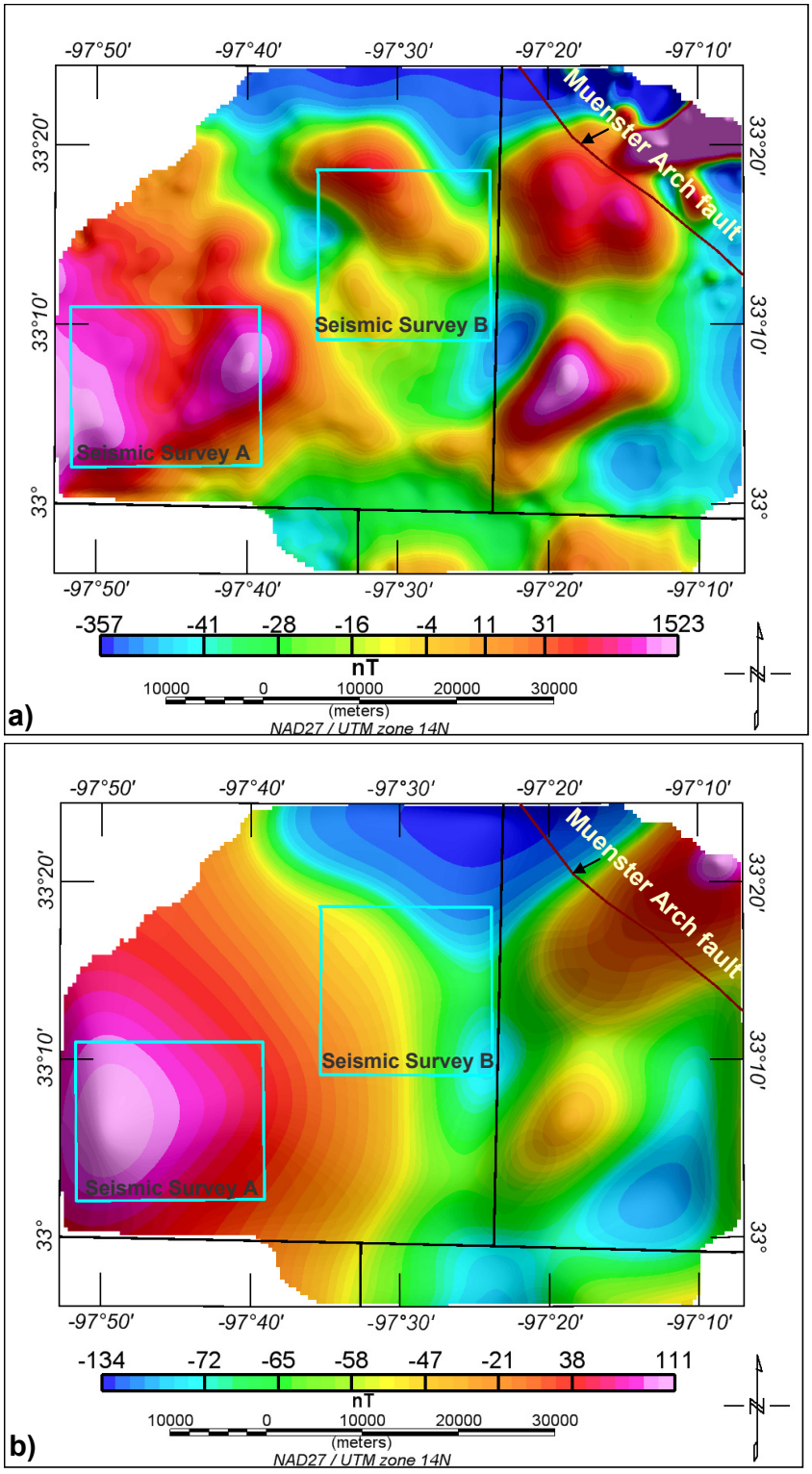


Figure 3.2. a) Reduced-to-pole (RTP) residual total magnetic intensity map (TMI) generated by subtracting 5 km upward continuation grid from TMI grid. Square cyan boxes shows the location of the seismic data used in this study. b) Map showing the 5 km upward continuation grid that was subtracted from the original TMI map to produce the RTP map shown in Figure 3.2a. Broad anomalies are related to deep regional features that masked the more local crustal features that are enhanced on the residual RTP map.

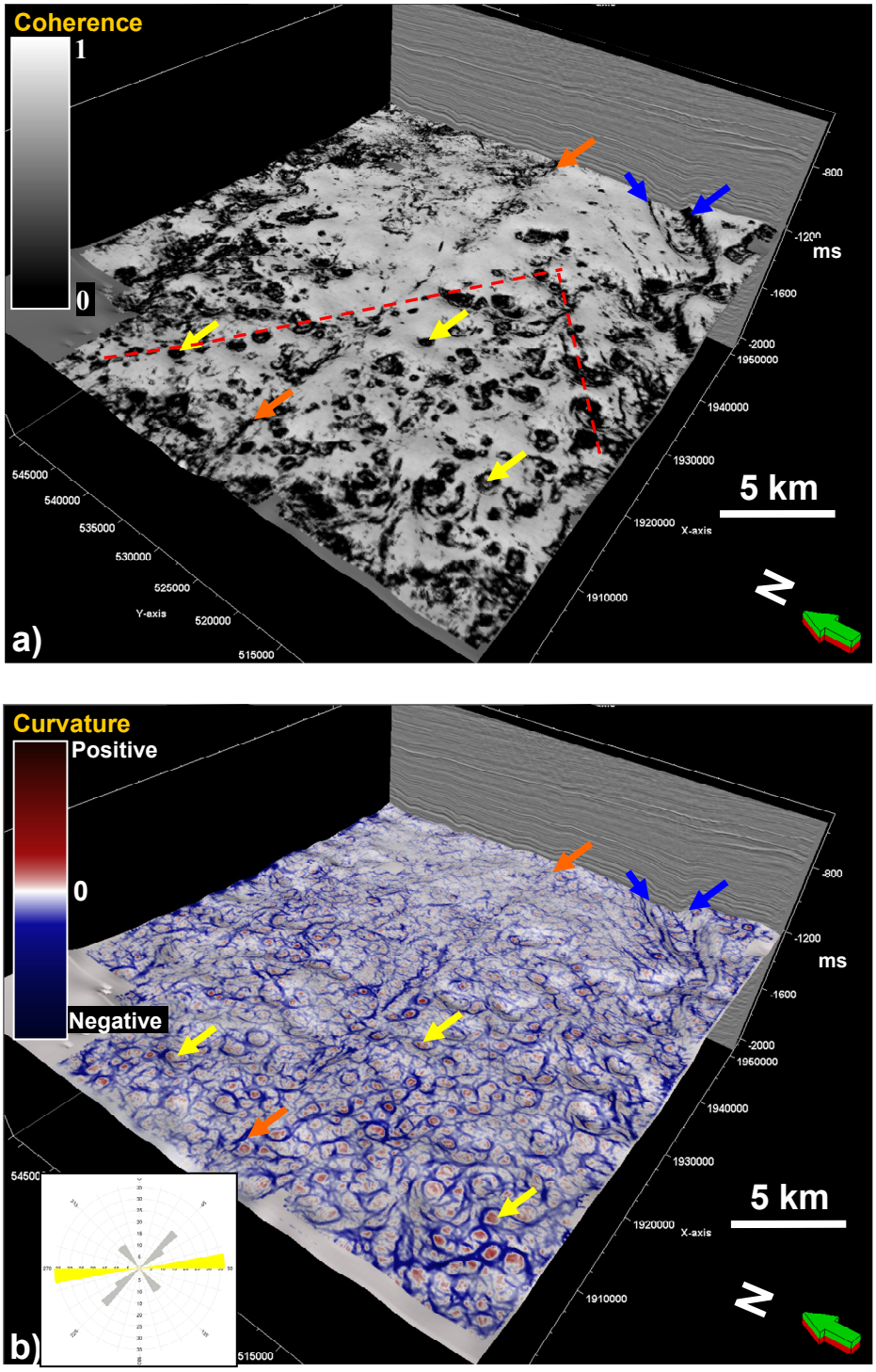


Figure 3.3. a) Coherence and b) Most-negative curvature horizon slices extracted at the Ellenburger formation level through seismic survey A. On the top horizon slice, the orange arrows (east-west lineaments) and blue arrows (northeast lineaments) are the major faults and strike-slip faults respectively that is consistent with Hakami et al. (2004) and Sullivan et al., (2006) interpretations. Yellow arrow and red-dash lines show the collapse features that is also strikes northeasterly and northwesterly. Inset rose diagram shows the trend of major lineaments mapped manually on the Ellenburger Formation surface.

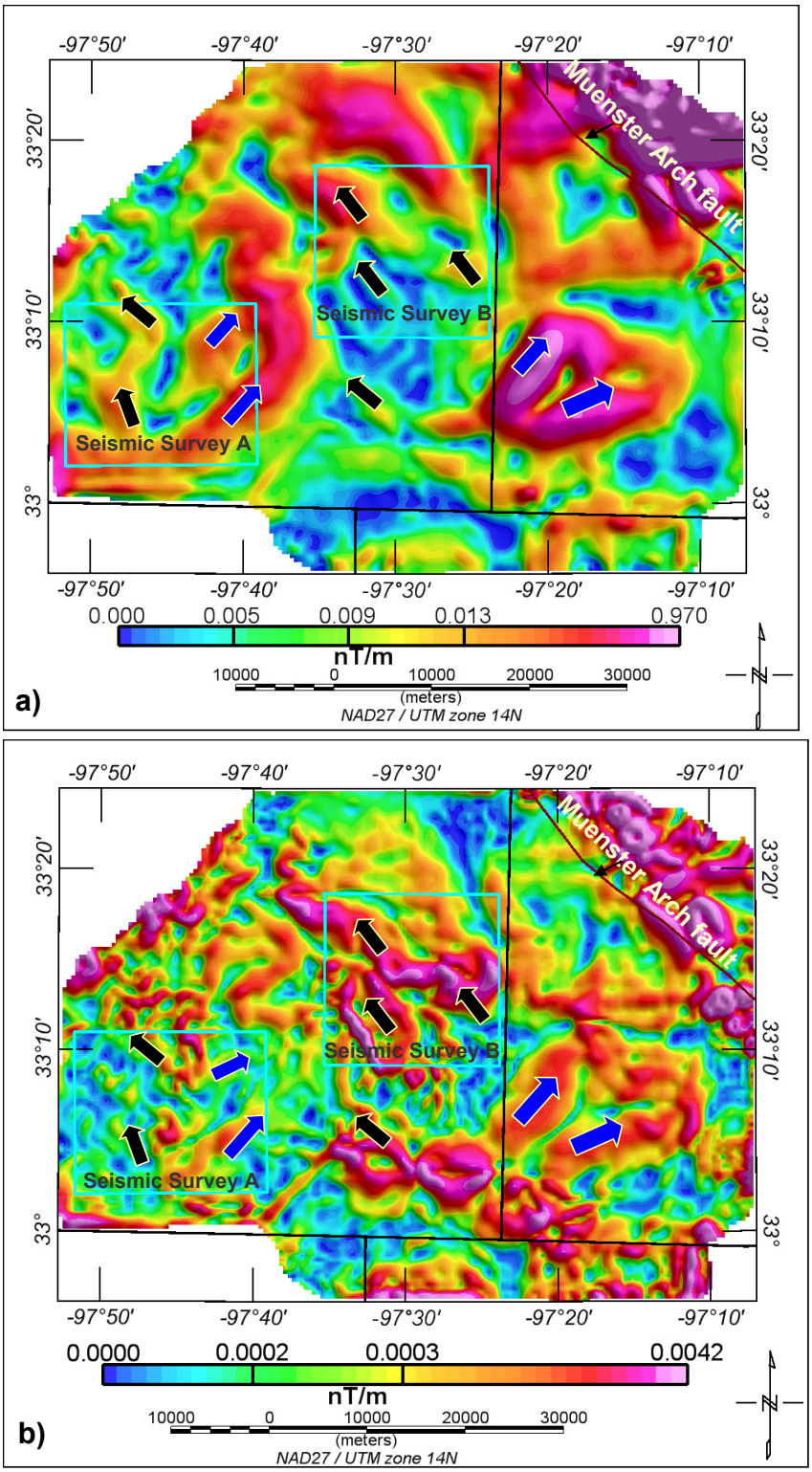


Figure 3.4. a) Horizontal gradient magnitude (HGM) of the TMI anomaly map shows where maxima are location of magnetic source edges. b) Total horizontal derivative of the tilt derivative lineaments orientations discussed in the text. The blue arrows located on the southeast section of the map was used independently to predict the kinds of intra-sedimentary structure to expect over that area.

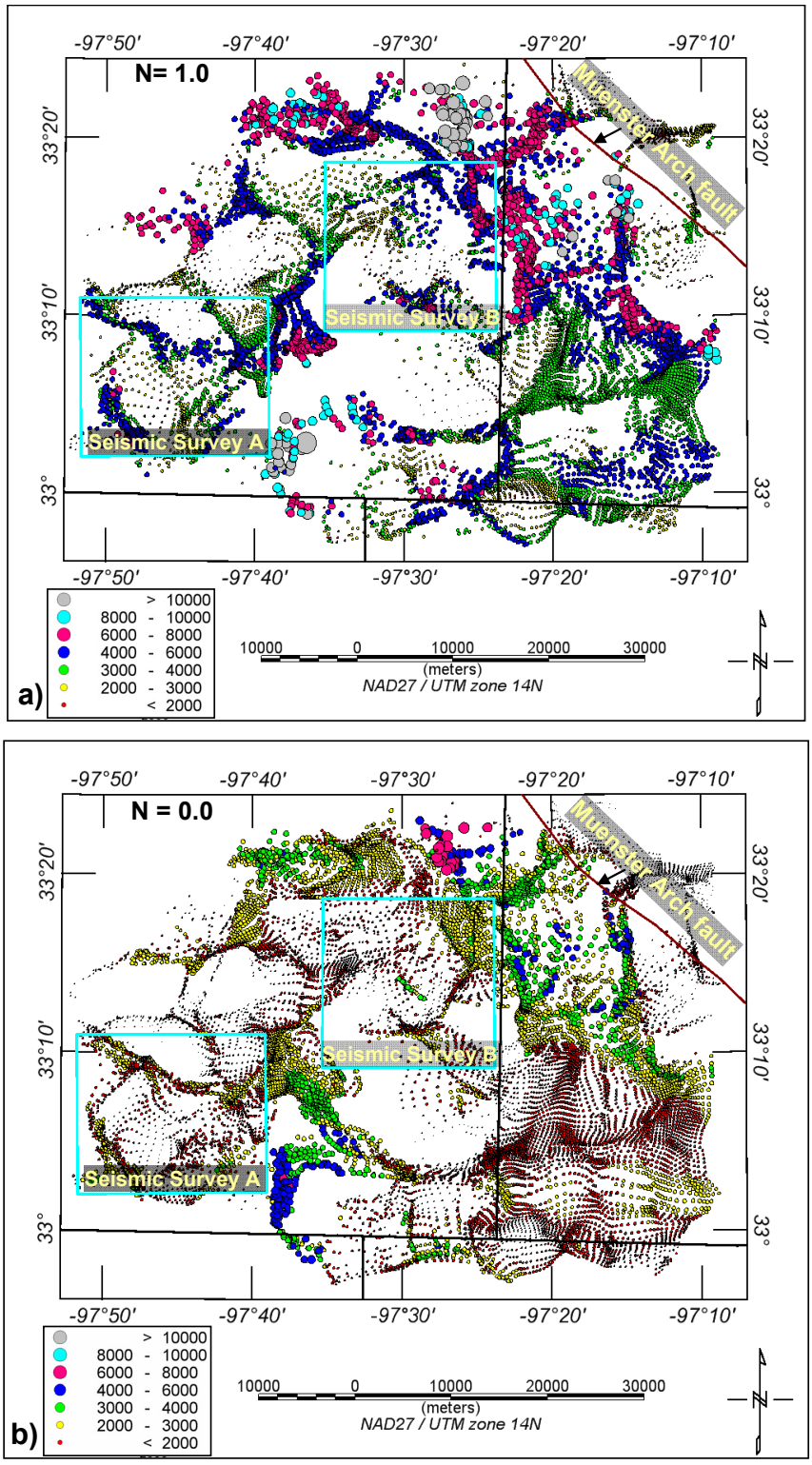


Figure 3.5. Euler deconvolution cluster plots computed using a structural index (N) of (a) 1.0 and (b) 0.0 are effective for delineating low-displacement faults and large-displacement faults, respectively

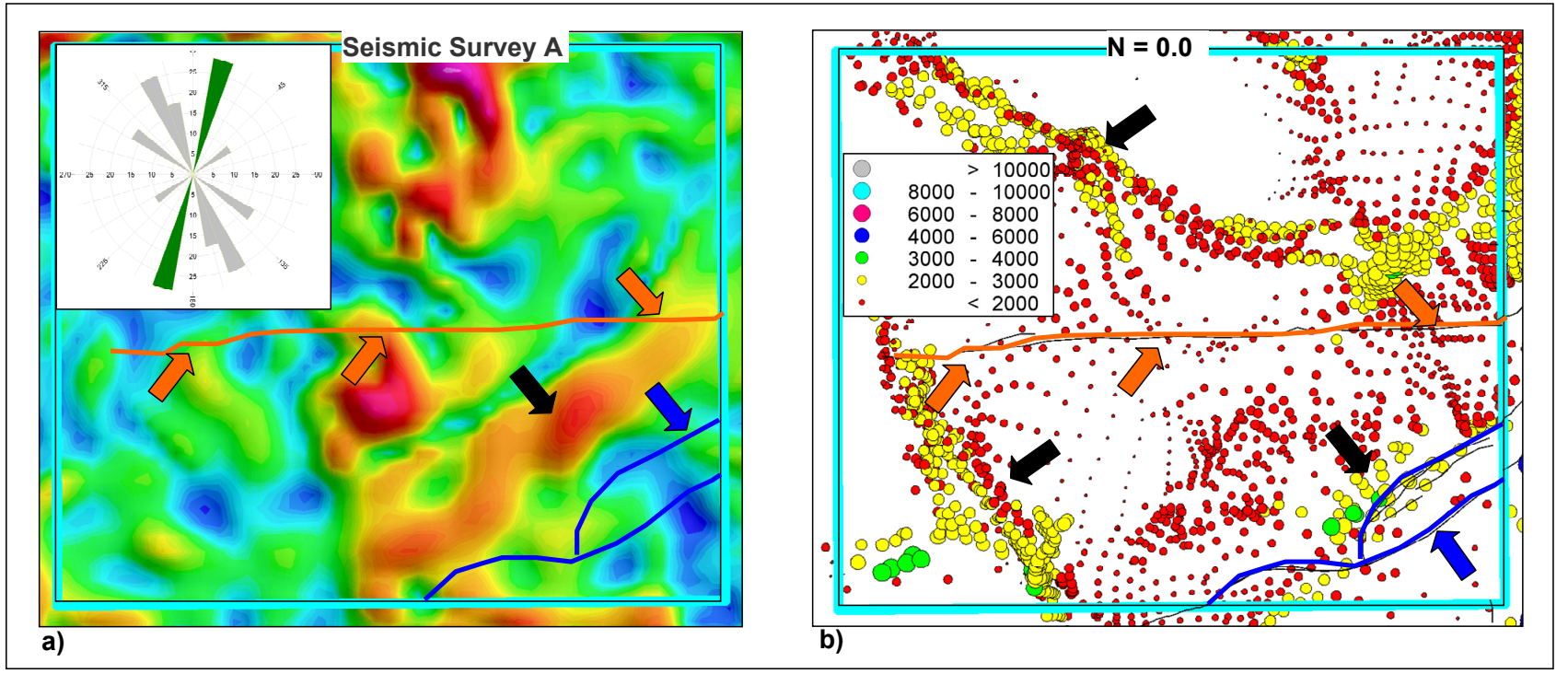


Figure 3.6 Zoomed-in section of (a) the horizontal gradient magnitude and b) the Euler deconvolution cluster plot with structural index of 0.0 from seismic survey A. Blue and orange lines are interpretation from seismic. The northeast faults (northeast black-arrow) appear parallel to linear trend from the Euler deconvolution estimation, which are reflecting basement structures. Inset rose diagram shows the trend of major lineaments mapped manually on the horizontal gradient magnitude map.

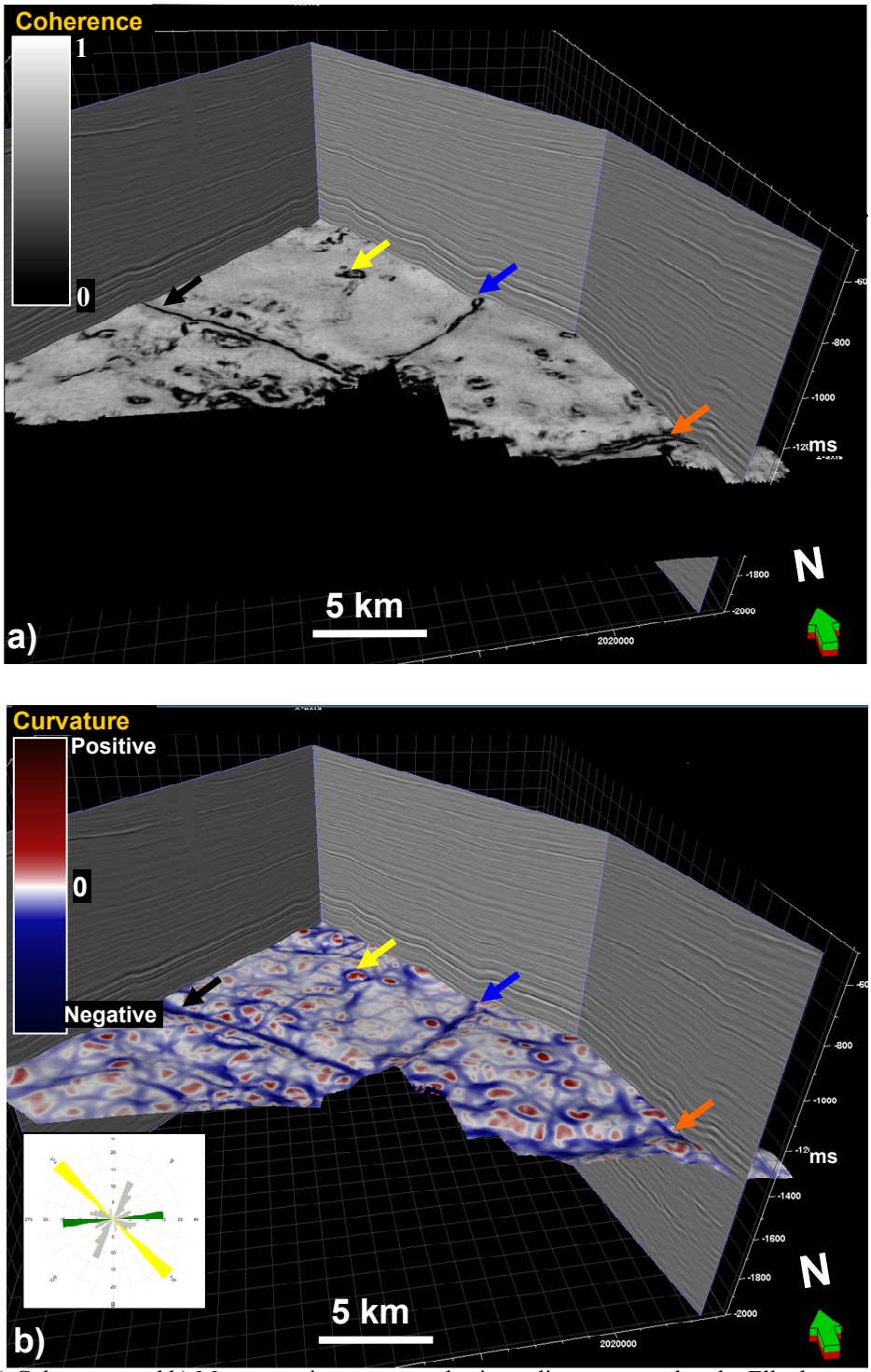


Figure 3.7. a) Coherence and b) Most-negative curvature horizon slices extracted at the Ellenburger formation level through seismic survey B. The orange arrows (east-west lineaments), blue arrows (northeast lineaments), and black arrows (northwest lineaments), are the major faults interpreted. Yellow arrow shows the collapse features. The northeast and northwest striking faults are parallel to the northeast striking present day stress field, the northeast trending Ouachita thrust front and the northwest trending Muenster Arch respectively. Inset rose diagram shows the trend of major lineaments mapped manually on the Ellenburger Formation surface.

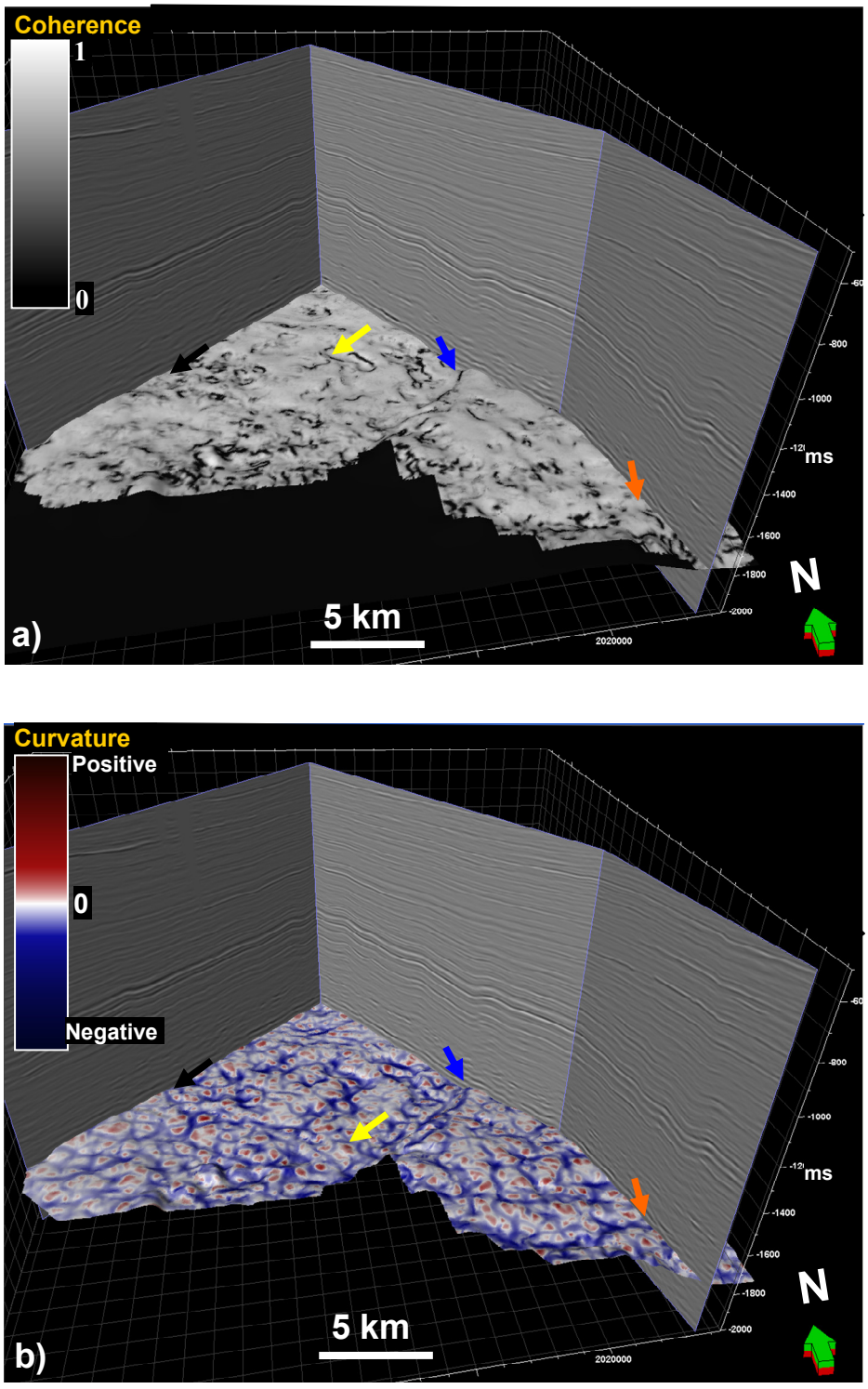


Figure 3.8. a) Coherence and b) Most-negative curvature horizon slices extracted near the top of basement surface through seismic survey B. Intra-sedimentary structures appears to penetrate the Precambrian basement.

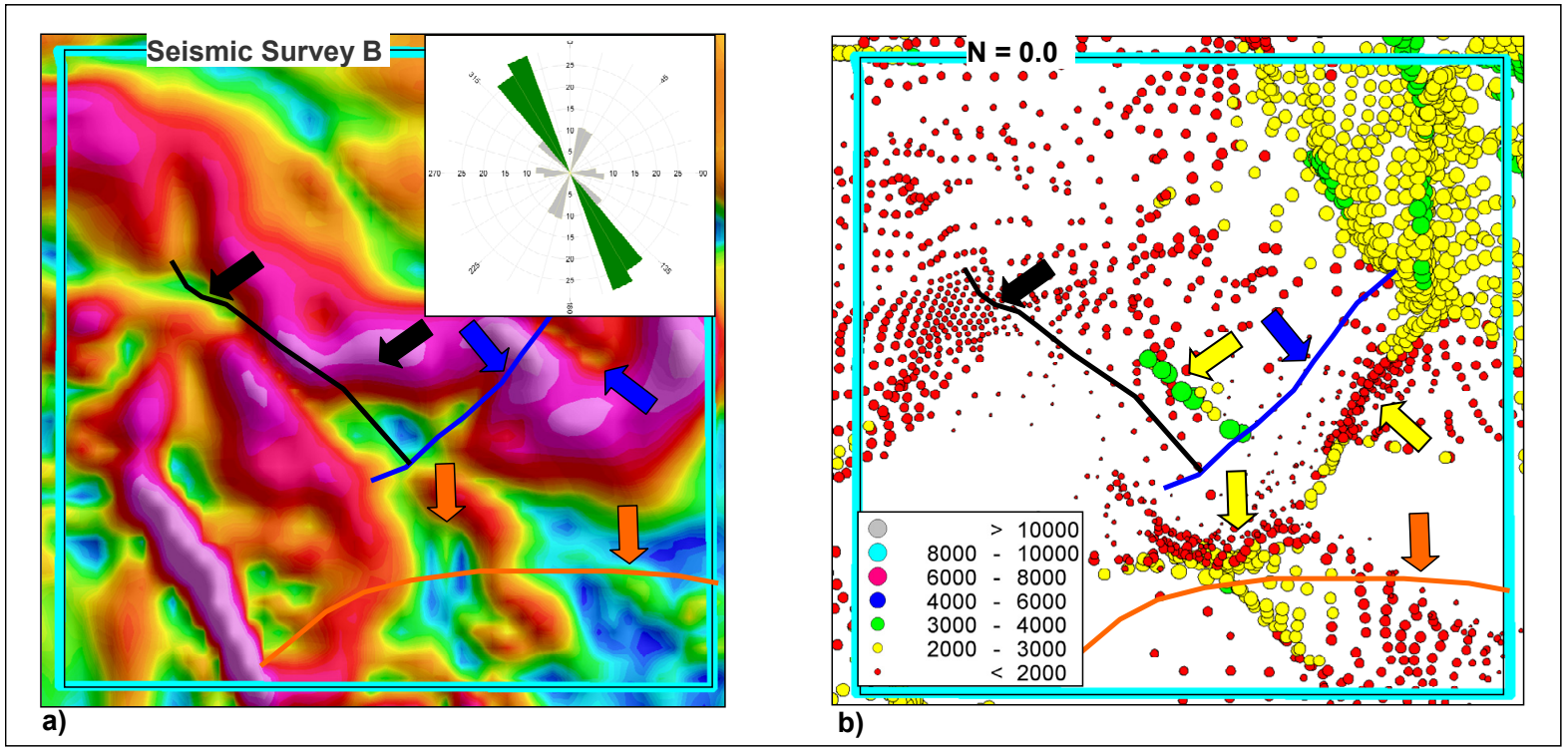


Figure 3.9. Zoomed-in section of (a) the horizontal gradient magnitude and b) the Euler deconvolution cluster plot with SI of 0.0 from seismic survey B. Blue, orange, and black lines are interpretation from seismic. The northeast, northwest, and east-west faults appear parallel to linear trend from the Euler deconvolution estimation, which are reflecting basement structures. Inset rose diagram shows the trend of major lineaments mapped manually on the horizontal gradient magnitude map.

## 3.9 References


Aktepe, S., K. J. Marfurt, and R. Perez, 2008, Attribute expression of basement faulting - Time versus depth migration: The Leading Edge, **27**, 360-367.

Barbosa, V. C. F., J.B.C. Silva, and W.E. Medeiros, 1999, Stability analysis and improvement of structural index estimation in Euler deconvolution: Geophysics, **64**, 48-60.

Barosh, P. J., 1995, A brief history of basement tectonics and the international basement tectonics conferences, *in* R. W. Ojakangas, A.B. Dickas, and J.C. Green, ed., Basement Tectonic **10**: Kluwer Academic Publisher, xvii-xxi.

Berger, Z., M. Boast, and M. Mushayandebvu, 2008, The contribution of integrated HRAM studies to exploration and exploitation of unconventional plays in North America: Reservoir, **35**, 42-48.

Blakely, R. J., 1996, Potential theory in gravity and magnetic applications: Cambridge University Press.

Blumentritt, C. H., K.J. Marfurt, and E.C. Sullivan, 2006, Volume-based curvature computations illuminate fracture orientations - Early to mid-Paleozoic, Central Basin Platform, west Texas: Geophysics, **71**, B159-B166.

Caran, S. C., C.M. Woodruff, and E.J. Thompson, 1981, Lineament analysis and inference of geologic structure - Examples from the Balcones/Ouachita trend of Texas: Transactions - Gulf Coast Association of Geological Societies, **XXXI**, 59-69.

Chopra, S., and K.J. Marfurt, 2005, Seismic attributes - A historical perspective: Geophysics, **70**, 3SO-28SO.

Chopra, S., and K.J. Marfurt, 2007, Seismic Attributes for Prospect Identification and Reservoir Characterization, *in* S. J. Hills, ed., Society of Exploration Geophysicists Geophysical Development Series No. **11**.

Elebiju, O. O., G.R. Keller, and K.J. Marfurt, 2008, New Structural mapping of basement features in Fort Worth Basin, Texas, using high-resolution aeromagnetic derivatives and Euler depth estimates: 78th Annual international meeting, SEG, Expanded Abstracts, **27**, 844.

Ewing, T. E., 1991, The tectonic framework of Texas: Text to accompany " The Tectonic Map of Texas": Bureau of Economic Geology - The University of Texas at Austin.

Flawn, P. T., A. Goldstein, Jr., P.B. King, and C.E. Weaver, 1961, The Ouachita system: University of Texas: Bureau of Economic Geology Report **6120**.

Gay Jr., S. P., 1995, The basement fault block pattern: its importance in petroleum exploaration, and its delineation with residual aeromagnetic techniques, *in* R. W. Ojakangas, A.B. Dickas, and J.C. Green, ed., Basement Tectonics **10**: Kluwer Academic Publisher, 159-207.

Gerhard, L. C., and S.B. Anderson, 1988, Geology of the Williston Basin (United States portion), *in* L. L. Sloss, ed., Sedimentary cover - North American Craton, U.S.: Boulder, Geological Society of America, The Geology of North America, **D-2**, 221-241.

Gersztenkorn, A., J.A. Sharp, and K.J. Marfurt, 1999, Delineation of tectonic features offshore Trinidad using 3D seismic coherence: The Leading Edge, **18**, 1000-1008.

Gibson, R. I., and P.S. Millegan, 1998, Geologic applications of gravity and magnetics: Case history: Society of Exploration Geophysicists - Geophysical References Series, No. **8**.

Glenn, W. E., and R.A. Badgery, 1998, High resolution aeromagnetic surveys for hydrocarbon exploration: Prospect scale interpretation: Canadian Journal of Exploration Geophysics, **34**, 97-102.

Goussev, S. A., R. A. Charters, H. H. Hassan, J. W. Peirce, and J. A. Genereux, 1998, HRAM fault interpretation using MAGPROBE depth estimates and non-traditional filtering: Canadian Journal of Exploration Geophysics, **34**, 30-39.

Grauch, V. J. S., and L. Cordell, 1987, Limitation of determining density or magnetic boundaries from the horizontal gradient of gravity or pseudogravity data: Geophysics, **52**, 118-121.

Grauch, V. J. S., M.R. Hudson, and S.A. Minor, 2001, Aeromagnetic expression of faults that offset basin fill, Albuquerque basin, New Mexico: Geophysics, **66**, 707-720.

Hakami, A. M., K.J. Marfurt, and S. Al-Dossary, 2004, Curvature attributes and seismic interpretation: Case study from Fort Worth Basin, Texas, USA: 74th Annual international meeting, SEG, Expanded Abstracts, **23**, 554.

Hale-Erlich, W. S., and J.L. Coleman, 1993, Ouachita-Appalachian juncture:a paleozoic transpressional zone in the southeastern USA: American Association of Petroleum Geologist Bulletin, **77**, 552-568.

Hansen, R. O., and E. deRidder, 2006, Linear feature analysis for aeromagnetic data: Geophysics, **71**, L61-L67.

Henry, J. D., 1982, Stratigraphy of the Barnett Shale (Mississippian) and associated reefs in the northern Fort Worth Basin, *in* C. A. Martin, ed., Petroleum geology of the Forth Worth Basin and Bend arch area: Dallas Geological Society, 157-178.

Jacques, J. M., 2003a, A tectonostratigraphic synthesis of the Sub-Andean basins: implications for the geotectonic segmentation of the Andean Belt: Journal of the Geological Society of London, **160**, 687-701.

Keller, G. R., J. M. Kruger, K. J. Smith, and W. M. Voight, 1989, The Ouachita system: A geophysical overview, *in* R. D. Hatcher, W. A. Thomas, and G. W. Viele, ed., The Appalachian-Ouachita Orogeny in the United States: Boulder, Colorado, Geological Society of America, The Geology of North America: Geological Society of America, **F-2**, 689-694.

Keller, G. R., and R.A. Stephenson, 2007, The Southern Oklahoma and Dniepr-Donets aulacogens: A comparative analysis, *in* R. D. J. Hatcher, M.P. Carlson, J.H. McBride, J.R. Martinez Catalan, ed., 4-D framework of continental crust: Geological Society of America, Memoir **200**, 127-143.

Kis, K. I., 1990, Transfer properties of the reduction of magnetic anomalies to the pole and to the equator: Geophysics, **55**, 1141-1147.

Lawrence, P., 1998, Seismic attributes in the characterization of small-scale reservoir faults in Abqaid field: The Leading Edge, **17**, 521-525.

Li, X., 2003, On the use of different methods for estimating magnetic depth: The Leading Edge, **22**, 1090-1099.

Li, X., 2006, Understanding 3D analytical signal amplitude: Geophysics, **71**, L13-L16.
Magoon, L. B., and W.G. Dow, 1994, The petroleum system, *in* L. B. Magoon, and W.G. Dow, ed., The petroleum system - from source to trap, **60**, 3-24.

McNaughton, D. A., 1953, Diltancy in migration and accumulation of oil in metamorphic rocks: AAPG Bulletin, **37**, 217-231.

Montgomery, S. L., D.M. Jarvie, K.A. Bowker, and R.M. Pollastro, 2005, Mississippian Barnett Shale, Fort Worth basin, north-central Texas: Gas shale play with multi-trillion cubic foot potential: American Association of Petroleum Geologist Bulletin, **89**, 155-175.

Mosher, S., 1998, Tectonic evolution of the southern Laurentian Grenville orogenic belt: Geological Society of America Bulletin, **110**, 1357-1375.

Nabighian, M. N., 1972, The Analytical Signal of two-dimensional magnetic bodies with polygonal cross-section: Its properties and use for automated anomaly interpretation: Geophysics, **37**, 507-517.

Nabighian, M. N., 1984, Toward a three-dimensional automated interpretation of potential field data via generalized Hilbert Transforms: Fundamental relations: Geophysics, **49**, 780-786.

Nabighian, M. N., V.J.S. Grauch, R.O. Hansen, T.R. LaFehr, Y. Li, J.W. Peirce, J.D. Phillips, and M.E. Ruder, 2005, The historical development of the magnetic methods in exploration: Geophysics, **70**, 33ND-61ND.

Neves, F., M.S. Zahrani, and S.W. Bremkamp, 2004, Detection of potential fractures and small faults using seismic attributes: The Leading Edge, **23**, 903-908.

Peirce, J. W., S. A. Goussev, R. A. Charters, H. J. Abercrombie, and G. R. DePaoli, 1998, Intra-sedimentary magnetization by vertical fluid flow and exotic geochemistry: The Leading Edge, **17**, 89-92.

Peirce, J. W., W.E. Glenn, and K.C. Brown, 1998a, High resolution aeromagnetic for hydrocarbon exploration - Special Issue: Presented at the Canadian Society of Exploration Geophysicists (CSEG) Forum.

Phillips, J. D., 2007, Geosoft executables (GX's) developed by the U.S. Geological Survey, version 2.0 with notes on GX development from Fortran code: U.S. Department of Interior, U.S. Geological Survey.

Plotnikova, I. N., 2006, Nonconventional hydrocarbon targets in the crystalline basement, and the problem of recent replenishment of hydrocarbon reserves: Journal of Geochemical Exploration, **89**, 335-338.

Pollastro, R. M., D.M. Jarvie, R.J. Hill, and C.W. Adams, 2007, Geologic framework of the Mississippian Barnett Shale, Barnett-Paleozoic total petroluem system, Bend arch-Fort Worth Basin, Texas: American Association of Petroleum Geologist Bulletin, **91**, 405 - 436.

Reid, A. B., J.M. Allsop, H. Granser, A.J. Millett, and I.W. Somerton, 1990, Magnetic interpretation in three dimensions using Euler deconvolution: Geophysics, **55**, 80-91.

Robinson, E. S., 1970, The upward continuation of anomalies in total magnetic intensity fields: Geophysics, **35**, 920-926.

Roest, W. R., J. Verhoef, and M. Pilkington, 1992, Magnetic interpretation using 3-D analytical signal: Geophysics, **57**, 116-125.

Salem, A., S. William, J.D. Fairhead, D. Ravat, and R. Smith, 2007, The meter reader - Tilt-depth method: A simple depth estimation method using first-order derivatives: The Leading Edge, **26**, 1502-1505.

Siebrits, E., J.L. Elbel, R.S. Hoover, I.R. Diyashev, R.T. Holditch, L.G. Griffin, S.L Demetrius, C.A. Wright, B.M. Davidson, N.P. Steinsberger, and D.G. Hill, 2000, Refracture reorientation enhances gas production in the Barnett Shale tight gas sand: Presented at the Society of Petroleum Engineers (SPE) Annual Technical Conference and Exhibition, SPE Paper 63030.

Simon, Y. S., 2005, Stress and fracture characterization in a shale reservoir, North Texas, using correlation between new seismic atrributes and well data: Master of Science, University of Houston.

Spaid-Reitz, M. K., and P.M. Eick, 1998, HRAM as a tool for petroleum system analysis and trend exploration: A case study of the Mississippi Delta survey, southeast Louisiana: Canadian Journal of Exploration Geophysics, **34**, 83-96.

Stone, C., 2008, Technology sweeps data from basement: HRAM "flies low" over subtleties: American Association of Petroleum Geologist Explorer, **29**, 22.

Sullivan, E. C., K. J. Marfurt, A. Lacazette, and M. Ammerman, 2006, Application of new seismic attributes to collapse chimneys in the Fort Worth basin: Geophysics, **71**, B111-B119.

Tarlowski, C., and I. Koch, 1988, On the problem of estimating depth to the magnetic basement: Geophysics, **53**, 1362-1363.

Thomas, W. A., 1989, The Appalachian-Ouachita orogen beneath the Gulf Coastal Plain between the outcrops in the Appalachian and Ouachita Mountains, *in* R. D. Hatcher, W. A. Thomas, and G. W. Viele, ed., The Appalachian-Ouachita Orogen in the United States: Boulder, Colorado, Geological Society of America, The Geology of North America: Geological Society of America, **F-2**, 537-553.

Thomas, W. A., and D.L. Baars, 1992, A North American continental-scale fracture zone (Abstract): Presented at the Structural styles in the Southern Midcontinent - a workshop; Abstract and Program, Oklahoma Geological Survey.

Thompson, D. T., 1982, EULDPH: A new technique for making computer-assisted depth estimates from magnetic data: Geophysics, **47**, 31-37.

Verduzco, B., D. J. Fairhead., C. M. Green, and C. MacKenzie, 2004, The meter reader - New insight into magnetic derivatives for structural mapping: The Leading Edge, **23**, 116-119.

Viele, G. W., 1989, The Ouachita Orogenic belt, *in* R. D. Hatcher, W. A. Thomas, and G. W. Viele, ed., The Appalachian-Ouachita Orogeny in the United States: Boulder, Colorado, Geological Society of America, The Geology of North America: Geological Society of America, **F-2**, 555-561.

Walper, J. L., 1982, Plate tectonic evolution of the Fort Worth basin,, *in* C. A. Martin, ed., Petroleum geology of the Forth Worth basin and Bend arch area: Dallas Geological Society, 237-251.

Wilson, F. W., and P. Berendsen, 1998, The role of recurrent tectonics in the formation of the Nemaha Uplift and Cherokee-Forest City Basins and adjacent structural features in eastern Kansas and Contiguous State, USA (abstact), *in* J. P. Hogan, and M.C. Gilbert, ed., Basement Tectonics 12 Central North America and other regions: Kluwer Academic Publishers, **12**, 301-303.

# Chapter 4: Integrated Geophysical Studies of the Basement Structures, the Mississippi Chert, and the Arbuckle Group of the Osage County, NE, Oklahoma (Paper to be submitted to the AAPG Bulletin)

## 4.1 Abstracts

We have used the integration of gravity, magnetic, and 3D seismic data to map features in the sedimentary column and to study relationship between sedimentary and basement features in the Osage County area. Volumetric seismic attributes such as coherence and curvature derived from 3D seismic data employed to better characterize subtle features such as collapse features, faulting and fracturing within the carbonate reservoirs that are difficult to image on conventional 3D seismic data. We conducted an integrated analysis that includes the use of 3D seismic data, seismic attributes, and derivative maps from potential field data to study the Mississippi Chert and the Arbuckle Group of Osage County, Oklahoma. We investigated the large gravity and magnetic anomalies and their association with the Mid-Continent Rift System (MCRS). Seismic attribute analysis of the Osage County carbonate reservoirs was effective in studying and identifying polygonal, highly coherent, and high amplitude lineaments that strike northwesterly and northeasterly within these reservoirs. The fracture lineament densities increase from the Mississippi Chert toward the Arbuckle Group and reduce toward the Reagan Sandstone. A one-to-one correlation between the Precambrian basement structures and the carbonate reservoir could not be established. However, basement structure lineaments were found to be parallel in orientation with the trend of lineaments seen within the Mississippian Chert and the Arbuckle Group. The northwest-striking

lineaments maybe related to the late-Paleozoic tectonism that affected both the Precambrian and Paleozoic section of Osage County. On the other hand, the northeast lineaments are related to the inherent structural grain of the northeast Oklahoma basement rock. Our analysis revealed prominent northeast trending anomalies that suggest that the MCRS extends into northern Oklahoma. However, geochronological data for basement rocks suggest that this extension would have to be limited to intrusive bodies that have little or no subcrops.

## 4.2 Introduction

Osage County located in northeastern Oklahoma and is bounded by the Ozark uplift to the east, the Nemaha uplift to the west, the Kansas state boundary to the north, and the Arkansas River to the southwest. This county is part of the gently southward-sloping stable shelf, which extends into the Anadarko and Arkoma basins (Thorman and Hibpshman, 1979) (Figure 4.1). Exposed deformed rocks within the county dip westward (Guo and Carroll, 1999).

Osage County, Oklahoma has been a prolific oil producing area since the discovery of the giant Burbank field in 1897. Although oil and gas exploration within the Osage County is as old as the seventeenth century, production has been mostly from the Cambrian-Ordovician Arbuckle Group that lies unconformably on top of the irregular Precambrian basement surface and from Mississippian Chert reservoirs (Thorman and Hibpshman, 1979; Franseen et al., 2004). The Mississippi Chert reservoir, informally called “Mississippi Chat” by drillers, is formed from exposed and diagenetically altered cherty limestone (Rogers, 2001). In Texas alone, Devonian fractured-chert reservoirs have produced about 700 million barrels of oil (Fu et al., 2006), many trillion cubic feet

of natural gas, and a hundred million more barrels of oil are yet to be produced from these reservoirs (Rogers and Longman, 2001).

For example, a vast majority of oil production from the Arbuckle reservoirs in Kansas and Oklahoma occurs on the Central Kansas uplift and the Nemaha uplifts respectively (Thorman and Hibpshman, 1979). In fact, the occurrence of these fracture-controlled reservoirs has been linked to Precambrian basement uplifts (Franseen et al., 2004), differential compaction and post Arbuckle weathering (Thorman and Hibpshman, 1979). However, what is not clearly established is the interaction between Precambrian basement structures and these fracture-controlled carbonate reservoirs.

Even with more than 50 years of production from chert reservoirs, a myriad of misconceptions and enigmas still surround these reservoirs. For example, chert reservoirs are generally associated with carbonate rocks that contain secondary porosity, but Rogers and Longman (2001) have documented a deep-marine clastic chert type of reservoir that produces from a primary porosity. These Monterey Cherts in California have never been sub-aerially exposed and were diagenetically stable in the subsurface where they became an early hydrocarbon accumulation site.

Chert reservoirs are structurally, depositionally, and diagenetically complex. Such complexities are reflected in their heterogeneity, which can be caused by faulting and fracturing (e.g. Thirty-one Chert reservoirs in the Three Bar field of the Permian Basin, Texas (Ruppel and Barnaby, 2001), and carbonate dissolution (e.g. Dickman field in Kansas (Nissen et al., 2006) resulting from transportation and deposition of siliceous sediments (Ruppel and Hovorka, 1995). These heterogeneities can act as hydrocarbon barriers creating compartmentalization when they are shale-filled or hydrothermally

altered. Otherwise, the fault and fractures that causes the heterogeneity can act as a fluid flow conduit (Davies and Smith, 2006). Thus, it becomes imperative to understand these structures and map their distribution within Osage County. The understanding of porosity and heterogeneity often associated with chert reservoirs is important for the exploration and management of such complex reservoirs.

For the last decade, independent operators have used conventional interpretation methodology from 3D seismic data to study the Midcontinent carbonate reservoirs. Increasingly, volumetric seismic attributes such as coherence, curvature, and amplitude gradients calculated from the 3D seismic data are being incorporated into the Mid-Continent exploration workflow to better characterize subtle carbonate features such as karsting, tectonic faulting and fracturing, and hydrothermal dissolution that are difficult to image from standard 3D seismic (e.g. Nissen et al., 2006). Seismic attributes that are sensitive to fractures and impedance have also been used to characterize porosity and field scale fractures that are associated with chert reservoirs (Fu et al., 2006). Studying chert reservoirs with the aid of seismic and seismic attribute data can effectively help delineate lineaments related to fault and fracture distribution within chert reservoirs.

In this paper, we present the results of potential field and seismic data analysis from several 3D seismic surveys acquired in Osage County, Oklahoma. Our efforts are directed at the fractured-controlled Ordovician Arbuckle dolomite and Mississippian Chert reservoirs that have been faulted, fractured, and diagenetically altered subaerial exposure and hydrothermal process. Our objective is to understand the interaction between Precambrian structures and the fractured controlled carbonate reservoirs. We attempt to establish an association between these structures and the karst reservoirs. In

addition, features identified within the Precambrian basement were compared with features within the sedimentary section as we examine possible links between these features. We believe that the results of this study will be useful in exploration for these reservoirs because knowledge about the geometry and their association with or without Precambrian basement will be improved.

We also conducted a regional integrated study utilizing seismic data, regional gravity, and regional aeromagnetic data to study the basement rocks and their associated potential field anomalies. Our methodology was directed at: 1) Investigating the extent of the 1100 Ma (MCRS) across Texas and Oklahoma. Authors such as Jones and Lyons (1964), Nixon and Ahern (1988), Robbins and Keller (1990), and Adams and Keller (1994) have used gravity and magnetic information to suggest that the MCRS extends further into west Texas and New Mexico than previously thought. 2) Studying the large Osage gravity anomaly and other intriguing anomalies that may or may not have a relationship with the MCRS. Density variation (Cook, 1956), deeper crustal sources (Denison, 1981), thinned crust, and Moho-bumps or anti-root (Roark, 1962) have been suggested as the cause of this anomaly because of its lack of correlation with regional structural geology.

## 4.3 Geologic Background

The present configuration of the Osage County area basement rocks reflects subtle large-scale Paleozoic movement; and according to Chenoweth (1968), the basement surface, which is an irregular erosional surface with series of domes, controls the overlying Paleozoic sedimentary distribution and thickness (Walters, 1946; Thorman et al., 1946).

Osage County (Figure 4.1) is surrounded by uplifts (Ozark, Nemaha, and Central Kansas). The Precambrian basement of these uplifts contains rocks that belong to the 1370 ± 30 Ma Southern Granite-Rhyolite (SGR) province that blankets most of the Midcontinent (Van Schumus et al., 1996). The intensely sheared and mylonitic Central Oklahoma granite group underlies the Nemaha uplift that bounds Osage County on the west (Figure 4.1). The uplift consists of a number of crustal blocks that are surrounded on the east and west by Middle Pennsylvanian reactivated faults (Luza et al., 1978).

Widespread within the Osage County area are distinct broad domes, covering an approximately 320-square-mile area (829 square kilometers) that spatially correlate with the Osage gravity anomaly (Figure 4.2). The western part of Osage County, which is less deformed than the eastern part, also contains fewer northeasterly and northwesterly striking domes, anticlines, and structural basins (Guo and Carroll, 1991).

Two sets of major Precambrian basement faults have been identified within Osage County. The northeast-southwest striking Labette fault that juxtaposes metarhyolitic rocks on the northwestern side (up-thrown) against rhyolitic rocks to the southeast (downthrown) extends northward from Payne County through Osage County and into southern Kansas. In addition, four other northwest-southeast striking faults cross the area (Denison, 1981; Guo and Carroll, 1999).

Common Paleozoic features that occur within the county include north-northeast and weakly defined northwest trending broad open-folds and en-echelon normal faults (Bass, 1942). These structures developed sporadically throughout Paleozoic time, and the dip of their flanks increases with depth mostly within the Cambrian and Ordovician strata (Thorman and Hibpshman, 1979).

## 4.4 Precambrian Geology of Northeast Oklahoma and Southeastern Kansas

The Northeast Precambrian rocks of Oklahoma and southeastern Kansas consist of petrographically, chronologically related intrusive and extrusive rocks and their metamorphic rocks equivalents. These rocks occur as a relatively thin veneer of shallow intrusive and extrusive rocks that cover unknown older basement rocks (Denison, 1981). These rocks are considered part of the widespread 1400 – 1340 Ma intracratonic magmatism that formed the "Western Granite-Rhyolite Province" (WGRP) or SGR (Bickford et al., 1986; Van Schmus et al., 1996), which overprints the earlier Proterozoic continental orogenic outer tectonic belt (Whitmeyer and Karlstrom, 2007) and extends from western Ohio to west Texas (Lidiak et al., 1966; Muehlberger et al., 1967). Relative ages of this Oklahoma rock units based on Rb/Sr isotopic dating is about 1285 Ma (Denison, 1981).

Basement rocks of northeastern Oklahoma can be classified into four igneous units: one volcanic and three granitic units (the Washington Volcanic Group (WVG), the Spavinaw Granite Group (SGG), the Osage Microgranite (OM), and the Central Oklahoma Granite Group (COGG)) (Figure 4.2) (Denison et al., 1966 and Denison, 1981).

### 4.4.1 Washington Volcanic Group (WVG)

The WVG unit covers a large portion of northeast Oklahoma and consists predominantly of porphyritic rhyolite, relic welded tuff texture, andesite and meta-rhyolite, which is the metamorphic equivalent of the rhyolite that occurs around its margin (Figure 4.2).

### 4.4.2 Spavinaw Granite Group (SGG)

This unit outcrops in Mayes County, Oklahoma and extends into southwestern Missouri (Figure 4.2). It consists of porphyritic micrographic granite, and these uniform epizonal granites are considered the subsurface equivalent of the irregularly shaped Wichita Mountain sills in southern Oklahoma (Denison, 1981).

### 4.4.3 Osage Microgranite (OM)

The Osage microgranite is uniform and a strongly porphyritic granite that is present in a very small area of northeastern Oklahoma (Figure 4.2) (mainly restricted to Osage County). The OM occurs as a relatively thin sill that intrudes into a thick rhyolite cover at shallow depth (Denison, 1981). Subsequent removal of the rhyolitic covering by erosion exposed the OM.

### 4.4.4 Central Oklahoma Granite Group (COGG)

The central Oklahoma granites are sometimes interpreted as the youngest rocks that occupy a vast area in northeastern Oklahoma (Figure 4.2). They are rimmed partly around the margins of the shallow intrusive and extrusive basement rocks of northeast Oklahoma, regionally metamorphosing the rhyolite into metarhyolite (Denison, 1981). Equivalent rocks of the COGG can be seen as outcrops in the eastern part of the Arbuckle Mountains.

## 4.5 Paleozoic Geology

The Paleozoic sequences in northeast Oklahoma reflect four episodes of north-south marine transgression and regression, and each of these sequences is bounded above

and below by a regional unconformity. Mesozoic and Cenozoic records are not present within northeast Oklahoma except for a late Cenozoic gravel deposit related to the glaciation and erosion in the Pleistocene time (Thorman and Hibpshman, 1979). Figure 4.3 shows a schematic lithologic column for Osage County.

A late Cambrian sea deposited granite wash or the Lamotte-Reagan Sandstone that probably represents reworked lag gravel deposits eroded from exposed basement, unconformably on the flanks or crest of the Precambrian basement (Keroher and Kirby, 1948).

The Arbuckle Group that unconformably overlies the Lamotte-Reagan Sandstone or directly overlies the Precambrian basement includes limestone, dolomite, and sandstone units. Where the Arbuckle Group directly overlies the Precambrian basement, the lower Arbuckle Group units onlap rugged Precambrian basement, and the upper Arbuckle Group is bounded at the top by a major interregional unconformity representing a major sea regression and subaerial exposure of the North America craton (Sloss 1963). Due to post-Arbuckle erosion and weathering, which enhances porosity and permeability, the upper Arbuckle Group contains of a series of karst sinkholes, collapse structures, and fractures and joints similar to its Ellenberger equivalent in the Fort Worth basin in Texas. It has been suggested that the distribution and alignment of these karst features in the Kansas Arbuckle Group are influenced by basement structures (Cansler and Carr, 2001). Thus, the complexity of the Arbuckle structures increases in structurally high areas (Franseen et al., 2004).

During the middle Ordovician, the Simpson Sea transgressed and regressed across Osage County depositing the Simpson Group. A shallow sea covered most of Oklahoma

during the Mississippian period depositing the Mississippian Limestone, which consists partly of limestone (chert) and dolomite that lies conformably on top of the Woodford Shale. Uplift and either surface/near surface erosion or in-situ weathering of the underlying Mississippian Limestone resulted in erosion and diagenetic alteration of the top of the this unit. The resulting irregular surface of this highly porous, hard, and tight Mississippian Chert and the dissolution of calcite create secondary porosity that makes the Mississippi Chert a potential hydrocarbon reservoir. In north-central Oklahoma and south-central Kansas, the Mississippian Chert present between the Pennsylvanian and Mississippian unconformity occurs as widespread, heterogeneous reservoirs that are generally not continuous (Rogers, 2001).

## 4.6 Previous Geophysical Works

In 1948, a joint effort between the U S Geological Survey and U S Coastal and Geodetic Survey was one of the first geophysical collaboration done in northeast Oklahoma. The effort resulted in the collection of regional gravity data around northeast Oklahoma and southeast Kansas. Cook (1956) recognized that the Osage anomaly did not correlate with regional geology. Roark (1962) suggested the cause of this anomaly to be due to crustal thinning, Moho antiroot or bump.

A lineament study that consisted of surface and subsurface fracture analysis was conducted by comparing satellite images and aerial photographs from Osage County (Guo and Carroll, 1999). The results of this study showed an orientation correlation between northeast-southwest and northwest-southeast surface lineaments with subsurface features.

### 4.6.1 Mid-Continent Rift System

The Middle Proterozoic Mid-Continent Rift System (MCRS) of North America is a 1100 Ma failed rift that extends for more than 1243 miles (2000 kilometers) (Hinze et al., 1997) from Lake Superior, through northwestern Wisconsin, southeastern Minnesota, southwestern Iowa, and southeastern Nebraska toward central Kansas. Jones and Lyons (1964), Nixon and Ahern (1988), Anderson and McKay (1989), Robbins and Keller (1990), and Adams and Keller (1994) suggested that dikes related with the MCRS mafic intrusion extend into Oklahoma. Other authors that have shared similar thoughts include Yarger (1985) and Xia et al. (1996). However, (Berendsen, 1997) and Bickford (1988) could not validate such an extension via drill holes. Repeated reactivation of Paleozoic structures (Berendsen, 1997), covering the MCRS by Phanerozoic cover, and rift offset (Xia et al., 1996) are some of the explanation given as the reason why the MCRS cannot be seen directly in Oklahoma.

## 4.7 Data and Methodology

### 4.7.1 Potential field data

The association of the MCRS with prominent gravity and magnetic anomalies makes the potential field methods an effective tool to investigate the MCRS. The datasets used in this study include aeromagnetic data that is part of the North American Magnetic Map project grid (http://crustal.usgs.gov/namad), which is the result of a combined effort of the United State Geological Survey (USGS), Geological Survey of Canada (GSC) and Consejo de Recursors Minerales of Mexico (CRM). This dataset contain grids obtained from the Geological Society of America's (GSA) Decade of North American Geology

(DNAG) program and is available for download at: (ftp://ftpext.usgs.gov/pub/cr/co/denver/musette/pub/open-file-reports/ofr-02-0414).

In addition to the aeromagnetic grid, gravity data points were downloaded from a community online gravity database that is maintained by Pan American Center for Earth and Environmental Studies (PACES) at the University of Texas at El Paso (UTEP) (http://research.utep.edu/paces). In addition, in the summer of 2008, I collected additional 200 gravity readings to better constrain the Osage anomaly. The gravity points were spaced at 200 m (656 ft) and acquired along existing roads using a LaCoste Romberg G-1115 gravimeter and a Worden 112 gravimeter. We reduced the gravity data using the standard data reduction program of Holom and Oldow (2007), which utilizes a Bouguer reduction density of 2.67 g/cc (2670 kg/m$^3$). The gravity spreadsheet used for this reduction conforms to the United State Geological Survey (USGS) and standard format of the working group of the North American Gravity Database Committee (Hildenbrand et al., 2002; Hinze et al., 2005). We compared the gravity spreadsheet results with results generated from the software written by Mike Webring of the USGS, which is the same program from which the PACES gravity datasets were derived,and were satisfied with the spreadsheet results. Thus, a simple residual Bouguer anomaly map was generated from all these gravity points (Figures 2 and 4a).

*Potential field data enhancement and filtering techniques*

Potential field anomalies contain a wide range of signals originating from various sources and depths, and there are times when a local anomaly needs to be extracted from a regional anomaly. The techniques of enhancing an anomaly of interest from the Precambrian basement allows us to be able to compare Precambrian basement structures

with sedimentary structures identified on seismic and seismic attribute data. All potential field enhancement and filtering are performed using modern magnetic and gravity processing and interpretation software.

The gravity and aeromagnetic data was gridded with a grid spacing of 5000m (16404 ft) and 1000 m (3281 ft) respectively. Before any interpretation could be done on aeromagnetic data, the data was reduced-to-the pole (RTP) in order to remove magnetic anomaly distortion caused by varying magnetization inclination and azimuth. This linear transformation transforms a total magnetic intensity field into a vertical component field such that the magnetic anomaly will lie directly over its causative source (Kis, 1990).

To highlight the effect of anomalies within the Precambrian basement, we generated a residual Bouguer anomaly and a residual total magnetic intensity (TMI) map from the complete Bouguer anomaly and the RTP TMI grids, which are shown in (Figure 4.4).

To highlight lateral or abrupt changes in magnetization, which indicate lateral changes in anomalies generally associated with faults or source contacts, we computed the horizontal gradient magnitude (HGM), tilt derivative, horizontal derivative of the tilt derivative and analytical signal for both gravity and aeromagnetic datasets. Derivative maps generated are shown in Figures 4.5. Although these edge-detecting derivatives enhance lateral discontinuities, it is the interpreter's responsibility to provide a geological acceptable interpretation. Mathematical foundation and details on these gradient methods are available in papers such as Grauch and Cordell (1987), Roest et al., 1992, Miller and Singh (1994); Blakely (1996), Verduzco et al. (2004), and Li (2006). For example, Grauch and Cordell (1987) cited an example of where the gradient from a sloping

interface could lead to maxima with two edges. This observation could be misinterpreted as two separate interfaces separating three geological units.

We also applied directional filters to our data. Directional filters isolate linear anomaly of interest that might have geological or tectonic implication to potential field map. Results from this filter allowed us to be able to compare anomaly trends associated with the MCRS. We were able to isolate anomalies that have inherent trends parallel to those of the (MCRS) and assess whether the MCRS extends southward into Oklahoma (Figure 4.6).

### 4.7.3 Seismic data

To understand the interaction between sedimentary features and structures within the Precambrian basement, we interpreted four different 3D seismic surveys that the Osage Nation and Spyglass Energy LLC provided us using modern interpretation software (Figure 4.1). The seismic data provide spatially and depth-limited structural details but at higher resolution than the potential field data. In addition, the seismic data give insight into the geometry and seismic expression of the chert reservoirs.

We began our interpretation by mapping the Arbuckle Group and the Mississippi Chert horizons. In addition to the time-structure map, we generated integrated seismic attributes for both horizons, which are designed to enhance geometric features such as fractures, faults, karst, and differential compaction that are not easily seen in the raw seismic data. The physical and geometrical features in the attribute use models of dip and azimuth, waveform similarity, amplitude, and frequency content from adjacent seismic samples, which can then be rendered on a computer for interpretation. Attributes that we found useful include coherence, most-negative and most-positive curvature, total energy

and energy-weighted coherent amplitude gradients; examples of their application and mathematical concepts in available in Chopra and Marfurt, 2007.

## 4.8 Data Analysis and Interpretation

Basement rocks generally display incoherent signals on seismic data. This is often due to lack of signal from basement depths or to processing flows that do not emphasize basement depths. Very seldom do we see coherent intra-basement reflection similar to that we observed on seismic data from Osage County (Figure 4.7). Beneath the base of the top of the basement and below the nearly horizontal Paleozoic section of Osage County, we identified many highly coherent dipping intra-basement reflectors. Between the bright intra-basement reflectors and the top of basement are reflecting sequences that we interpret to be meta-igneous or meta-sedimentary (Figure 4.8). McBride et al. (2003) identified similar broad "basinal" sequences bounded below by three highly coherent layers beneath the Paleozoic Illinois basin.

Generally, within the granite-rhyolite province, dipping intra-basement reflectors are associated with volcanics (Hinze et al., 1997; Richard et al., 1997). For example, Schaming and Rotstein (1990), and Schlich et al. (1993) interpreted dipping intra-basement reflectors on seismic data from the Kerguelen Plateau in south Indian Ocean, as basaltic flows that are associated with volcanic margin. Hinze et al. (1997) and Richard et al. (1997) also interpreted dipping intra-basement reflectors seen in the southern margin of the MCRS of western Lake Superior and Pre-Mount Simon basins of western Ohio as Keweenawan volcanic and eastern granite-rhyolite rocks respectively.

The Osage intra-basement reflectors display a positive reflection coefficient (positive acoustic boundary) that is caused by an increase in acoustic impedance resulting

in a red (trough) blue (peak) red (trough) pattern (see Figure 4.7 inset). The base of the intra-basement reflector displays a decrease in acoustic impedance marked by a change from peak to trough. The increase in acoustic impedance at the top intra-basement reflector (similar to what can be observed at a hard water bottom) also has a positive impedance change.

### 4.8.1 Seismic description of Osage basement reflectors

To understand the nature and geometry of these bright coherent intra-basement reflectors, we mapped the intra-basement reflectors from the available 3D seismic data. The intra-basement reflectors exhibit a basinal geometry with the high end occupying the northeastern end of the survey (Figure 4.8a). This kind of geometry is also similar to the sill geometry described in Hansen et al. (2004). On Figure 4.8b, the geometry observed is similar to growth or detachment faults. However, the intra-basement reflectors crosscut each other in Figure 4.8c. This crosscutting relationship is generally seen in an igneous intrusion setting and according to the law of crosscutting relationship; a younger igneous intrusion always crosscut an older igneous body that it cuts through. Inset in Figure 4.8b indicates the general orientation of the reflectors to be northwest. Using the intra-basement reflectors dip, we classify these reflectors into two groups (I and II). Reflectors in group I dip south-southwest and reflectors in group II dip to the east (Figure 4.8c). In addition to these geometries, other 3D data interpreted show interactions of intra-basement features with younger sedimentary strata (Figure 4.9a-c). This suggests that both the intra-basement reflectors and the Paleozoic section have been affected by the same tectonic event.

Based on the crosscutting relationship of the intra-basement features shown in Figure 4.8c, reflector group II (blue line) crosscuts reflector group I, which implies that reflector group I, which strikes northwesterly, is oldest.

The areas of the 3D seismic surveys (Figure 4.1) is part of the granite-rhyolite province (Denison, 1981); thus, we interpret the basement reflectors as being from the lower portion of the eastern granite-rhyolite province units.

### 4.8.2 Potential field expression of basement features

*Anomaly Identification and Interpretation*

The potential field anomalies analyzed around Osage County generally display simple Bouguer gravity anomalies and complex magnetic anomalies (Figures 4.2). We specifically investigated the broad gravity high "Osage anomaly" (OS1 on Figure 4.4a) (Cook, 1956; Denison, 1981) that occupies a vast majority of Osage County, the elongate north-northwest gravity high anomaly that occurs west of the Nemaha uplift (OS2 on Figure 4.4a), and the elongated north-northeast gravity high that abuts against the Wichita uplift (OS3 on Figure 4.4a). Robbins and Keller (1990) indentified gravity anomaly OS3 and interpreted this anomaly via 2D gravity modeling as dense Keweenawan volcanic rock. Our integrated approach was based on understanding these anomalies in the context of all the available geological and geophysical data.

The broad high anomaly on the residual anomaly map (OS1) (~ 20 mGal, ~150 nT) has an approximate length and width of 99 km and 75 km respectively (Figures 4.4). This suggests that the source of this high density, high magnetic susceptibility could be deep and broad. Gravity and magnetic derivative maps suggest a northwest trending anomaly (Figures 4.5). However, the directional filtering map in Figures 4.6 suggests

both a northwesterly and northeasterly trending anomaly. OS1 anomaly occurs within the Osage Microgranite and Washington Volcanic Group. At locations where the Spavinaw Granite Group are present, this kind of prominent high gravity response is lacking (Figures 4.4).

High gravity and magnetic value (~18 mGal, ~200 nT) dominate the 83 km long and 48 km wide OS2 anomaly (Figures 4.4). Occurring south of the MCRS relics, gravity, a magnetic derivative map, and directional filter maps (Figures 4.5 and 4.6) suggest a northwest trending anomaly. The high frequency nature of this elongate anomaly suggests a shallow source.

The anomaly that abuts against the Wichita uplift (~10 mGal) is a 75 km long and 33 km wide and trends northeast (OS3; Figures 4.4 - 4.6). The magnetization displayed by this elongated anomaly (-250 nT to the north +115 nT to the south) is complex but forms a distinct signature.

Based on the gravity data and its derivative maps alone, one could assert that the MCRS extends across Oklahoma, abutting against the Southern Oklahoma aulacogen (Figure 4.5).

Directional filters aimed at enhancing trends of the anomalies show that the OS1 anomaly has both northwestern and northeastern trending components. OS2 has a characteristic northwest and northeast anomaly trend while OS3 anomaly exhibits trend that is consistent with the northeast trend displayed by the MCRS (Figures 4.6). Thus, OS2 anomaly can be interpreted to be related to be part of the MCRS, the same conclusion cannot be made about the OS1 anomaly.

Age dating from Precambrian wells available from the work of Denison (1981) and Van Schmus et al. (1993) only provide one date as young as the MCRS. The Texaco Inc. Kohpay well (Table 4.1), which is the only well that penetrated the Osage Microgranite and close to OS1 gave a Rb/Sr age of 1183 ± 46 Ma (Figure 4.6). However, the wells to basement are sparse to the south and the anomalies could be from intrusion that do not subcrop. In a similar case, a massive subcrop 1.1 Ma mafic intrusions from the Central basin platform of west Texas, which have been missed by previous wells, was penetrated by the Nellie #1 well that that was drilled into about 5 km of basement rocks. The well was centered on a gravity anomaly maximum and a well that is just 5 km north surprisingly tested a granitic and metamorphic basement rocks (Keller et al., 1989).

### 4.8.3 Seismic attribute expression of chert reservoirs from Osage County

*Mississippi Chert and Arbuckle Group Time-Structure and Seismic Attribute Mapping*

We evaluated Mississippi and Arbuckle Group reservoirs comparing structures and lineation on both seismic and seismic attribute data. Structural mapping of both reservoirs shows generally southeast dipping undulating horizons (Figures 4.10). The chert horizons display an irregular surface that is typical in a karsted carbonate region. Structural complexity increases from the shallow Mississippi Chert to the deeper Arbuckle Group. We also noted an east-west feature in the southern portion of the seismic data (Figures 4.10).

Coherence, curvature, total energy, and inline gradient attributes computed from the seismic data facilitates mapping of karst features and associated fracture patterns. The coherence horizon-slice map near the Mississippi Chert shows the presence of circular low-coherence features that we interpret as collapse features (red arrows on Figure

4.11a). At the Arbuckle Group level, the incoherent features are more dominant. We noticed that some of these low coherence features contain very coherent linear features (Figures 4.12a and 4.13a).

Figures 4.11b-4.14b shows the most-negative horizon slice that enhances valley or bowl shaped features. We notice that most-negative curvature attributes enhance the lineaments that we interpret as fractures and faults. We also identified increase number of lineaments especially at the top and within the Arbuckle Group (Figures 4.11b-4.13b). We manually mapped most of the coherent and most-negative lineaments plotted them as a rose diagram. The rose diagram plots in Figures 4.12b-4.14b inset indicate two sets of orthogonal lineaments (northeast-southwest and northwest-southeast). We suggest that the northeast striking lineaments are similar to the solution-enhanced faults and fractures reported by Nissen et al. (2006) in the Mississippian reservoir of the Dickman field in Kansas. The long anomalous northeast-striking lineament (yellow lineament) on the rose diagram is the fault seen on the southeast corner of the most-negative curvature horizon slice (Figures 4.12b-4.14b).

Based on our interpretation, the density of the northwest striking lineaments increase toward the top and below the Arbuckle Group (Figures 4.11b-4.13b). However, lineaments densities is reduced within the Reagan Sandstone that lies on top the basement rocks (Figure 4.14b). The blended image of the most-negative curvature (Figure 4.15), the total energy (Figure 4.16), and the coherence (Figure 4.13a) attributes with the inline gradient attribute (Figure 4.17), show these lineaments to be nearly polygonal in shape. The lineaments occur as high amplitude and high total energy (Figures 4.18-4.20). Figure

4.20 also shows these lineaments to be highly coherent and we suggest that the amplitude and coherent nature of these lineaments can be due to the content material within them.

Based on the seismic analysis result, we suggest that lineaments over the Mississippi Chert and Arbuckle Group have a general northeasterly and northwesterly strike. Our finding is consistent with a surface and subsurface remote sensing study of lineaments conducted by Guo and Carroll (1999). These authors also identified a northeast-southwest and northwest-southeast striking surface lineament, which correlated with subsurface lineaments (Figures 4.21).

*Precambrian Basement Lineaments*

Rose diagrams from regional maps of the potential field derivatives sensitive to basement structures, display lineaments that are parallel to the northwest and northeast strike direction of lineaments identified from the local seismic and seismic attributes images (Figures 4.22). However, the northwest-striking anomalies on both derivatives map shown in Figures 4.22, appear longer with more lineament density than the northeast striking anomalies. Thus, we suggest that the northeast-southwest Precambrian structures reflect the regional inherent structural fabric of northeastern Oklahoma.

Based on the similarity in orientation of the lineaments seen within the Paleozoic section and Precambrian basement of Osage County, we suggest that the Precambrian basement controls the Mississippian Chert and Arbuckle Group reservoirs.

## 4.9 Conclusions

This paper describes an integrated geophysical analysis that utilizes seismic data and potential field data to study Precambrian basement controls on carbonate reservoirs in Osage County in northeast Oklahoma. Seismic attribute analysis of the Mississippi

Chert and the Arbuckle Group of Osage County was effective in studying and identifying lineaments within these reservoirs.

Our fracture analysis study on the most-negative curvature and rose diagram revealed that lineaments within the study area strike northeast-southwest and northwest-southeast. These lineaments interpreted as fractures and their density increase from the Mississippi Chert downward toward the Arbuckle Group but decreases from the Arbuckle Group toward the Reagan Sandstone. These lineaments also appear as polygonal and are highly coherent with high amplitude on the most-negative curvature, coherence, and total energy attributes respectively.

Basement structure lineaments were found to be parallel in orientation with the trend of lineaments seen within the Mississippian and Arbuckle Group. The northwest-striking lineaments are suggested to be related to the late-Paleozoic tectonism that affected both the Precambrian and Paleozoic section of Osage County. On the other hand, the northeast lineaments are related to the inherent structural fabric of the basement rock. Thus, we suggest that the Precambrian basement controls the Mississippian Chert and Arbuckle Group reservoirs. Thus, for Mississippi Chert and Arbuckle group exploitation, structurally high areas that are fractures will be the primary target area to explore for these reservoirs. In addition, highly coherent area with high total energy is good indicator of a viable chert reservoir. Therefore, these parameters mentioned above are what explorers in Osage County should look for when exploiting for Mississippi Chert and Arbuckle Group reservoirs.

In our investigation of the possible extension of the Mid-Continent Rift System (MCRS) through Oklahoma and toward the Texas border, the potential field anomalies

indicates that the Osage anomaly (OS1) centered within Osage County is not related to the MCRS. Based on the orientation of the OS2 and OS3 anomalies, which occur west of the Nemaha uplift and abut the Wichita uplift respectively, we suggested that both anomalies are related to MCRS extension through Oklahoma. However, we could not substantiate this conclusion with a geochronological age dating data at this time.

## 4.10 Acknowledgements

We express sincere thanks to the Osage Nation for the use of their seismic data for research and education. We also want to thank Charles Wickstrom and Shane Matson for access to more recently acquired proprietary surveys, and more importantly, for their geologic insight into the complexities of the Osage County region. Geosoft provided the education license for the potential field data processing and interpretation "Oasis Montaj". The seismic interpretation would not have been possible without the gracious donation of the Petrel interpretation software by Schlumberger. Ha Mai of the Attribute Assisted Seismic Processing and Interpretation (AASPI) helped with the generation of codes used to compute the attributes. We thank Rockware for the online free trial of the RockWork14 demo-software used to generate the rose diagram. Lastly, we would like to thank the Oklahoma Geologic Survey for insightful geological comments and logistic support.

I appreciate the assistant of Matt Cosatt during the collection of the gravity data in the summer of 2007.

Table 4.1. Wells in north-central Oklahoma that penetrates Precambrian basement. The depth to the top of basement is listed under column title "BASEMENT TOP (ft)". Column title "BASEMET (ft)" is the subsea depth, which is the basement depth relative to mean-sea-level (MSL). Isotope ages were compiled from Denison (1981) and Van Schmus et al. (1996).

| API | OPERATOR | LEASE | WELL # | QUARTER | SECTION | TOWNSHIP | RANGE | YEAR | TOTAL DEPTH (ft) | SURFACE ELEVATION (ft) | BASEMENT TOP (ft) | BASEMENT THICKNESS (ft) | BASEMENT (ft) | LATITUDE | LONGITUDE | ROCK AGE | SOURCE | ISOTOPE AGE |
|---|---|---|---|---|---|---|---|---|---|---|---|---|---|---|---|---|---|---|
| 13320229 | PAWNEE PETROLEUM CO. | RENTIE | 1 | W2 NW NE | 23 | 9N | 6E | 1968 | 7261 | 886 | 7224 | 37 | -6338 | 35.24469 | -96.64333 | 1242 ± 21 Ma | Denison, (1981) | Rb/Sr |
| 03715553 | CENTRAL COMMERCIAL | JOHNSON HAY | 3 | SW NW SW | 10 | 17N | 10E | 1930 or 1937 | 4282 | 793 | 4278 | 4 | -3485 | 35.96382 | -96.24289 | 1212 ± 48 Ma | Denison, (1981) | Rb/Sr |
| 11330447 | TEXACO INC. | OSAGE C | 1A | C NE SW | 24 | 20N | 11E | 1965 | 3690 | 1002 | 3634 | 56 | -2632 | 36.19272 | -96.08434 | 1286 ± 24 Ma | Denison, (1981) | Rb/Sr |
| 11303718 | NORBLA OIL | LYMAN | 2 | NW SE SW | 24 | 22N | 9E | 1963 | 2972 | 860 | 2933 | 39 | -2073 | 36.36426 | -96.29443 | 1281 ± 48 Ma | Denison, (1981) | Rb/Sr |
| 11315912 | CITIES SERVICE OIL CO. | OSAGE LOT | 1-SWD | NW SE NE | 8 | 23N | 11E | 1953 | 3032 | 762 | 3007 | 25 | -2245 | 36.48741 | -96.14216 | 1233 ± 50 Ma | Denison, (1981) | Rb/Sr |
| 11306916 | TEXACO INC. | L KOHPAY | 16WS | C NE NE N | 29 | 25N | 8E | 1963 | 2848 | 1088 | 2813 | 35 | -1725 | 36.62072 | -96.45967 | 1183 ± 46 Ma | Denison, (1981) | Rb/Sr |
| 07101424 | ANDERSON-PRICHARD OIL CORP | J WELSH | 28 | NW NE SW | 17 | 28N | 1E | 1918;1956 | 4408 | 1138 | 4406 | 2 | -3268 | 36.90384 | -97.22348 | 1228 ± 56 Ma | Denison, (1981) | Rb/Sr |
| | EAGLE PICHER MINING CO. | BEAVER | 43-C | NE NW NE | 19 | 29N | 23E | unknown | 1650 | 833 | 1610 | 40 | -777 | 36.98608 | -94.85449 | 1383 ± 8 Ma | Van Schmus et al., (1996) | Zircon |
| 10937486 | CITIES SERVICE CO. | FARLEY | 5 | SW NE NW | 19 | 11N | 2W | 1947 | 8344 | 1249 | 8272 | 72 | -7023 | 35.41797 | -97.45326 | 1220 ± 73 Ma | Denison, (1981) | Rb/Sr |
| 10300893 | OKLAHOMA NATURAL GAS CO. | HARDROW | 1 | NW SE | 15 | 23N | 2W | 1964 | 5508 | 959 | 5464 | 44 | -4505 | 36.46829 | -97.39674 | 1381 ± 29 Ma | Denison, (1981) | Rb/Sr |
| 00321255 | CHAMPLIN PETROLEUM CO. | RAY N SMITH | 1 | E2 SE NW | 1 | 27N | 10W | 1985 | 7300 | 1161 | 7239 | 61 | -6078 | 36.84963 | -98.22701 | 1380 ± 24 Ma | Van Schmus et al., (1996) | Zircon |
| | AMAX | DAC | 2 | SE SE NE | 6 | 20N | 23E | | 1723 | 1165 | 1674 | 49 | -509 | 36.24235 | -94.88778 | 1270 ± 32 Ma | Denison, (1981) | Rb/Sr |
| 11701034 | SINCLAIR OIL & GAS CO. | LOUISA M JONES | 46 | W2 SE SW | 20 | 21N | 8E | 1962 or 1988 | 2945 | 961 | 2929 | 16 | -1968 | 36.27682 | -96.47240 | 1224 ± 51 Ma | Denison, (1981) | Rb/Sr |
| 14502643 | HENDERSON OIL CO | KELLEY | 1 | SW SW NW | 18 | 17N | 17E | 1965 | 2505 | 553 | 1828 | 677 | -1275 | 35.95263 | -95.54615 | 1299 ± 26 Ma | Denison, (1981) | Rb/Sr |

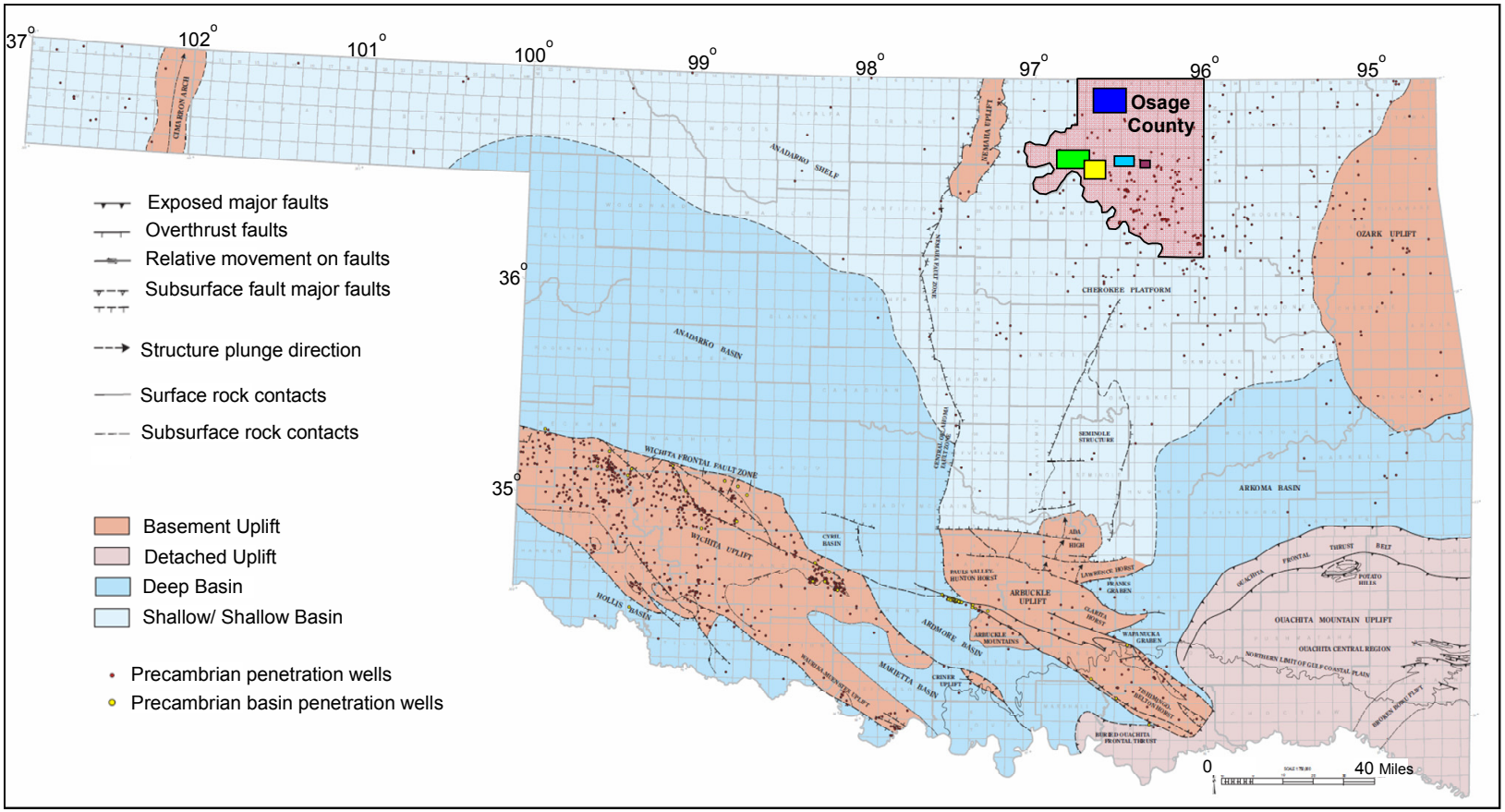


Figure 4.1. Map shows the major geologic province in Oklahoma, geologic boundaries, structural boundaries, the study area (Osage County), seismic data used for this study (colored boxes), and wells that penetrate the basement. Potential field anomalies around the Osage county, Nemaha uplift, and Anadarko basin were investigated. (Map adapted from Northcutt and Campbell, 1995 Map).

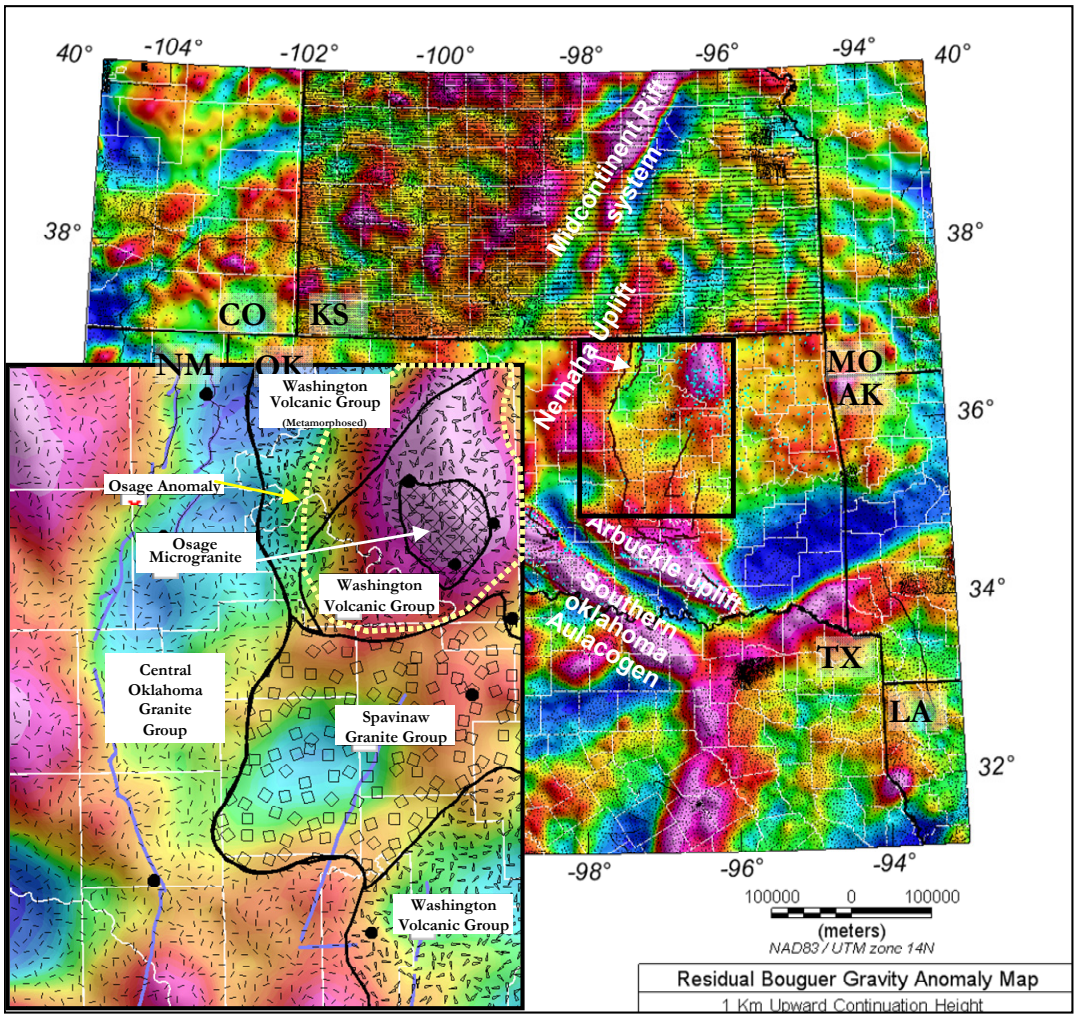


Figure 4.2. Simple residual Bouguer anomaly map of the Midcontinent United States. Inset map shows the basement rocks identified by wells in central Oklahoma overlain on residual Bouguer anomaly map. Dashed yellow line shows the outline of the Osage anomaly that lacks spatial correlation with regional structural geology. (See texts for description of the basement rocks). (Map modified after Denison's (1981) map of basement rocks in central Oklahoma). Inset map shows the Osage anomaly and gravity points collected in the summer of 2008 as part of dataset for this study. Black dots represent gravity stations. Pink-fault boundaries downloaded from (http://www.ogs.ou.edu/geolmapping.php )

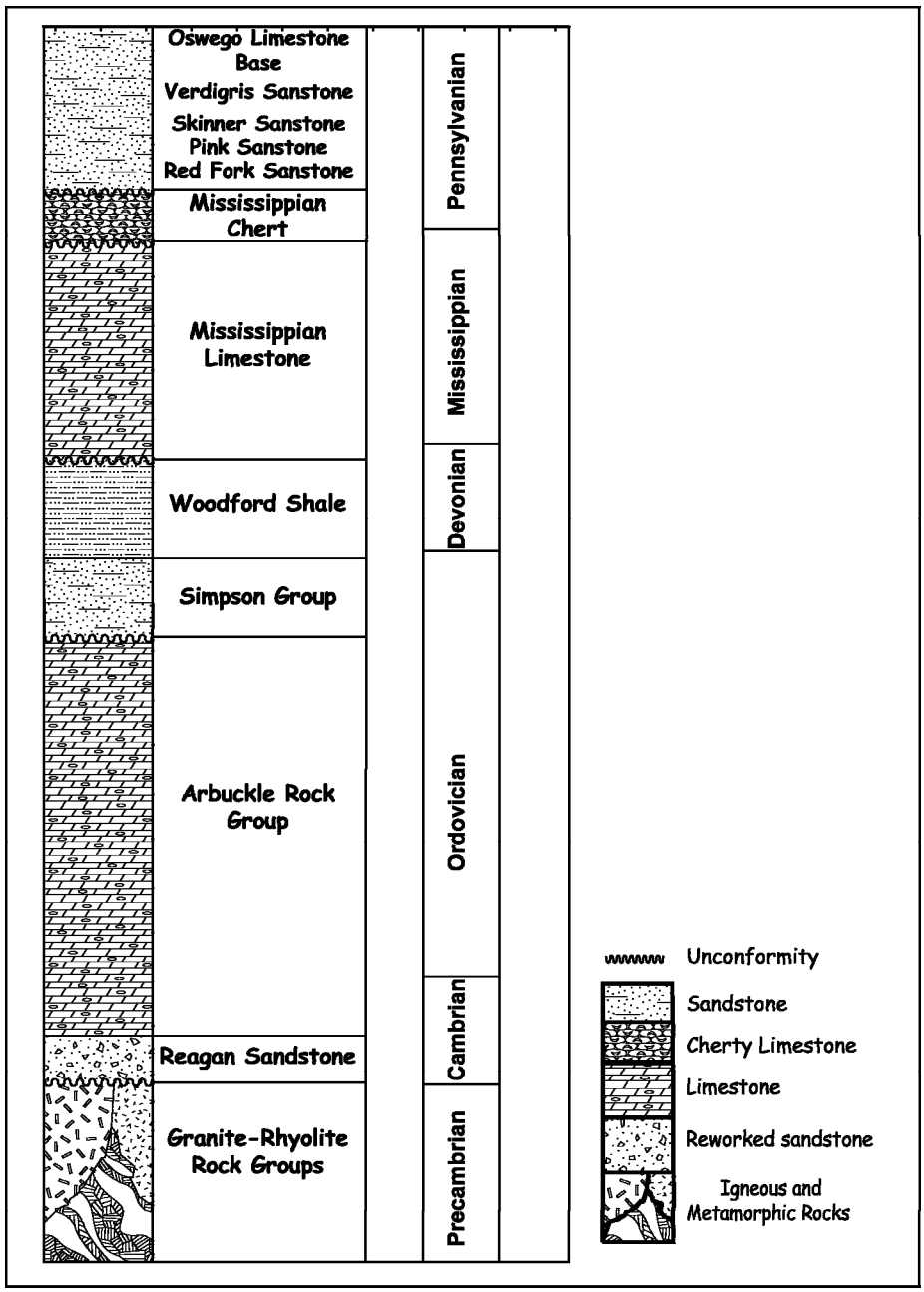


Figure 4.3. Schematic stratigraphic column for Osage County. Extracted from Zeller (1968), Thorman and Hibpshman (1979), and Franseen (2004).

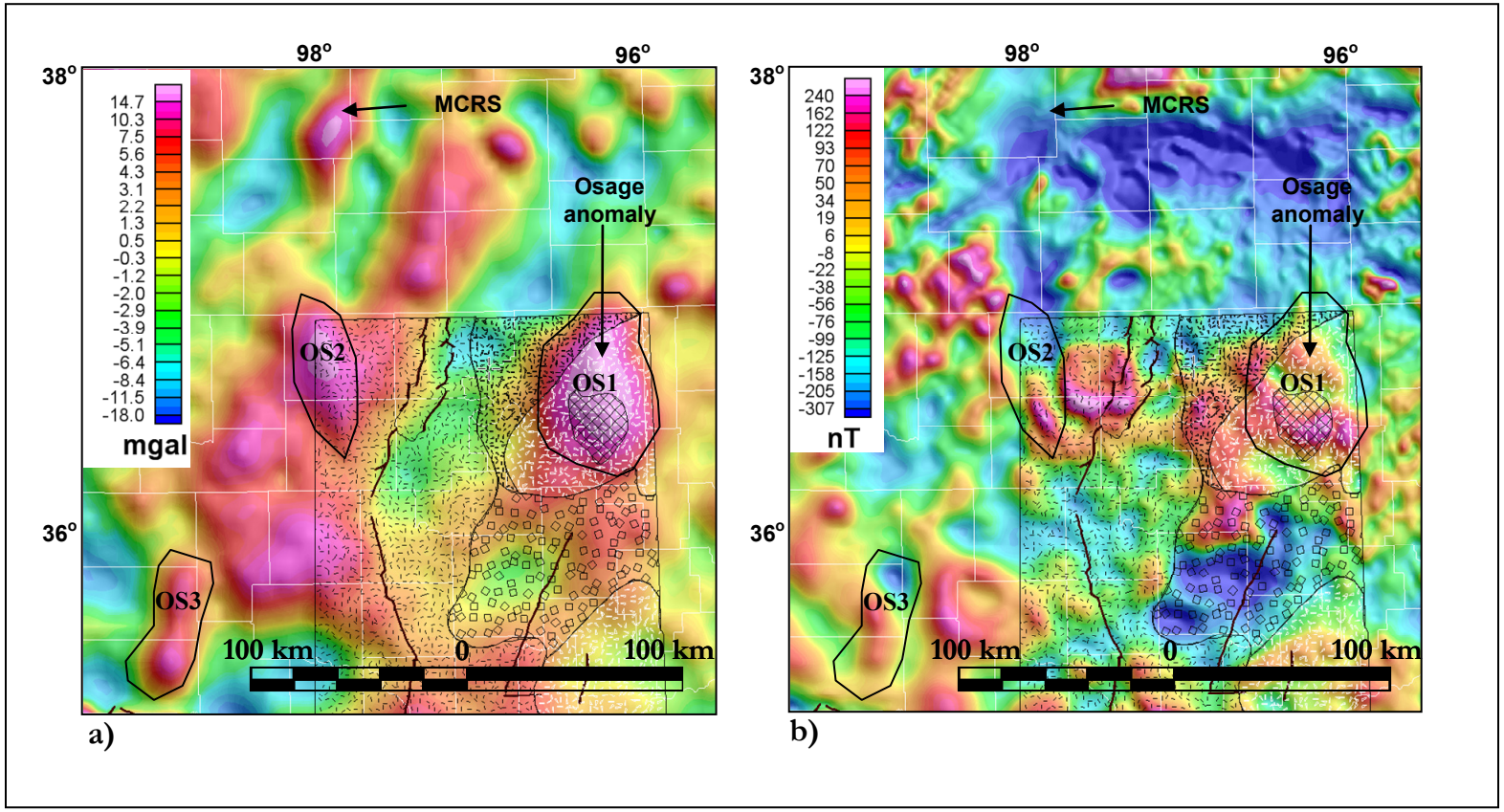


Figure 4.4. (a) Residual Bouguer anomaly map (b) Total magnetic intensity (TMI) map showing the relic of the MRS, Osage anomaly, other anomalies investigated in this study, as well as the Precambrian basement geology of Osage County. Magnetic anomaly over the anomalies and the relics of the MCRS are complex and inconclusive when compared with the gravity anomaly in (a).

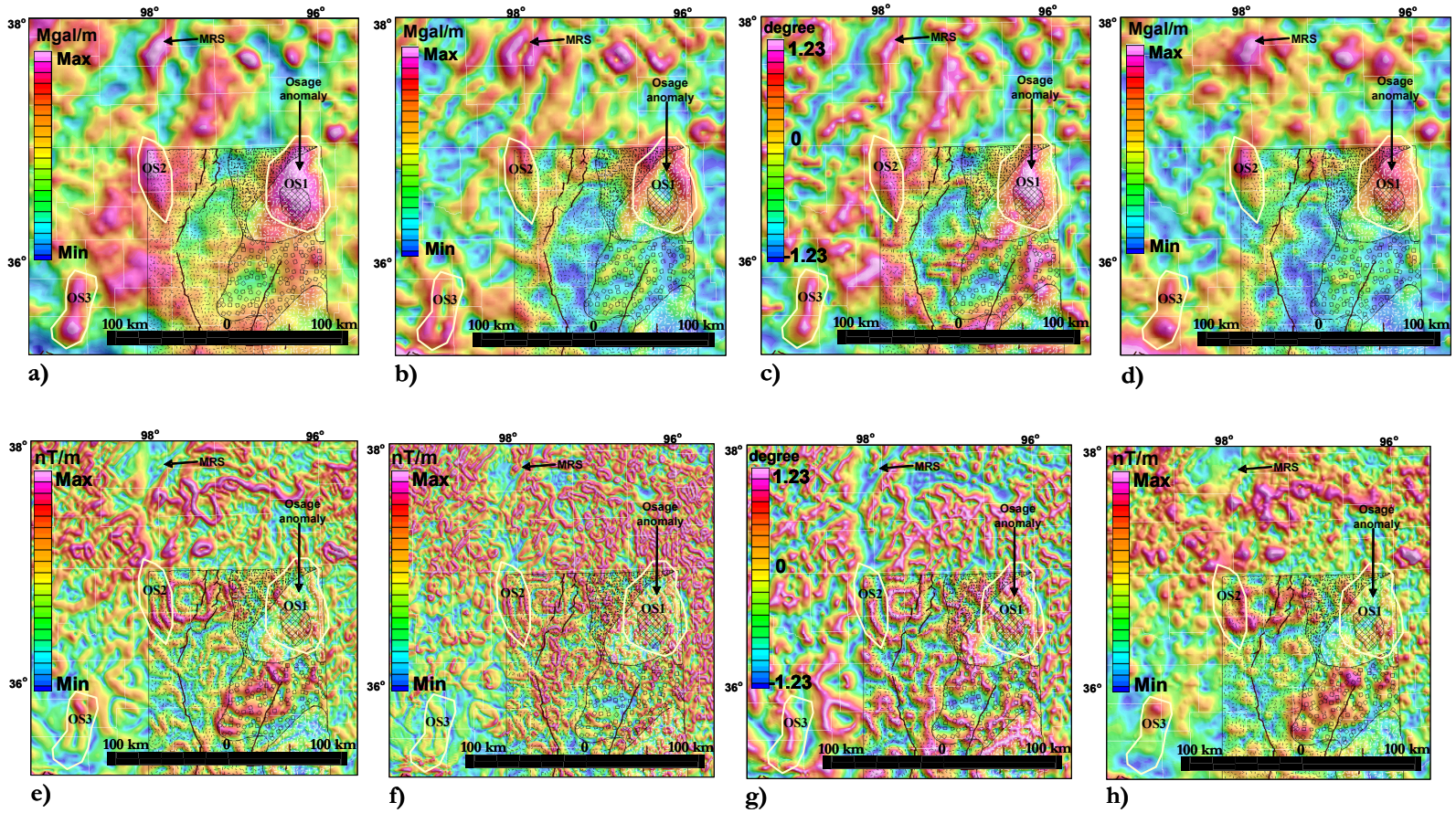


Figure 4.5. Derivative maps computed on the residual gravity grid. (a) First vertical derivative (b) Horizontal gradient magnitude (c) Tilt derivative and (d) Analytical signal. Corresponding derivative maps on TMI anomaly grid. (e) Horizontal gradient magnitude (f) Horizontal derivative of the tilt derivative (g) Tilt derivative and (h) Analytical signal. (See text for interpretation).

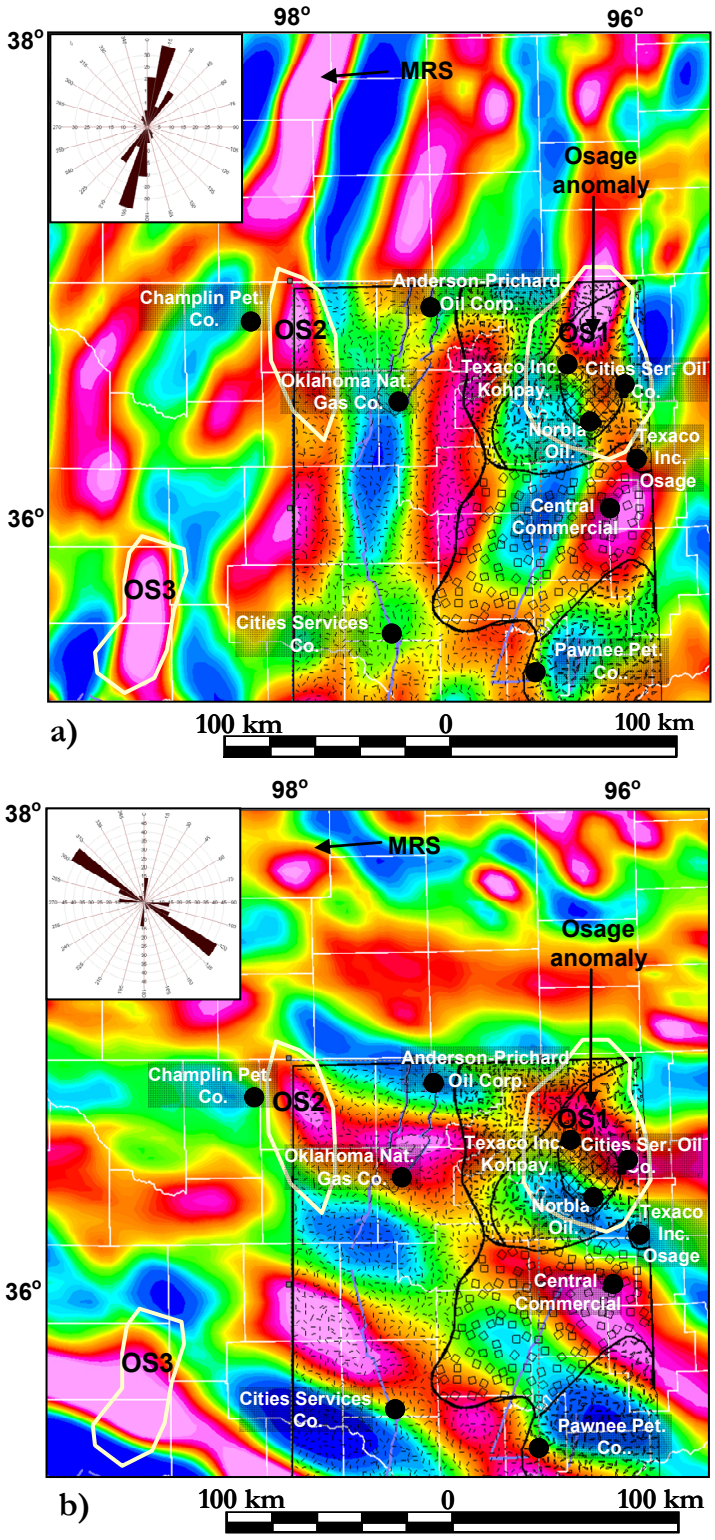


Figure 4.6. Directional filter of the 90 km high-pass filtered Bouguer anomaly map that enhances (a) northeast structures related to the MRS and (b) northwest structures. Age dating from Precambrian well (black dots) were from Van Schmus et al.'s (1993) and Denison's (1981) work. Inset map shows rose diagram showing anomaly trends (a) northwest and (b) northeast

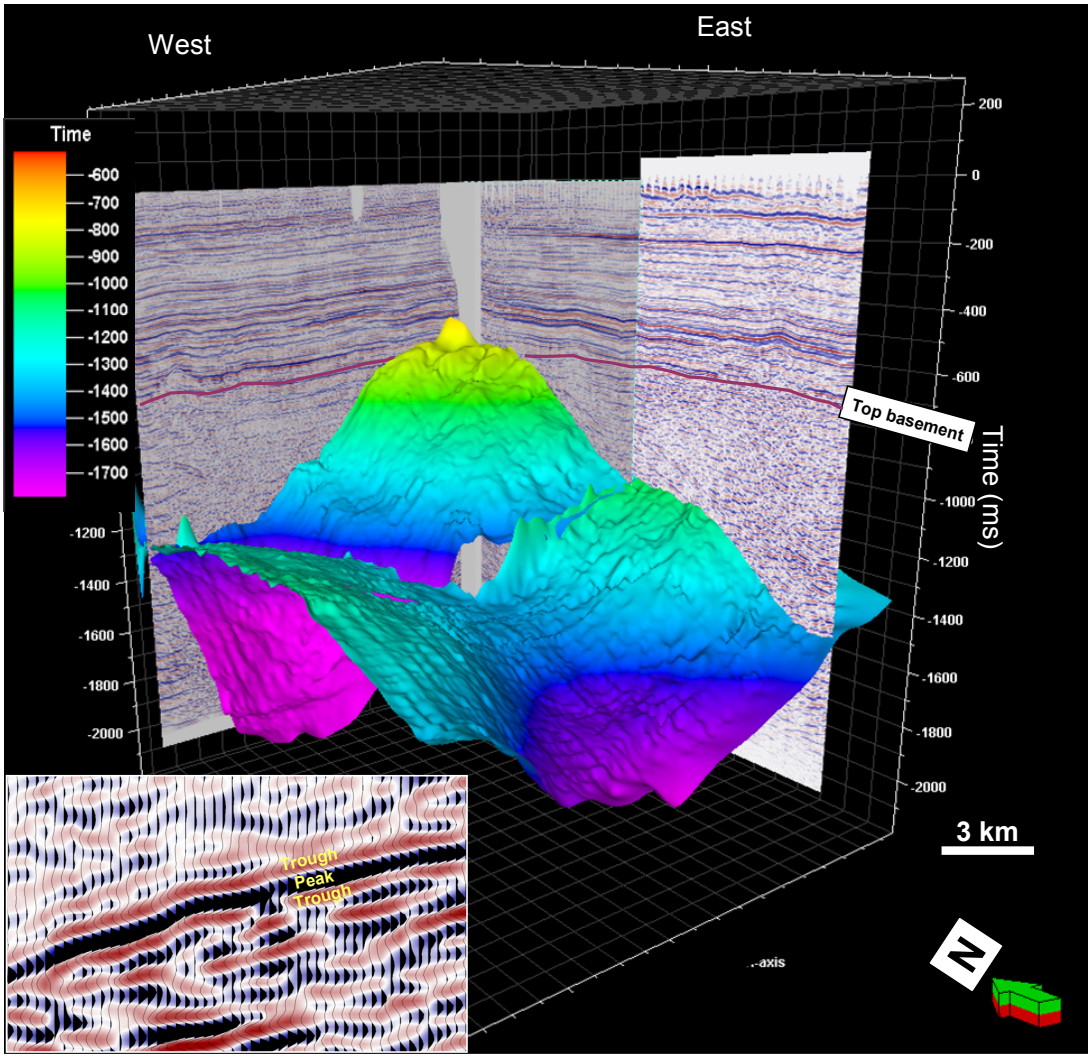


Figure 4.7. 3D Visualization of seismic data from Osage county showing the geometry of intra-basement reflectors beneath the nearly horizontal Paleozoic section. Inset shows the top of the intra-basement reflector and polarity of one of the seismic lines.

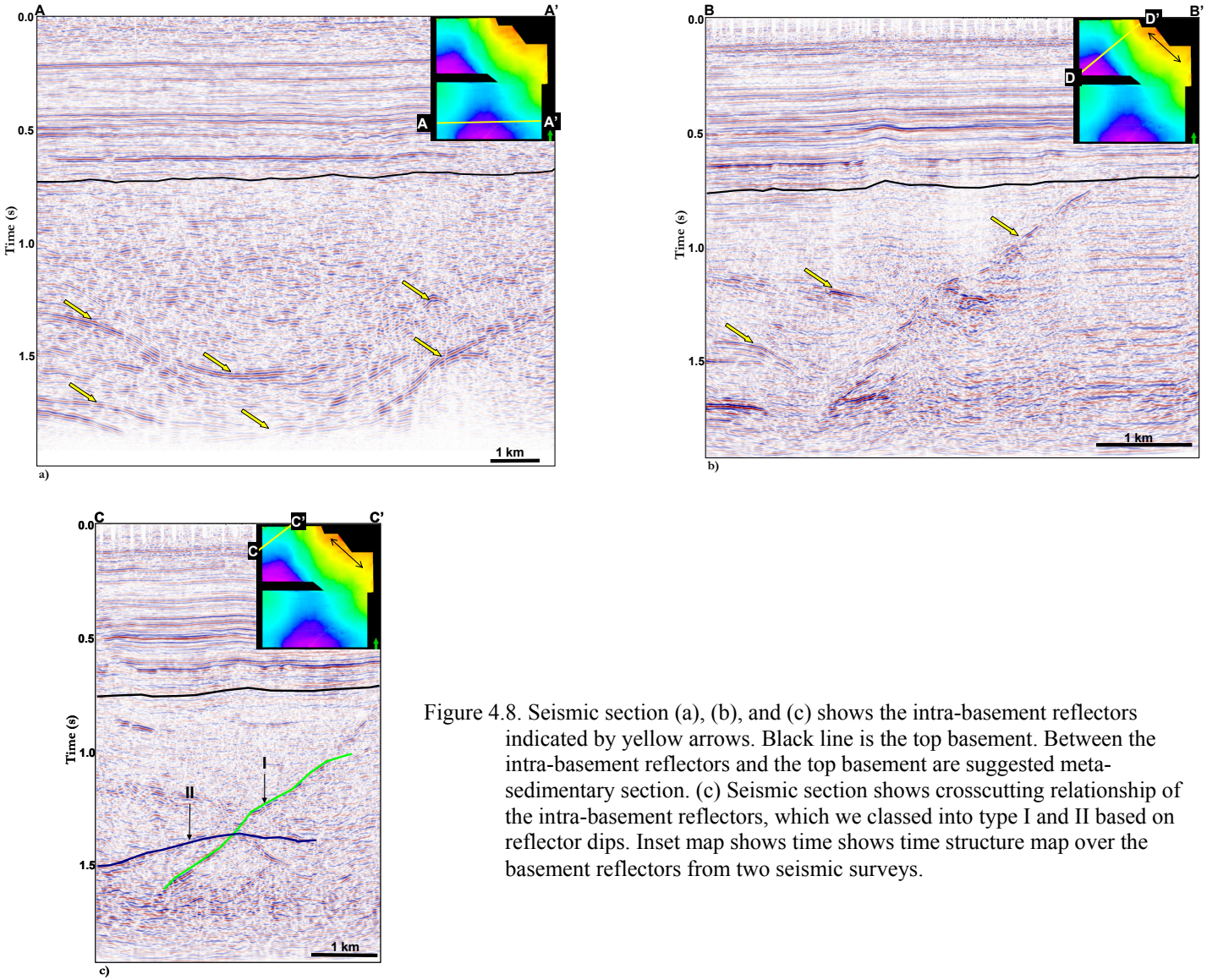


Figure 4.8. Seismic section (a), (b), and (c) shows the intra-basement reflectors indicated by yellow arrows. Black line is the top basement. Between the intra-basement reflectors and the top basement are suggested meta-sedimentary section. (c) Seismic section shows crosscutting relationship of the intra-basement reflectors, which we classed into type I and II based on reflector dips. Inset map shows time shows time structure map over the basement reflectors from two seismic surveys.

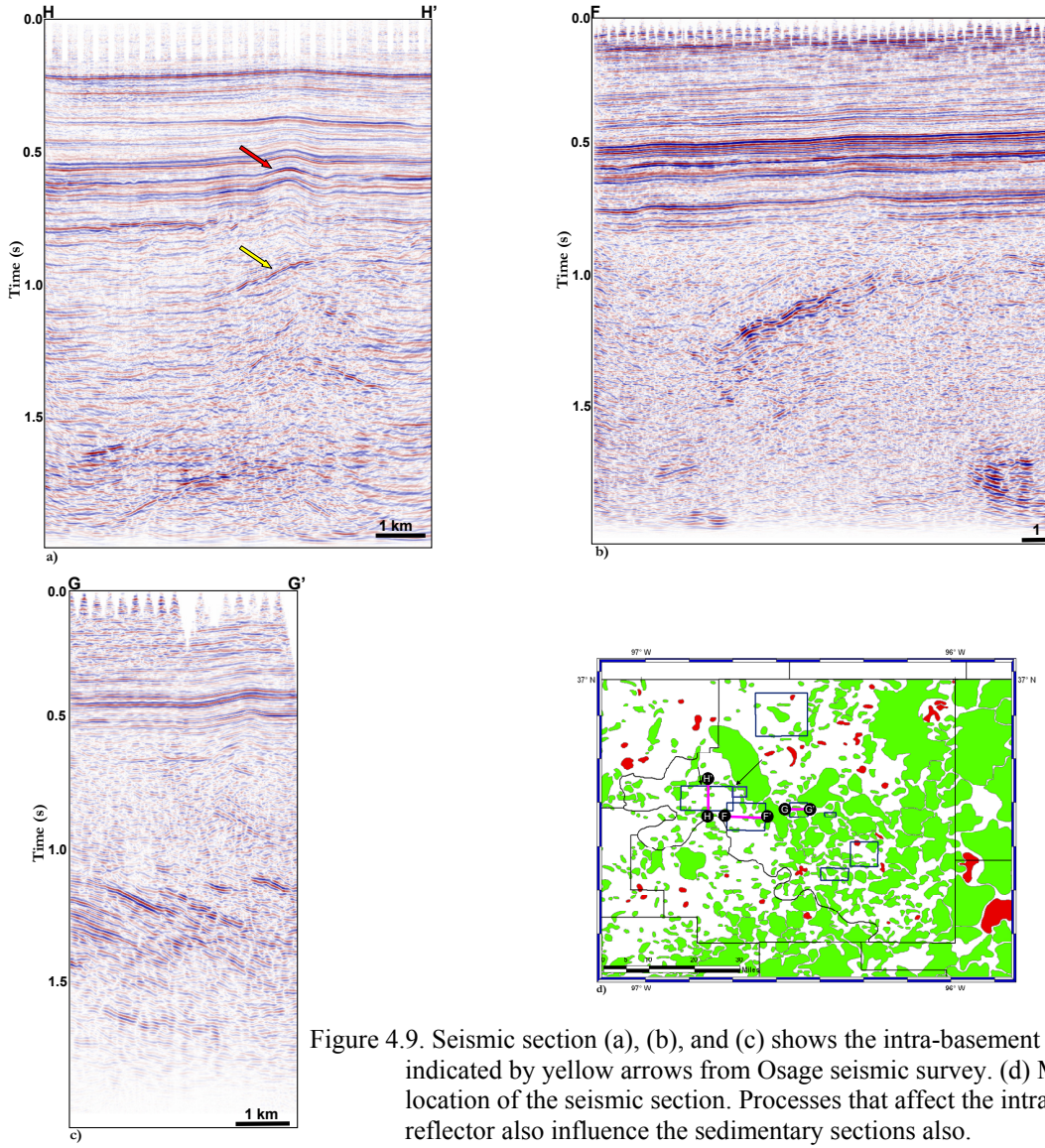


Figure 4.9. Seismic section (a), (b), and (c) shows the intra-basement reflectors indicated by yellow arrows from Osage seismic survey. (d) Map showing the location of the seismic section. Processes that affect the intra-basement reflector also influence the sedimentary sections also.

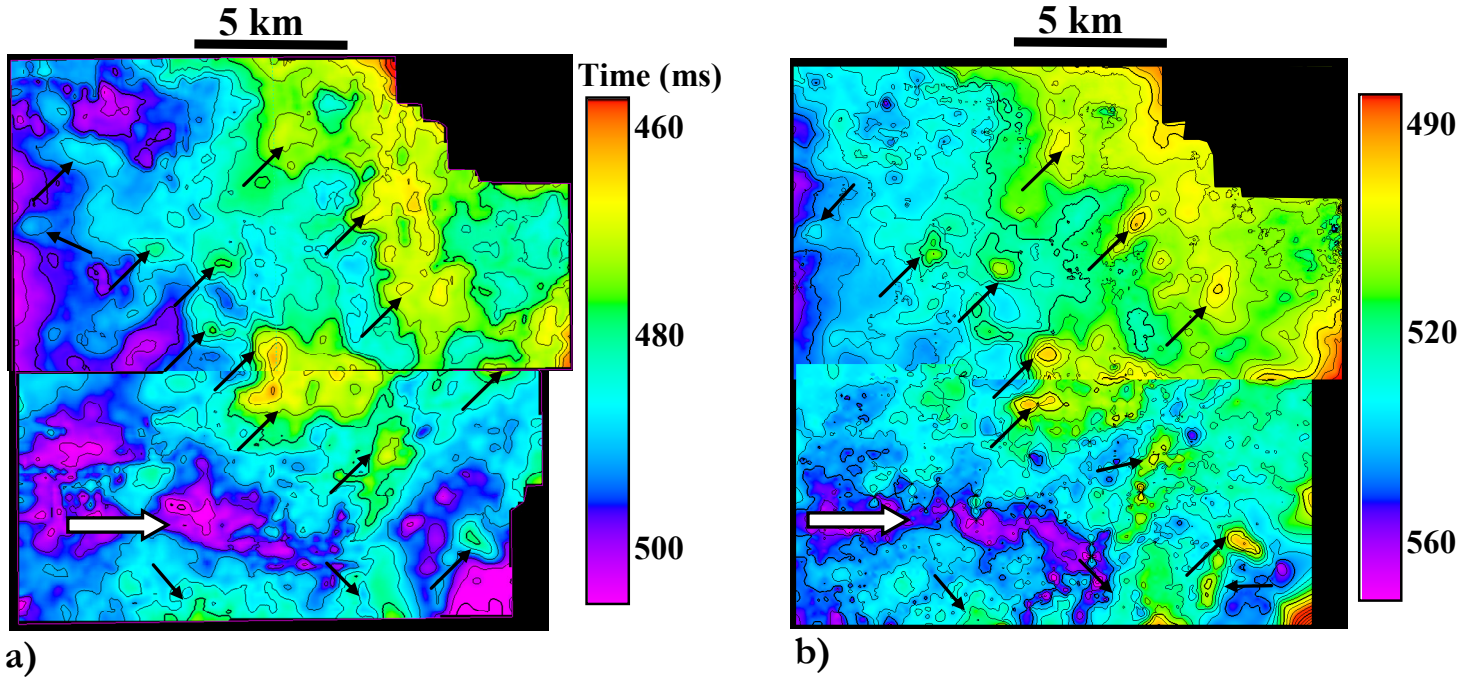


Figure 4.10. Time structure map on (a) the Mississippi Chert and (b) top of Arbuckle Group from two Osage county surveys. Map shows a general southeast dipping undulating and irregular surface. Features marked with black arrows suggest residual hills associated with a karsted carbonate region.

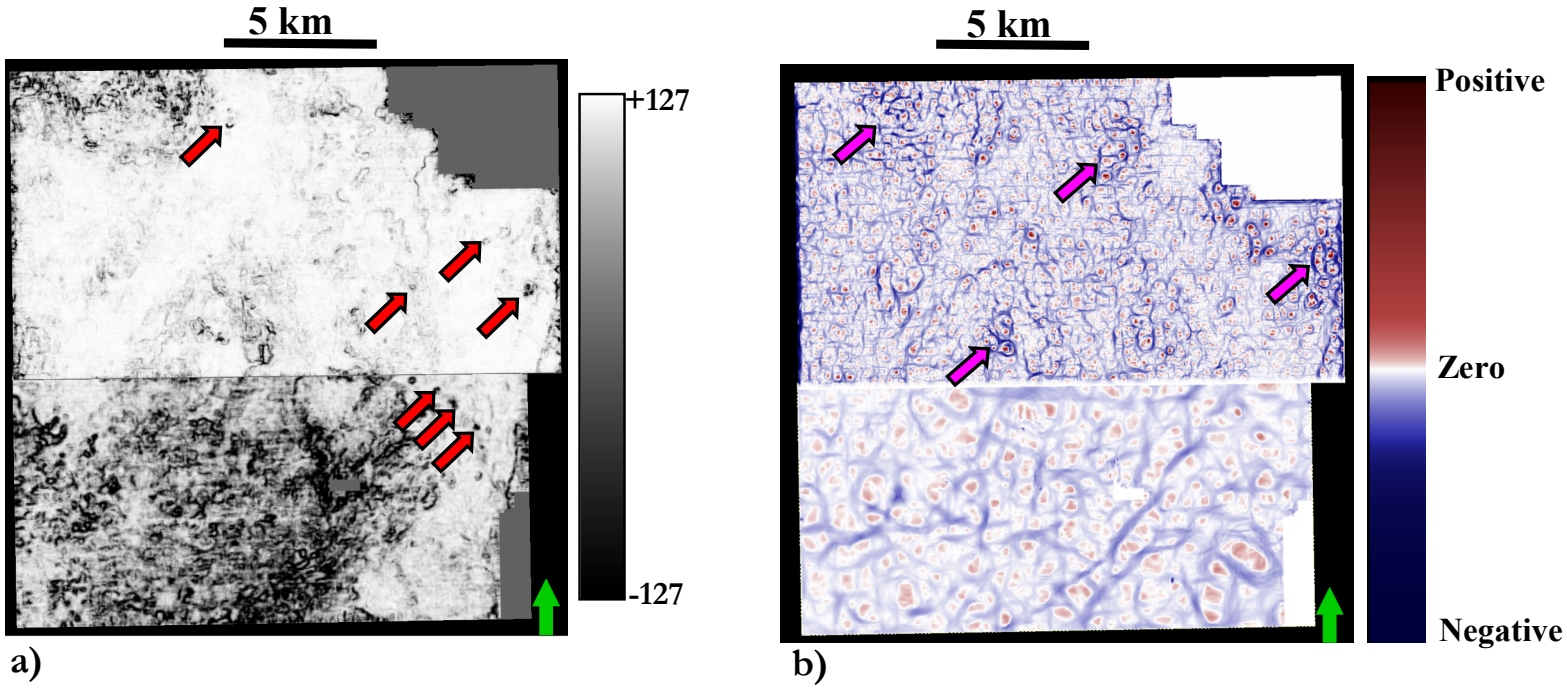


Figure 4.11. (a) Coherence and (b) most-negative curvature horizon slice along Mississippi Chert from two Osage county surveys with overlain time-structure contours. Red-arrows indicate the location of collapse features, magenta-arrows indicate networks of fracture lineaments enhanced by curvature attributes. Circular features dominate curvature along the Mississippi Chert and no preferred order of lineament is identified.

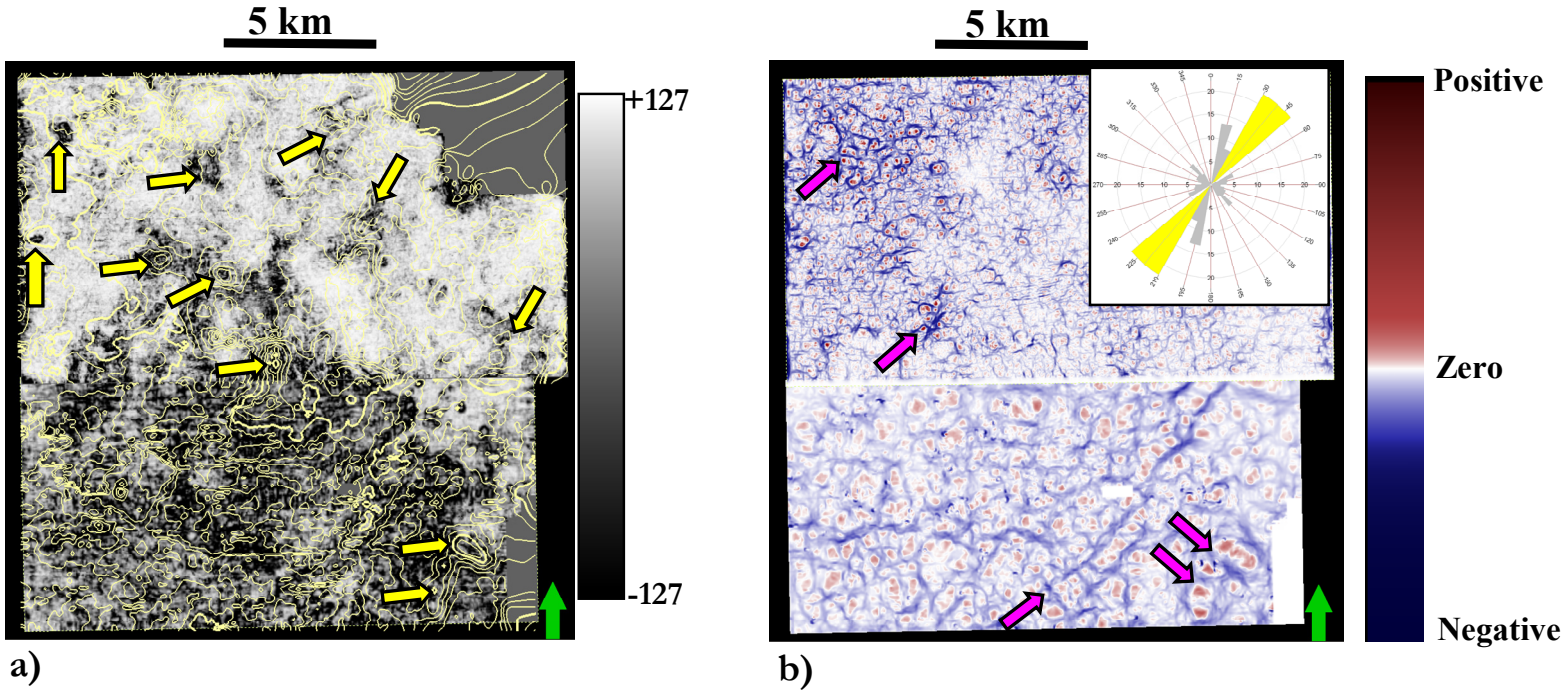


Figure 4.12. (a) Coherence and (b) most-negative curvature horizon slice at the top of Arbuckle Group from two Osage county surveys with overlain time-structure contour. Magenta-arrows indicate networks of fracture lineaments enhanced by curvature attributes, and yellow arrows indicate low coherence feature that spatially correlate with structurally high area. We manually mapped these lineaments to generate the inset rose diagram shown in Figure 4.12b. Inset rose diagram show lineaments orientation and density, which increases below Arbuckle Group (see Figure 4.13. Anomalous northeast trending lineament (yellow petal) on the rose diagram correspond to the northeast trending lineament that we interpreted as fault located on the southeast corner of the lower survey.

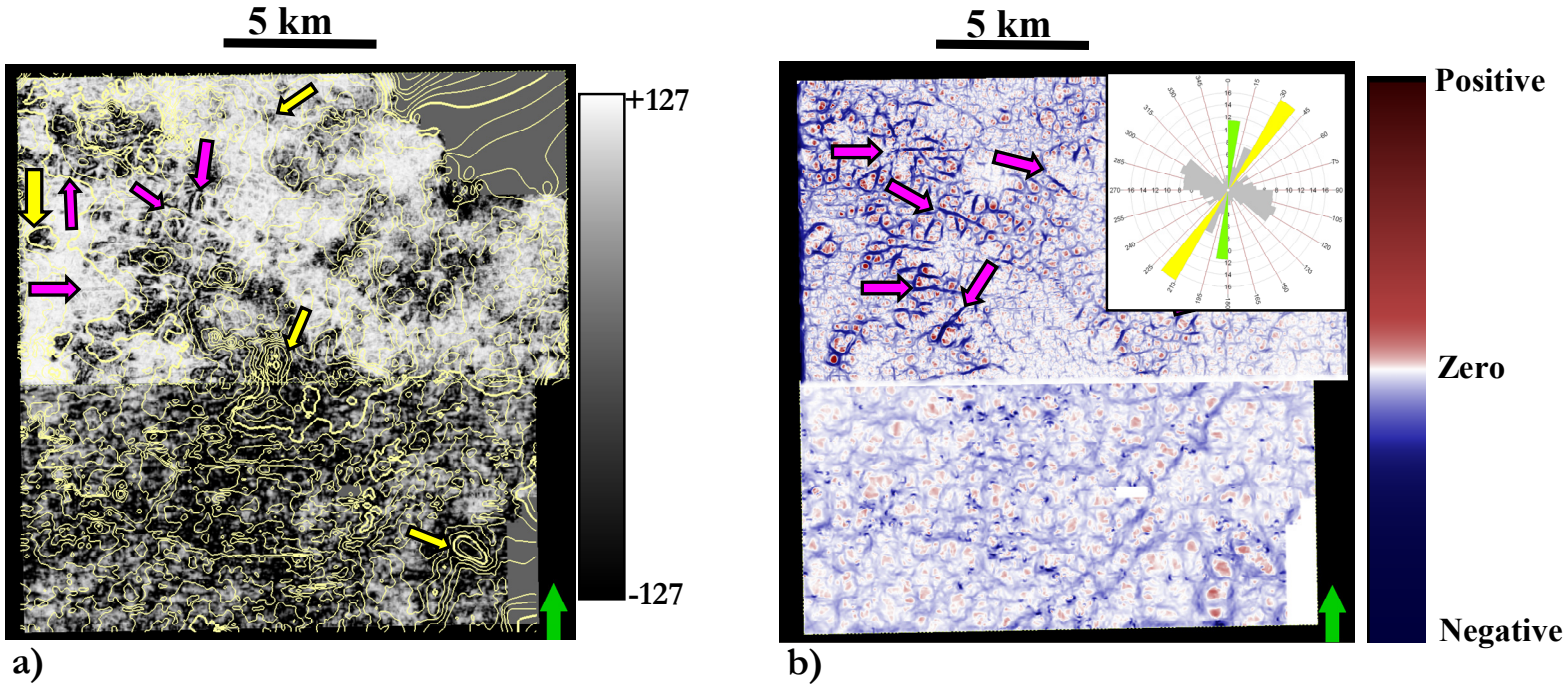


Figure 4.13. (a) Coherence and (b) most-negative curvature horizon slice below Arbuckle Chert from two Osage county surveys with overlain time-structure contour. Magenta-arrows indicate networks of fracture lineaments enhanced by curvature attributes, and yellow arrows indicate low coherence feature that spatially correlate with structurally high area. We manually mapped these lineaments to generate the inset rose diagram shown in Figure 4.13b. Circular features dominate curvature along the Mississippi Chert and no preferred order of lineament is identified. Inset rose diagram show lineaments orientation and density, which increases below Arbuckle Group. Anomalous northeast trending lineament (yellow petal) on the rose diagram correspond to the northeast trending lineament that we interpreted as fault located on the southeast corner of the lower survey.

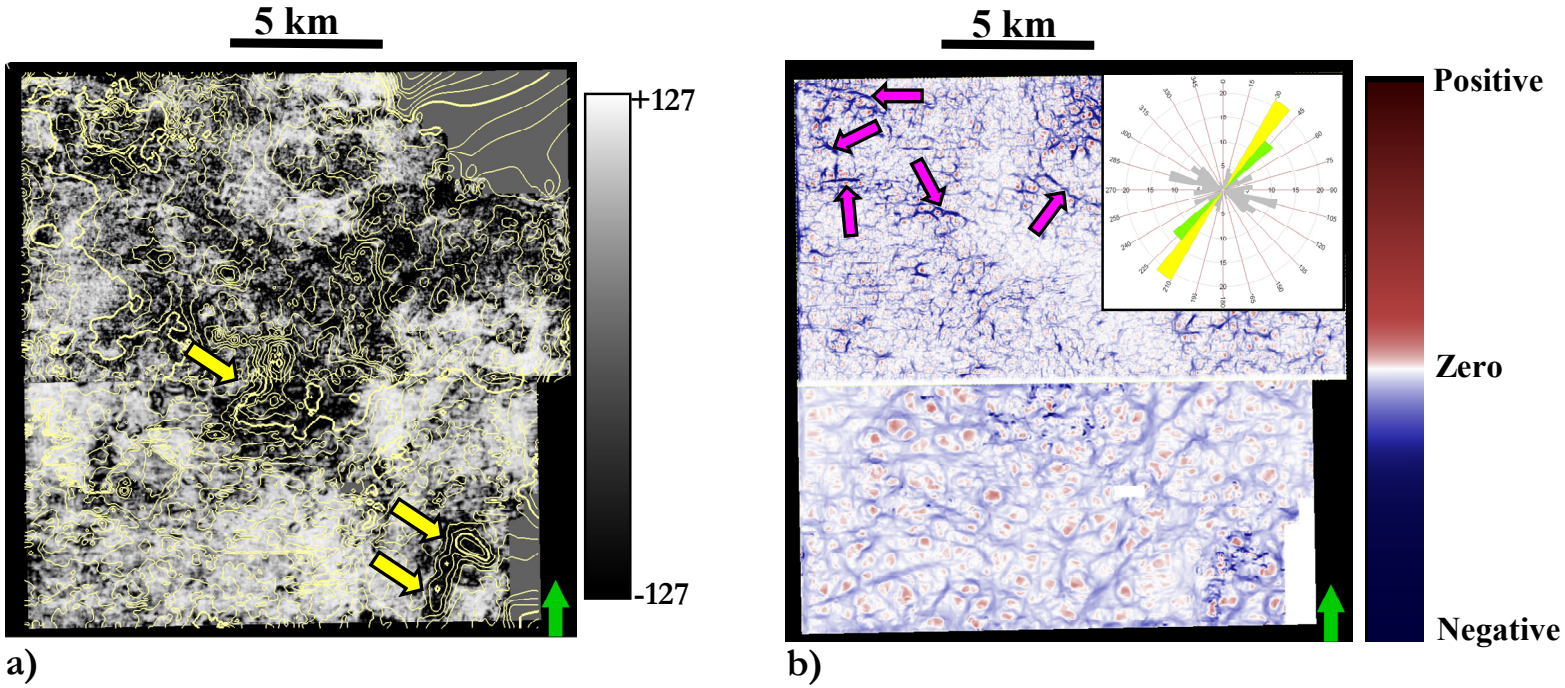


Figure 4.14. (a) Coherence and (b) most-negative curvature horizon slice near the Reagan Sandstone from two Osage county surveys with overlain time-structure contour. Red-arrows indicate the location of collapse features, magenta-arrows indicate networks of fracture lineaments enhanced by curvature attributes, and yellow arrows indicate low coherence feature that spatially correlate with structurally high area. We manually mapped these lineaments to generate the inset rose diagram shown in Figure 4.11f-h. Circular features dominate curvature along the Mississippi Chert and no preferred order of lineament is identified. Inset rose diagram show lineaments orientation and density, which increases below Arbuckle Chert. Anomalous northeast trending lineament (yellow petal) on the rose diagram correspond to the northeast trending lineament that we interpreted as fault located on the southeast corner of the lower survey. Toward the Reagan sandstone and the basement, the density of the northwest trending lineaments diminishes.

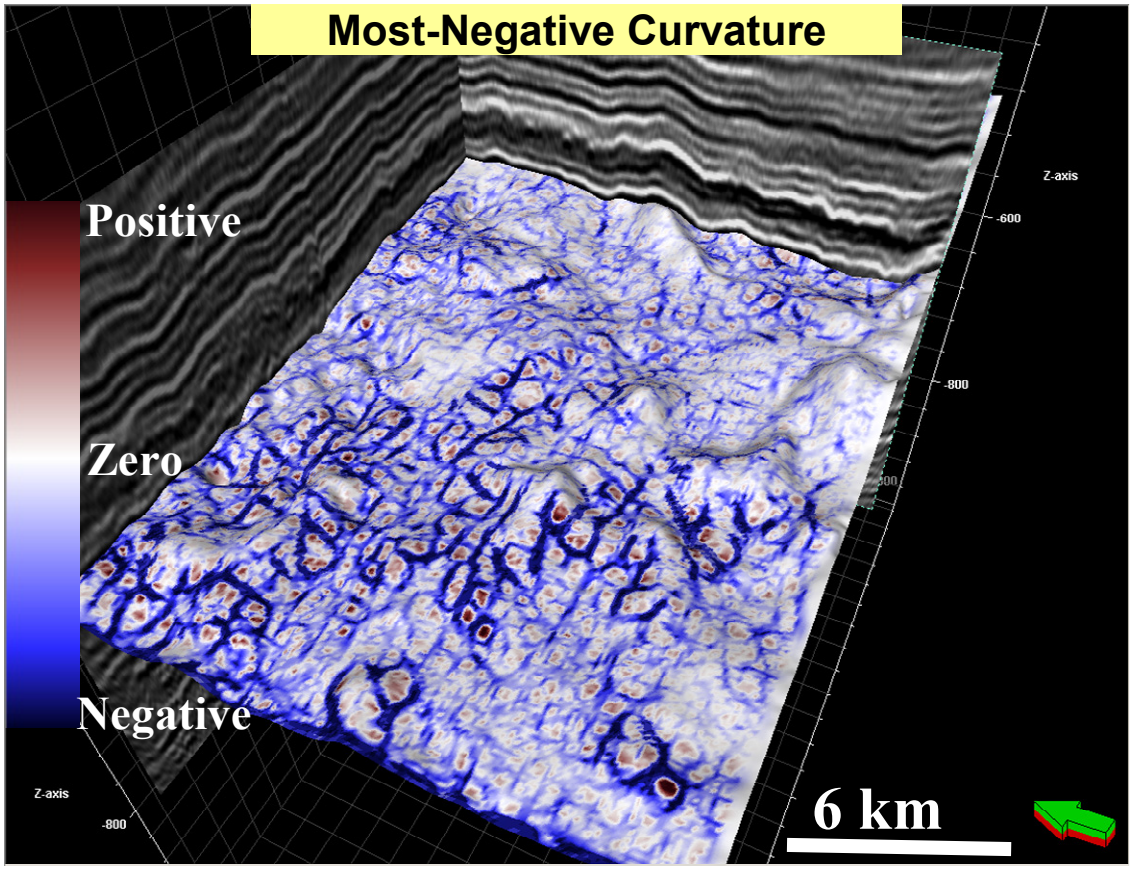


Figure 4.15. Most-negative curvature attribute extracted below the top Arbuckle Group. This attribute show the polygonal shape of the lineaments.

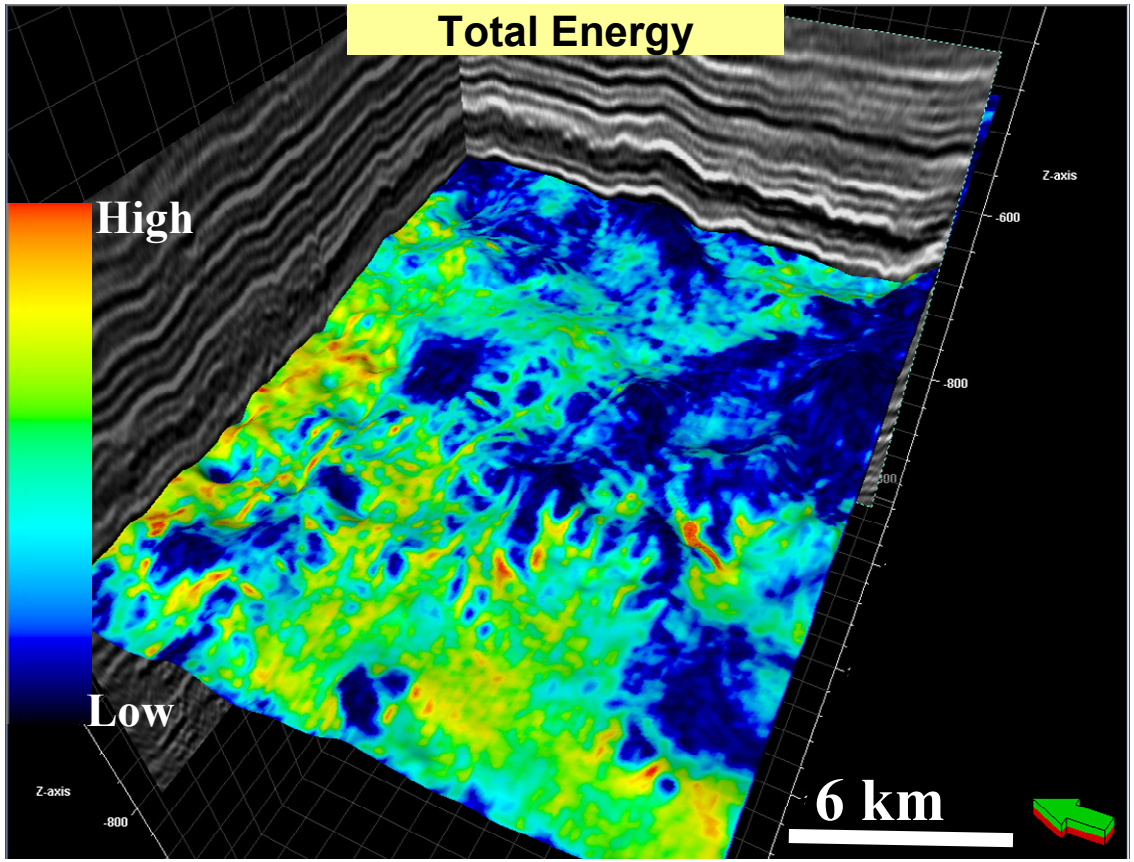


Figure 4.16. Total energy attribute extracted below the top Arbuckle Group. This attribute show the high amplitude nature of the lineaments.

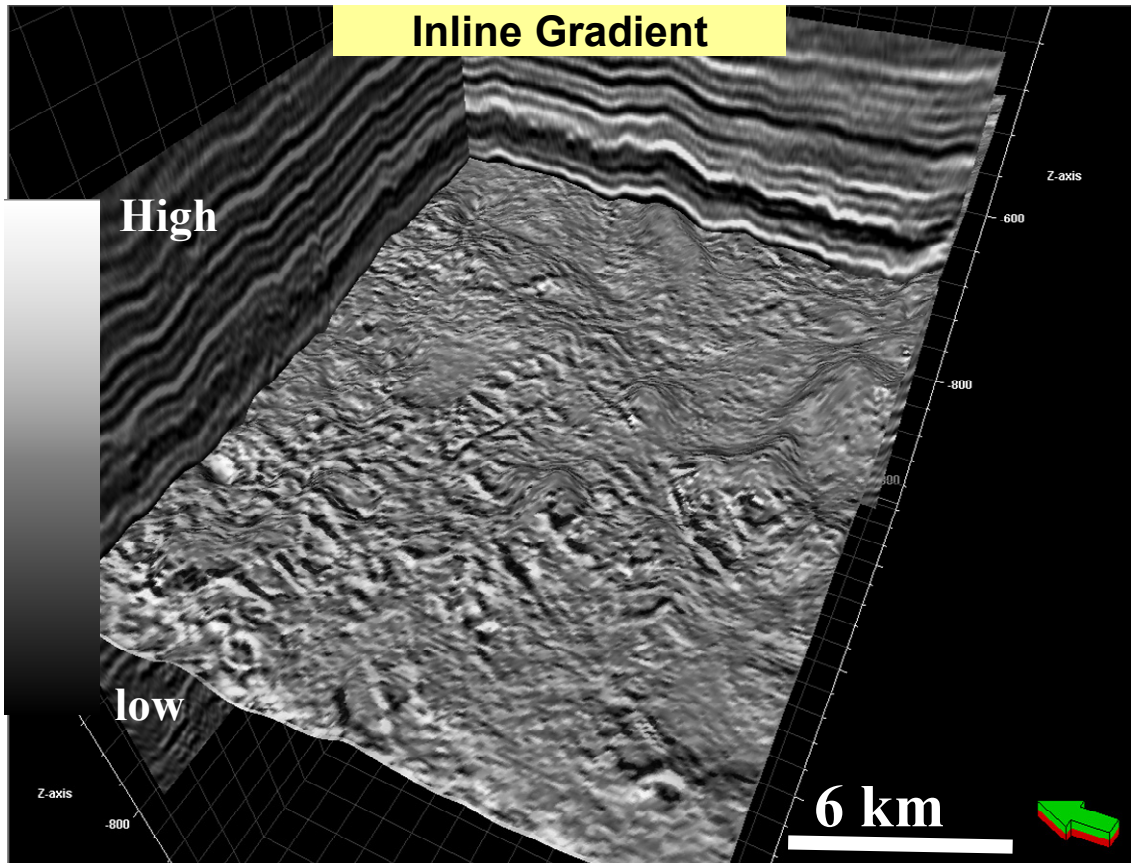


Figure 4.17. Inline gradient extracted below the top Arbuckle Group. This attribute show the polygonal shape of the lineaments.

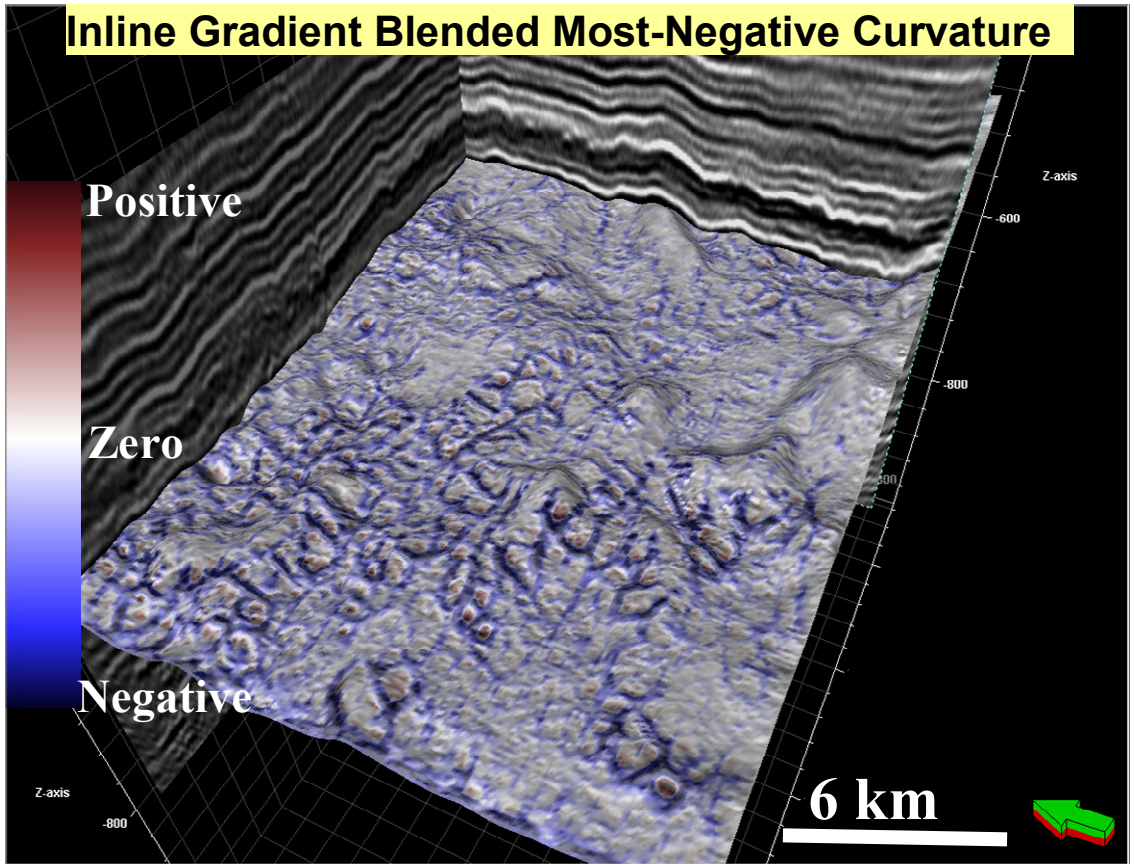


Figure 4.18. Co-rendering most-negative attributes with inline gradient. This attribute combination better enhances the lineaments shape with added benefit of a shaded relief display.

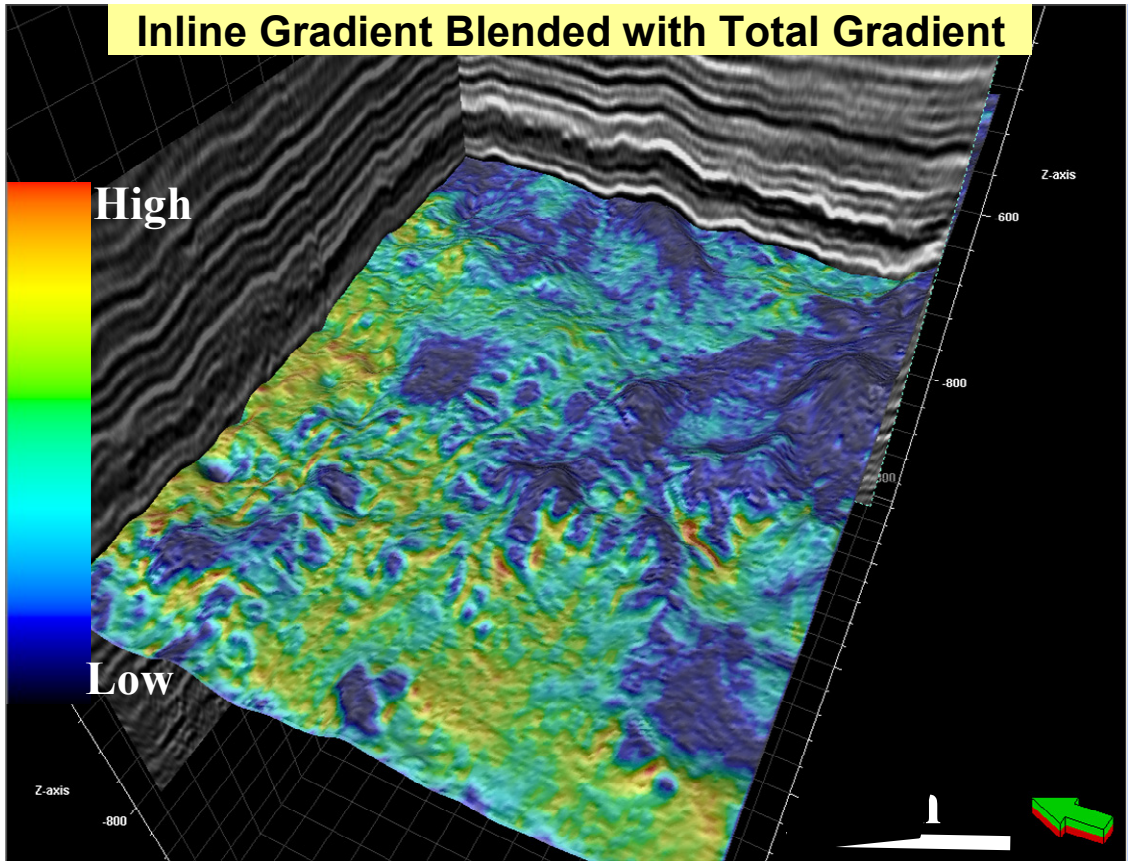


Figure 4.19. Co-rendering total gradient attributes with inline gradient. This attribute combination better enhances the lineaments amplitude with added benefit of a shaded relief display.

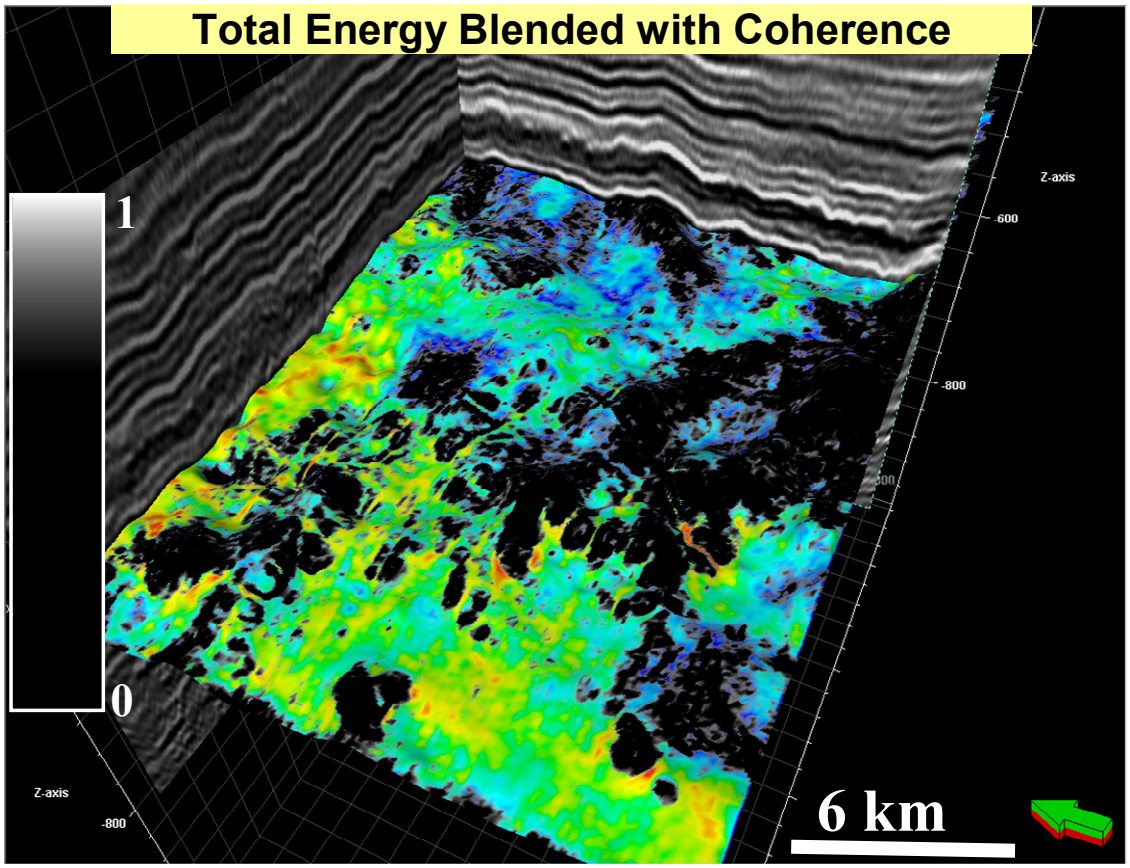


Figure 4.20. Co-rendering coherence attributes with inline gradient. This attribute combination better enhances the lineaments coherent nature with added benefit of a shaded relief display.

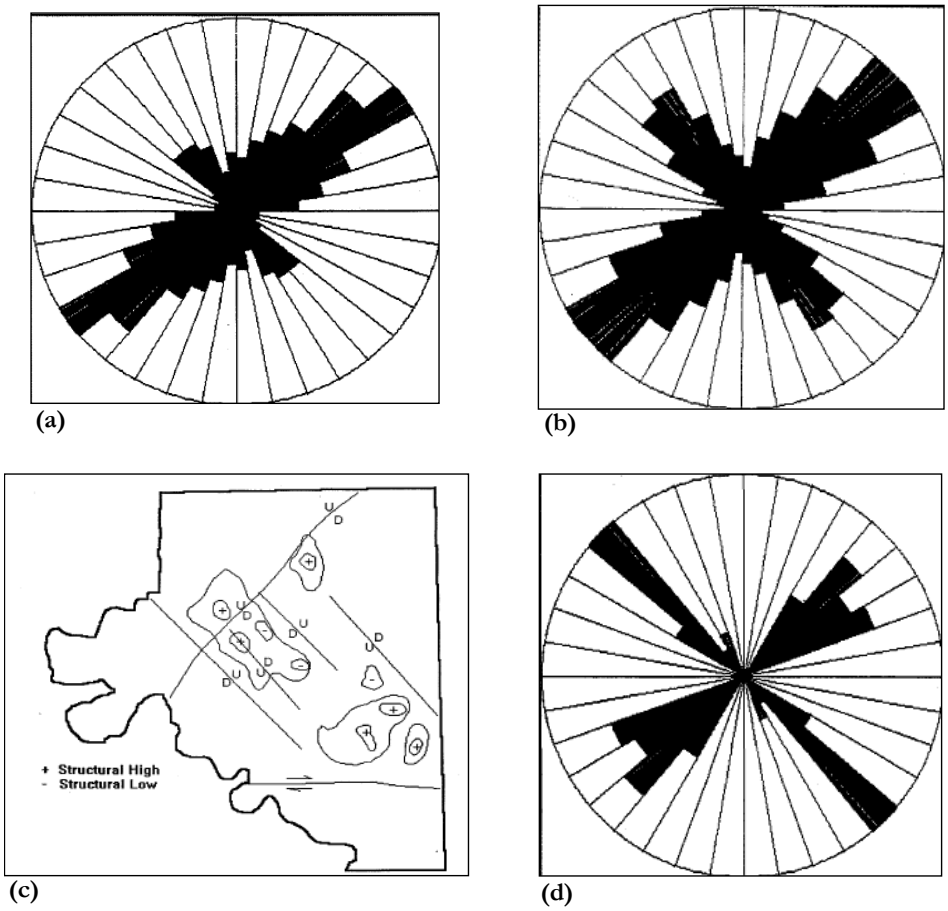


Figure 4.21. Rose diagrams showing the lineaments trend computed from aerial photograph and satellite images of (a) surface and (b) subsurface structures within the Osage County. (c) Schematic diagram shows the trend of structures within the Precambrian basement. (d) Major lineament trend within the Osage County trends northeast-southwest and northeast-southeast (Adapted from Guo and Carroll, 1999).

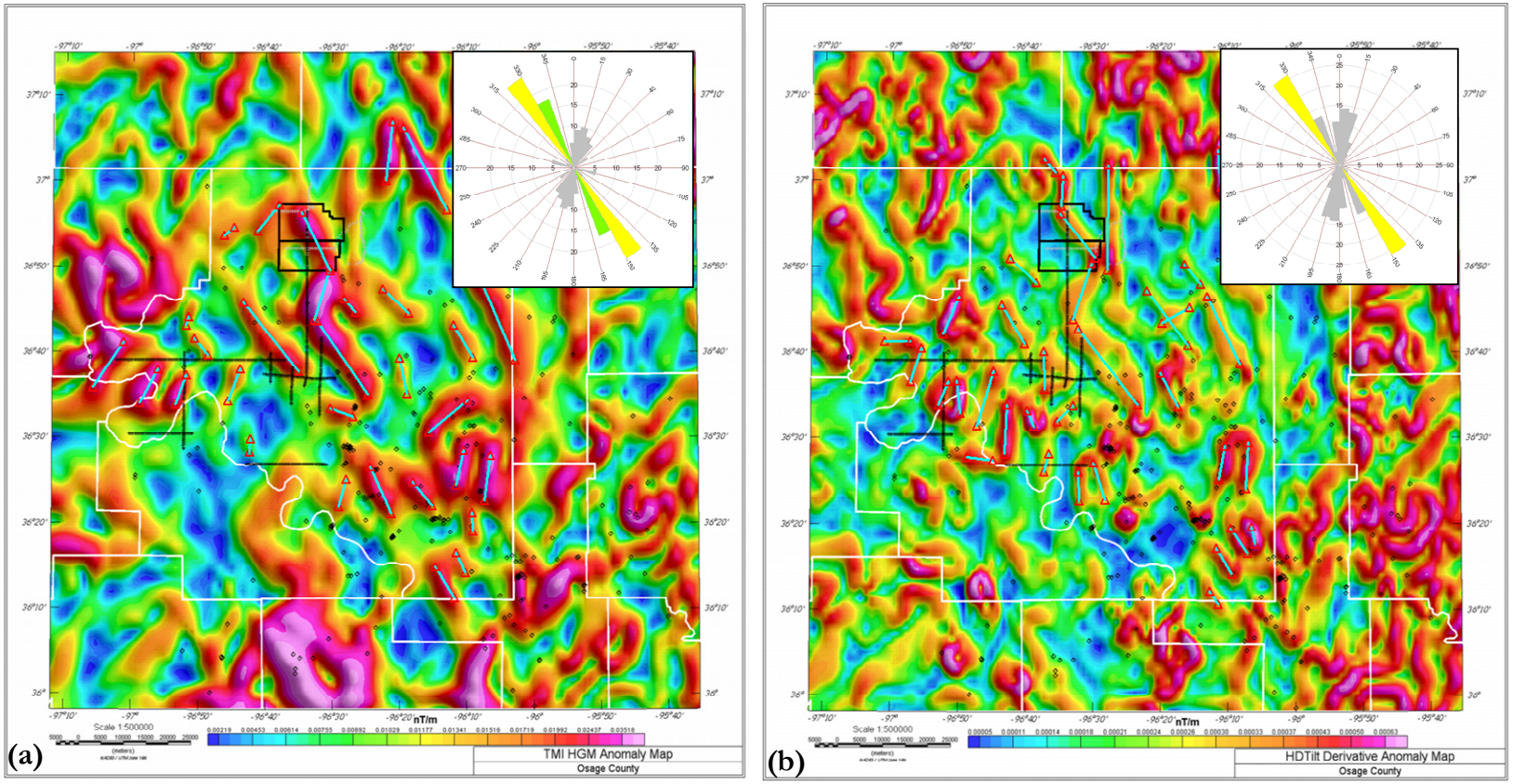


Figure 4.22. (a) Horizontal gradient magnitude and (b) horizontal derivative of the tilt derivative map with corresponding rose diagrams showing Precambrian structural trends.

## 4.11 Reference


Adams, D. C., and G.R. Keller, 1994, Possible extension of the Midcontinent Rift in west Texas and eastern New Mexico: Canadian Journal of Earth Science, **31**, 709-720.

Anderson, R. A., and R.M. McKay, 1989, Clastic rocks associated with the Midcontinent Rift System in Iowa: United State Geological Survey Bulletin **1989-I**.

Bass, N. W., 1942, Summary of subsurface geology with special reference to oil and gas - Part II: U.S. Geological Survey Bulletin, **900-K**, 343-393.

Berendsen, P., 1997, Tectonic evolution of the Midcontinent Rift System in Kansa, *in* R. W. Ojakangas, A.B. Dickas, and J.C. Green, ed., Middle Proterozoic to Cambrian rifting, Central North America: Geological Society of America, Geological Society of America Special Paper **312**, 235-241.

Bickford, M. E., W. R. Van Schmus, and I. Zietz, 1986, Proterozoic history of the midcontinent region of North America: Geology, **14**, 492-496.

Bickford, M. E., 1988, The formation of continental crust: Part 1. A review of some principles: Part 2. An application to the Proterozoic evolution of southern North America: Geological Society of America Bulletin, **100**, 1275-1391.

Blakely, R. J., 1996, Potential theory in gravity and magnetic applications: Cambridge University Press.

Cansler, J. R., and T.R. Carr, 2001, Paleogeomorphology of the sub-Pennsylvanian unconformity of the Arbuckle Group (Cambrian- Lower Ordovician): Kansas Geological Survey 2001-55.

Chenoweth, P. A., 1968, Early Paleozoic (Arbuckle) overlap, southern Mid-Continent, United States: American Association of Petroleum Geologists Bulletin, **52**, 1670-1688.

Chopra, S., and K.J. Marfurt, 2007, Seismic Attributes for Prospect Identification and Reservoir Characterization, *in* S. J. Hills, ed., Society of Exploration Geophysicists Geophysical Development Series No. **11**.

Cook, K. I., 1956, Regional gravity survey in northeastern Oklahoma and southeastern Kansas: Geophysics, **21**, 88-106.

Davies, G. R., and L.B. Smith Jr., 2006, Structurally controlled hydrothermal dolomite reservoir facies: An overview: American Association of Petroleum Geologists Bulletin, **90**, 1641-1690.

Denison, R. E., E.A. Hetherington Jr., and G.S. Kenny, 1966, Isotopic-age dates from basement rocks in Oklahoma: Oklahoma Geology Notes, **26**, 170-176.

Denison, R. E., 1981, Basement rocks in northeastern Oklahoma: Oklahoma Geological Survey Circular, **84**, 1-84.

Ewing, T. E., 1991, The tectonic framework of Texas: The University of Texas at Austin.

Franseen, E. K., A.P. Byrnes, J.R. Cansler, D.M. Steinhauff, and T.R. Carr, 2004, The geology of Kansas - Arbuckle Group: Kansas Geological Survey - Current Research in Earth Science, **250**.

Fu, D. T., E.C. Sullivan, and K.J. Marfurt, 2006, Rock-Property and seismic-attribute analysis of a chert reservoir in the Devonian Thirty-one Formation, West Texas, U.S.A.: Geophysics, **71**, B151-B158.

Grauch, V. J. S., and L. Cordell, 1987, Limitation of determining density or magnetic boundaries from the horizontal gradient of gravity or pseudogravity data: Geophysics, **52**, 118-121.

Guo, G., and H.B. Carroll, 1999, A new methodology for oil and gas exploration using remote sensing data and surface fracture analysis: Prepared for United States Department of Energy, Assistant Secretary for Fossil Energy.

Hansen, D. M., J.A. Cartwright, and D. Thomas, 2004, 3D seismic analysis of the geometry of igneous sills and sill junction relationships, *in* R. J. Davies, J.A. Cartwright, S.A. Stewart, M. Lappin, and J.R. Underhill, ed., 3D Seismic Technology: Application to the Exploration of Sedimentary Basins: Geological Society, London, Memoir, **29**, 199-208.

Hildenbrand, T. G., A. Briesacher, G. Flanagan, W.J. Hinze, A.M. Hittelman, G.R. Keller, R.P. Kucks, D. Plouff, W. Roest, J. Seeley, D.A. Smith, and M. Webring, 2002, Rational and operation plan to upgrade the U.S gravity database: U.S. Geological Survey Open-File Report 02-463.

Hinze, W. J., D.J. Allen, L.W. Braile, and J. Mariano, 1997, The Midcontinent Rift System: A major Proterozoic continental rift, *in* R. W. Ojakangas, A.B. Dickas, and J.C. Green, ed., Middle Proterozoic to Cambrian Rifting, Central North America, Geological Society of America Special Paper **312**, 7-35.

Hinze, W. J., C. Aiken, J. Brozena, B. Coakley, D. Dater, G. Flanagan, R. Forsberg, T. Hildenbrand, G.R. Keller, J. Kellogg, R. Kucks, X. Li, A. Mainville, R. Morin, M. Pilkington, D. Plouff, D. Ravat, D. Roman, J. Urrutia-Fecugauchi, M. Véronneau, M. Webring, and D. Winester, 2005, New standards for reducing gravity database: The North American gravity database: Geophysics, **70**, J25-J32.

Holom, D. I., and J.S. Oldow, 2007, Gravity reduction spreadsheet to calculate the Bouguer anomaly using standardized methods and constants: Geosphere, **3**, 86-90.

Jones, V. L., and P.L. Lyons, 1964, Vertical-intensity magnetic map of Oklahoma.

Keller, G.R., J.M. Hills, M.R. Baker, and E.T. Wallin, 1989, Geophysical and geochronology constraints on the extent and age of mafic intrusions in the basement of west Texas and eastern New Mexico: Geology, 17, 1049-1052

Keroher, R. P., J.J. Kirby, 1948, Upper Cambrian and Lower Ordovician rocks in Kansas: Kansas Geological Survey Bulletin, **72**, 140.

Kis, K. I., 1990, Transfer properties of the reduction of magnetic anomalies to the pole and to the equator: Geophysics, **55**, 1141-1147.

Li, X., 2006, Understanding 3D analytical signal amplitude: Geophysics, **71**, L13-L16.

Lidiak, E. G., R.F. Marvin, H.H. Thomas, and M.N. Bass, 1966, Eastern area, pt. 4 of geochronology of the Mid-Continent region, United States: Journal of Geophysical Research, **71**, 5427-5438.

Luza, K. V., R.L. Dubois, P. Foster, J.E. Lawson, and L. Koff, 1978, Seismicity and tectonic relationships of the Nemaha uplift in Oklahoma: Oklahoma Geological Survey.

McBride, J. H., D.R. Kolata, and T.G. Hildenbrand, 2003, Geophysical constraints on understanding the origin of the IIIinois basin and its underlying crust: Tectonophysics, **363**, 45-78.

Miller, H. G., and V. Singh, 1994, Potential field tilt - a new concept for location of potential field sources: Journal of Applied Geophysics, **32**, 213-217.

Muehlberger, W. R., R.E. Denison, and E.G. Lidiak, 1967, Basement rocks in continental interior of United States: American Association of Petroleum Geologists Bulletin, **51**, 2351-2380.

Nissen, S. E., T.R. Carr, and K.J. Marfurt, 2006, Using new 3-D seismic attributes to identify subtle fracture trends in Mid-Continent Mississippian Carbonate Reservoirs: Dickman Field, Kansas: Search and Discovery Article #, **40189**.

Nixon, G. A., and J.L. Ahern, 1988, Southern extension of the Midcontinent geophysical anomaly; evidence for Keweenawan rifting in north-central Oklahoma: Geological Society of America Abstract with Programs, **20**, A234.

Northcutt, R. A., and Campbell, J.A., 1995, Geologic provinces of Oklahoma: Oklahoma Geological Survey.

Richard, B. H., P.J. Wolfe, and P.A. Potter, 1997, Pre-Mount Simon basins in western Ohio, *in* R. W. Ojakangas, A.B. Dickas, and J.C. Green, ed., Middle Proterozoic to Cambrian Rifting, Central North America: Geological Society of America Geological Society of America Special Paper **312**, 243-252.

Roark, J. J., 1962, Earth crust measurements by seismograph in Oklahoma - An interim report Geophysical Society of Tulsa Proceedings, 1959-1961: Presented at the 30th Annual meeting of the Society of Exploration Geophysicists.

Robbins, S. L., and G.R. Keller, 1990, Complete Bouguer and isostatic residual gravity maps of the Anadarko Basin, Wichita Mountains, and surrounding areas, Oklahoma, Kansas, Texas, and Colorado: United State Geological Survey Bulletin, **1866-G**, G1-G11.

Roest, W. R., J. Verhoef, and M. Pilkington, 1992, Magnetic interpretation using 3-D analytical signal: Geophysics, **57**, 116-125.

Rogers, J., and M.W. Longman, 2001, An introduction to chert reservoirs of North America: American Association of Petroleum Geologists Bulletin, **85**, 1-5.

Rogers, S. M., 2001, Deposition and diagenesis of Mississippian chat reservoir, north-central Oklahoma: American Association of Petroleum Geologists Bulletin, **85**, 115-129.

Ruppel, S. C., and S.D. Hovorka, 1995, Controls on reservoir development in Devonian Chert: Permian Basin, Texas: American Association of Petroleum Geologists Bulletin, **79**, 1757-1785.

Ruppel, S. C., and R.J. Barnaby, 2001, Contrasting styles of reservoir development in proximal and distal chert facies: Devonian Thirty-one Formation, Texas: American Association of Petroleum Geologists Bulletin, **85**, 7-33.

Schaming, M., and Y. Rotstein, 1990, Basement reflectors in the Kerguelen Plateau, south Indian Ocean: Indications for the structure and early history of the plateau: Geological Society of America Bulletin, **102**, 580-592.

Schlich, R., Y. Rotstein, and M. Schaming, 1993, Dipping basement reflectors along volcanic passive margins - new insight using data from Kerguelen Plateau: Terra Nova, **5**, 157-163.

Sloss, L. L., 1963, Sequences in the cratonic interior of North America: Geological Society of America, Bulletin, **74**, 93-114.

Thorman, C. H., and M.H. Hibpshman, 1979, Status of mineral resource information for the Osage Indian Reservation, Oklahoma :Administrative Report **BIA-47**: U.S. Geological Survey and Bureau of Mines.

Van Schmus, W. R., M. E. Bickford, and K. C. Condie, 1993, Early Proterozoic crustal evolution, *in* J. C. Reed, M. E. Bickford, R. S. Houston, P. K. Link, D. W. Rankin, P. K. Sims, and W. R. Van Schmus, ed., Precambrian conterminous U.S.: Boulder, Geological Society of America, The Geology of North America, **C-2**, 270-281.

Van Schmus, W. R., M. E. Bickford, and A. Turek, 1996, Proterozoic geology of the east-central mid-continent basement, *in* B. A. Van der Pluijm, and Catacosinos, P.A., ed., Basement and basin of eastern North America: Geological Society of America Special Paper **308**, 7-32.

Verduzco, B., D. J. Fairhead., C. M. Green, and C. MacKenzie, 2004, The meter reader - New insight into magnetic derivatives for structural mapping: The Leading Edge, **23**, 116-119.

Walters, R. F., 1946, Buried Precambrian hills in northeastern Barton County, central Kansas: American Association of Petroleum Geologists Bulletin, **30**, 660-710.

Whitmeyer, S.J., and K.E. Karlstrom, 2007, Tectonic model for the Proterozoic growth of North America: Geosphere, **3**, 220-259

Xia, J., D.R. Sprowl, and D.W. Steeples, 1996, A model of Precambrian geology of Kansas derived from gravity and magnetic data: Computers & Geosciences, **22**, 883-895.

Yarger, H. L., 1985, Kansas basement study using spectrally filtered aeromagnetic data, *in* W. J. Hinze, ed., The Utility of Regional Gravity and Magnetic Anomaly Maps: Society of Exploration Geophysicists, 213-232.

# Chapter 5: A Geophysical Study of Peru's Subandean Basins and Their Regional Setting (Paper to be submitted to the Journal of South America Earth Sciences)

## 5.1 Abstract

The integration of potential field data with seismic and well data has helped define the major structural features and regional architecture of the Ucayali basin area of Peru. Horizontal gradient magnitude and the horizontal derivative of the tilt derivative of the total magnetic intensity (TMI) data suggest two trends of basement lineaments. The northwest-southeast trending lineaments interpreted as Precambrian basement structures are sub-parallel to the late Paleozoic fold and thrust belts that resulted from the shortening associated with the formation of the Andes. These fold and thrust belts were reactivated along the zones of weaknesses that already existed in the Precambrian basement. The east east-northeast lineaments are located beneath the Fitzcarrald Arch that lies above the buoyant Nazca ridge. We interpret this lineament as part of the Ene Pisco – Abancay Fitzcarrald tectonic lineament, which is one of the five tectonic domains in these region and is oriented east-northeast. Gravity modeling suggests that the crustal thickness beneath the Peru increases from the north of the Ucayali basin toward the south.

Regional gravity modeling, which was constrained with seismic profile data, showed that the dip of the subduction zone and the crustal thickness increase southward as earthquake studies have inferred. Two dominant wavelengths of anomalies can be identified on the integrated local gravity models. We interpret the longer wavelengths to

be due to relief on the Precambrian basement that probably dates from the rifting that broke-up the Neoproterozoic Rodinian supercontinent and produced a passive margin that remained largely undisturbed until at least the late Paleozoic. Major structures such as the Cushabatay, the Contaya, and the Shira Uplifts are also identified on the models

## 5.2 Introduction

The Andes and associated structures form one of earth's largest orogenic belts. However, in terms of modern geophysical studies, Peru is relatively unstudied. Petroleum exploration has caused interest in this region to increase, and sparsely explored Peruvian Subandean structures such as the Ucayali and Marañon basins (Figure 5.1) have been subject of some recent regional research and petroleum evaluations (e.g., Chung, 1999; PARSEP, 2002). In addition, there have been many lithospheric-scale studies of the Altiplano and Andes south of Peru.

In eastern Peru, Chung (1999) conducted a regional gravity and magnetic analysis of the basement structures. A high correlation between the Andean structures and positive gravity anomalies, and intra-basement structures (faults and/or intrusive bodies) control on the structural style of the Ucayali basin were noted. We have access to new data in the area of the Ucayali and Marañon basin and have undertaken a new integrated study of this region with the goal of providing a new insight into the underlying geology of these Subandean basins. In this study, we have expanded on what has been done previously by carefully conducting a highly integrated analysis of the Ucayali basin region in particular. Our focus was on improving the understanding the geometry of the Ucayali basin as well as the underlying basement structure and its interaction with Paleozoic or younger structures. Reactivation of some pre-existing basement faults system has been known to

control paleo-depositional, deformation, metamorphism, and magmatic history within the Subandean foreland basin (Jaillard et al., 200; Jacques, 2003). North-south Subandean intrabasin highs and major basin-bounding arches such as the Cushabatay uplift and the Contaya uplift are associated with basement fault reactivation and many of these basement features are difficult to map on seismic reflection data (Figure 5.1). However, potential field data can effectively be used to map such basement features. We used derivative maps generated form aeromagnetic data to map the basement structures of the Subandean basins.

From a regional perspective, the Peruvian Andes play a crucial role in understanding the northern Andes and the Central Andes, which are characterized by an accretionary style of subduction and a high plateau style of orogenesis respectively (Gerbault and Hérail, 2005). Key efforts in this area have been focused on understanding the structure, geometry and effect of the subducting oceanic Nazca plate on continental deformation and the along strike variation of the structural styles of the Andean foreland (Kley et al., 1999). Authors such as Jordan et al. (1983) and Tassara (2005) have investigated the relationships between flat-slab subduction (5-10$^{o}$) along the Andean margin (latitude 2$^{o}$-15$^{o}$S) (Jacques, 2003) and volcanism. Studying interaction such as this can provide a laboratory understanding of processes such as intraplate seismicity and volcanic activity. In this study, we developed a regional geophysical cross-section across the Peruvian Andes to the Subandean basins, using all available resources and published results (e.g., Sobolev and Babeyko, 2005; Tassara et al., 2006; Mamani et al., 2008) to understand the intraplate interactions. Our goal for compiling this information was to provide constraints for construction of an integrated 2D gravity model across the region

to describe the regional architecture and major structural features. We also investigated the slab geometry beneath the Peruvian Andes. Various authors such as Ramos (1999), Jacques (2003), and Sobolev and Babeyko (2005) have suggested a flat-slab subduction (5– $10^{o}$dip) of a young buoyant oceanic crust with no associated active volcanism for study area.

## 5.3 Geologic Setting and Tectonic History

The Andes are a segmented and a highly complex 8000 km long mountain chain that extends along the western boundary of the South American plate (e.g., Jordan et al., 1983; Ramos, 1999; Jaillard et al, 2000). The Andean chain consists of Western and Eastern Cordillera that resulted from the Cenozoic tectonic shortening of the Nazca plate subsiding beneath the South American plate margin and present day active processes. The Western Cordillera of the Andes consists of deformed metamorphic rocks and Mesozoic sediments that are intruded by plutons and are unconformably covered by abundant volcanic rocks. The Eastern Cordillera, which is bordered to the west by a near continuous east-verging fold and thrust belt, consists of uplifted zone of Pre-Mesozoic metamorphic rocks and deformed Mesozoic sedimentary rocks with subordinate intrusions and volcanic rocks of primarily Paleozoic –Tertiary age (Litherland et al., 1994; Jaillard et al, 2000).

Gansser (1973) classified the Andes along-strike into northern, central, and southern segments. Along-strike variations in the subducting oceanic plate slab dip to beneath the South American plate that range from flat to normal have been noticed by several authors (e.g., Jordan et al., 1983; Wortel, 1984; Kley et al., 1999; Ramos, 1999). Jacques (2003) further classified the Andes into five main tectonostratigraphic domains

(northern, western, central, eastern, and southern) based on intracontinental deformation and basement fault behavior along the Andean domains - based on intracontinental deformation and basement fault dominance along the Andean foreland's length. These tectonostratigraphic domains are characterized by east-northeast and northwest basement lineaments that are interpreted as reactivated old, deep crustal fracture systems that were formed during the early tectonic history of the Andes.

Mountain building processes that formed the Andean are generally considered to have been initiated during the Mid- or Late Cretaceous (Jacques, 2003). However, complex history of the Andes began with the formation of the proto-margin of Gondwana. During the Phanerozoic - Early Paleozoic era (Pan-African-Brasiliano Orogeny) several different continental blocks and cratonic terranes were accreted against the late Proterozoic margin of Gondwana constituting the Pre-Andean orogenic processes. In the Late Paleozoic, the Andes experienced the first subduction related mountain buildup during the Alleghanian and Gondwanan Orogeny (Ramos and Aleman, 2000).

Various tectonic processes dominated the Pangaea break-up that occurred during the Early Mesozoic rifting of the continental margin of the Andes. This extensional period is characterized by northwest-southeast trending grabens. In the Late Permian to Early Triassic Andean orogenesis was initiated by eastward subduction of the oceanic Nazca plate beneath the continental South American plate. In Peru, this orogenesis formed the "Andean Convergent arc" via continued subduction, transpression and crustal thickening (Jacques, 2003). In addition, a complex series of fore-arc, intra-arc and retro-arc basins were developed during this time. Related transpressional and transtensional

processes created a series of en-echelon horsts and grabens with northeast-southwest and northwest-southeast trends that crossed the Andes (Ramos and Aleman, 2000).

### 5.3.1 Peruvian Subandean Basin Tectonic History

The Peruvian subandean foreland that includes the Marañon, Ucayali, and Madre de Dios basins occupies the Eastern Cordillera and extends from Venezuela in the north to Chile and Bolivia in the south. These north-south elongated foreland basins are bounded on the west by the Andes zone of deformation and on the east by the stable cratonic shield (Jacques 2003). Occupying the western tectonic domain, the Peruvian foreland basins are associated with the Nazca Ridge flat-slab with dips of 5-10$^{o}$ (Suárez et al., 1983; Ramos, 1999) (Figure 5.2).

These currently active sub-Andean basins have experienced a long deformation and basin formation history that is part of the complex fold and thrust belt system of the Andes, which is actively been explored for hydrocarbons (Mathalone and Montoya, 1995). The western and eastern edges of the basins are characterized by a thin-skinned deformation in a narrow fold and thrust belt and basement-involved, thick-skinned deformation, respectively (Jacques, 2003; Espurt et al., 2008).

After the Late Mesozoic Peruvian orogenesis, which left the Ucayali and the Marañon basins relatively underformed, early Cenozoic "Incaic compressional deformation" is suggested to be responsible for most of the central Andes compression, which caused a regional flexural tilting (Mathalone and Montoya, 1995). The Late Miocene Quencha-III compressional event affected the Subandean basins the most, and this event shaped the Andes into it present modern configuration. The Quencha-III event resulted in a series of thick and thin-skin basement thrusting and inversions that

partitioned and dissected the Peruvian sub-Andean basins at the zones with inherent northwest structural fabric. Reactivated structures such as the Contaya and Cushabatay uplifts were also developed also during this time. Similarly, normal and reverse faults, thrust anticlines, inversion structures and other related hydrocarbon traps and seals structures were formed at this time (Mathalone and Montoya, 1995).

## 5.4 Datasets and Methodology

### 5.4.1 Gravity Dataset

The onshore gravity dataset used for this project are made available by GETECH via the Hess Corporation. These grids were part of the datasets compiled from the South America Gravity Project (SAGP) and Global Continental Margins Gravity Studies (GCMGS) respectively. The onshore grids (Figure 5.1) were processed with a reduction density of 2.67 g/cc.

The complete Bouguer anomaly map shown in Figure 5.3 was generated with a grid spacing of 5 km. The sparse distribution of the gravity points initially raised some concern because large regions of interest were devoid of gravity stations. Our solution to this problem involved careful construction of gravity profiles for modeling and integrated analysis of all the data available to us.

*Gravity Data Enhancement*

In order to achieve our objective of defining the major structural elements within the Ucayali basin area and understanding its deep structure, the regional effect of the Andes has to be removed from the complete Bouguer gravity map. For our purpose, the term ‘regional’ refers to sources with deep origins such as the Andes crustal root. The

term ‘residual’ refers to fields created by shallow to intermediate sources such as intra-basement features.

Separating a complete Bouguer anomaly map into residual anomalies resulting from local mass distributions and regional anomalies can be a somewhat difficult task. To separate out the regional anomaly from the complete Bouguer anomaly map, we employed an upward continuation to estimate the regional anomaly values (Figure 5.4). The upward continuation of potential field data is not new to processing and is a form of low-pass filtering. It permits the viewing of potential field at different levels over an anomaly source and acts as a standard separation filter for potential field data (Hughes et al., 1947; Henderson, 1949; Robinson, 1970; Jacobsen, 1987). It enhances long wavelength signals by attenuating higher frequency signals due to shallow sources without producing any side effects that require additional correction

To produce residual maps reflecting shallow crustal features (Figure 5.5), we carefully selected an upward continued level that reflected the regional anomalies and then simply subtracted the corresponding grid from the complete Bouguer anomaly grid. From this standpoint, the subtraction of the regional anomaly map from the complete Bouguer map is a form of high pass filter, without the artifacts that often characterized high-pass filters maps. We generated a series of regional anomaly maps at various upward continuation heights ranging from 10 km – 160 km. We observed that an upward continuation height of 30 km produced a map that appeared to best represent the prevailing regional trends and the desired smooth regional in the Ucayali basin region. Thus, the residual anomaly map used in this study was generated by subtracting a

regional anomaly (30 km upward continued grid) from the original complete Bouguer anomaly grid (Figure 5.5).

### 5.4.2 Magnetic Dataset

The aeromagnetic dataset consisted of a country wide total magnetic intensity (TMI) grid for Peru, compiled from the South American Magnetic Project (SAMMP) of GETECH (Figure 5.6). These data consists of individual surveys that were flown at different heights and flight-line spacing that were gridded at a 1 km spacing, merged, and reduced to a mean ground clearance elevation of 1 km.

*Magnetic Data and Data Enhancement*

Prior to any interpretation can, the data was reduced-to-the equator (RTE). The RTE technique ameliorates problems that are typically associated with low-latitude data and transforms nonzero inclination anomaly into an anomaly that would be observed with the same body with zero inclination. Low-latitude data (our dataset) at about 15 degrees latitude becomes unstable for a reduction-to-the pole (RTP) application (Kis, 1990). The caveat of the RTE transformation is that it has the tendency to create a change of anomaly sign, such that a maximum will appear as a minimum. However, this typically occurs very near the equator.

To highlight lateral or abrupt changes in magnetization that can suggest faults or source contacts, we computed the horizontal gradient magnitude (HGM), and the tilt derivative. These derivatives (Figures 5.7 & 5.8) are edge-detecting derivatives that enhance lateral discontinuities in a TMI grid (Grauch and Cordell, 1987; Roest et al., 1992; Miller and Singh, 1994; Blakely, 1996; Verduzco et al., 2004; Li, 2006). It is still

up to the interpreters to devise a geologically meaningful interpretation to what is seen on these gradient maps.

We also attempted to estimate depth to the top of Precambrian basement using the Euler deconvolution method. The Euler deconvolution method is an automated depth estimation method (Thompson, 1982) that can help determine the location or depth to the shallowest or deepest reasonable magnetic source or edges for various geological sources such as, dikes, faults, magnetic contacts, and extrusives (Phillips, 2007). It uses the structural index (SI) to describe the geometry of the desired geologic structure and as a geological constraint (Reid, 1990; Barbosa et al., 1999).

The depth to magnetic basement grid (Figure 9) was constructed based on a processed not observed 1 km clearance total magnetic intensity grid. However, results generated from such a grid need to be analyzed with caution. Two important issues arise; first, if we do not know exactly where the magnetometer was located, we have no datum from which to compute the depth to basement. Second, magnetic depth estimates are dependent on the magnetic field gradients, and the terrain clearance heavily affects field gradients. Nevertheless, the depth to basement results obtained from the mean terrain clearance magnetic grid still proved to be very useful, but its limitations should be kept in mind. In fact, this map provides a constraint in the gravity modeling and was used to produce the series of overlays discussed below.

## 5.5 Integrated Interpretation and Modeling

### 5.5.1 Anomaly Interpretation

The horizontal gradient magnitude map and the horizontal derivative of the tilt derivative of the TMI map (Figures 5.7 and 5.8) show mainly northwest-southeast (black

arrows) and east-northeast (green arrows) anomaly trends. The northwest lineaments displayed on these maps are consistent with the northwest-southeast trend direction of the Subandean fold and thrust belt. The similarity in trend between the basement lineaments and the fold and thrust belt suggest that the Late Paleozoic fold and thrust belt that resulted from the shortening associated with the early formation of the Andes are following the zones of weaknesses already existing in the Precambrian basement.

The east-northeast lineaments are sub-parallel to the east-west regional shortening associated with the Late Miocene Quencha III orogeny that is the recent phase of Andean orogenesis (Mégard, 1984). These lineaments are located in the southern part of the Ucayali basin and the northern part of the Fitzcarrald Arch. They display a complex structural architecture (Espurt et al., 2008) beneath the Fitzcarrald Arch, which has been interpreted to be located over the buoyant Nazca ridge (Espurt et al., 2007). Although the Nazca ridge trends N45$^{o}$E, the present day plate convergent suggest a N78$^{o}$E trend, which is roughly parallel to the strike of these lineaments.

Regionally, the east-northeast lineaments are also sub-parallel to the Ene Pisco – Abancay Fitzcarrald tectonic lineament, which is one of the five tectonic domains described in Jacques (2003). This zone is interpreted as an old, deep fracture system that has been repeatedly reactivated during the tectonic development of the Andean region forming different zones of deformation with the overlying cover.

The depth to the shallowest Precambrian basement map in Figure 5.9 suggests the basement deepens northwesterly beneath the Ucayali basin. A large proportion of this basin (southeastern) has an estimated depth that is less than ~ 5 km. Beneath the Marañon basin, the Precambrian basement is much deeper (~ >10 km).

### 5.5.2 Gravity Profile Construction - Gravity Point Extraction

Although we had to work with grids of gravity and elevation data, we went to considerable lengths to reconstruct gravity values and elevations at the locations of actual gravity points whose locations were provided by GETECH. The OASIS MONTAJ modeling software is not set-up to easily handle the selection of randomly distributed gravity points on a straight-line profile, but this step was crucial given the erratic distribution of data points and the topographic relief present. The points were manually selected along the profile lines, and repetitive points were eliminated. We implemented a technique to extract selected points from the randomly distributed gravity points in order to construct profiles for the integrated gravity modeling.

### 5.5.3 Regional Gravity Models

After constructing the series of gravity and magnetic maps, we chose two regional profiles along where gravity data points were available for modeling (northeast - southwest trending black lines in inset map of Figure 5.10). These profiles extended completely across Peru starting from the Pacific coast. Initial model densities and subducting plate geometries were extracted from Tassara et al., (2006) paper. The integrated modeling was done employing the Geosoft GM-SYS modeling software. Formation top and total depth (TD) information from wells were used as constraint in the gravity modelling. Density estimates for the main sedimentary packages were extracted from the density logs.

Modeling of these profiles created a good regional framework from which to work in the area within the Ucayali basin. The models also showed that the dip of the subduction zone and the crustal thickness is increasing northward as earthquake studies

have inferred (Figure 5.10). This variation in dip has implications for foreland deformation in this area because the change of dip in the plate induces stresses that are oblique to the subduction zone and the Andes. According to Jacques (2003), several transfer zones are needed to account for the splitting of the plate slip vector into strain and displacement along different parts of the Andean Belt. These induce stresses are manifested for example, at the junction between the Peruvian flat-slab and the more steeply dipping slab to the south (e.g. The Nazca Ridge – Fitzcarrald Lineaments) (Jordan et al., 1983). This broad zone has gone through basement-involved deformations that include contraction and reverse fault (Ramos, 1999) and the stresses and strains are dissipate throughout the zone of deformation along the flat-slab Peruvian Andes.

### 5.5.4 Local Gravity Modeling

Based on these long profiles, the locations of wells, and the locations of seismic lines, we chose and model three local profiles across the Ucayali basin. The locations of these profiles were chosen based on the locations of actual gravity readings, the locations of deep wells, and the locations of seismic lines. In the case of these profiles, we modeled the residual gravity values and used the magnetic depth to basement estimates (Figure 5.9) as constraints. The lack of a regional trend in these profiles indicates that we successfully separated the gravity field into its regional and local components (Figures 5.11, 5.13, and 5.15). Density units for the modeling were defined based on density log information and lithologic descriptions. Our approach was to create relatively simple models since we lacked the information to justify a more complex density structure. We also chose density contrasts for the units that were skewed toward making the contrast large, which is actually a conservative approach in that it reduces the dimension of

structures required. We preferred to model anomalies as being related to geologic structures rather than intra-basement features such as intrusions unless necessary. The only area on the local profiles that required a departure from this approach was the southwest end of Local Profile A where the present of salt was indicated.

Using normalized density values from density logs as much as possible, the density units we defined are as follows: (1) Precambrian basement/upper crust - 2.7 g/cc; (2) Paleozoic (and pre-Cretaceous Mesozoic) sedimentary rocks - 2.5 g/cc; (3) Cretaceous and younger sedimentary rocks - 2.2 g/cc; and (4) Salt – 1.9 g/cc. Also to the extent possible, formation tops from the wells constrained contact boundaries between density units (see Table 5.1). Seismic reflection profiles were also used where available (Figure 5.12, 5.14, and 5.16).

*Local Profile A*

Local Profile A is the longest and extends for about 500 km. The modeling was constrained by four wells (Shanusi-1, Yurimaguas-2, Loreto-1, and Samiria Sur-1) whose total depths (TD) and formation tops are plotted on the model (Figure 5.11). This model has a vertical exaggeration of ~4. The southwest and northeast portions of the profile are gravity highs, but the central portion of the profile is a broad gravity low that we modeled as being the result of the thickening of the Paleozoic section. In areas with a thin Paleozoic section, the Precambrian basement lies at a relatively shallow depth of ~5 km. A number of local gravity anomalies were modeled as structural highs and lows, which we interpret to be result of a series of horst blocks and grabens (See Figure 5.11). However, it is possible that intra-basement density contrasts could explain some of these anomalies

*Local Profile B*

Local Profile B extends for about 250 km (Figure 5.13) and is parallel to Local Profile A. Two wells (Orellana-3 and La Frontera-1) are located close enough to this profile to serve as constraints. As in the case of Local Profile A, the southwest end of the profile is a gravity high and lies along the same northwest trend in the residual gravity maps (Figure 5.5). However, there is enough gravity data to show that the intervening area between these highs is low relative to them. As in Local Profile A, areas with thick Paleozoic sections and considerable basement relief are indicated (Figure 5.14).

*Local Profile C*

The central portion of Local Profile C (Figure 15) is characterized by a broad region with residual gravity values near zero. This gravity high corresponds with the location of the Shira uplift, the basement depth from the model is about 6 km, and it is shallower than it is surrounding (Figure 5.16). Because this area is flanked by gravity lows, it appears to indicate a larger structural high than is actually present. Inspection of Figures 5.5 and 5.16 shows that the profile passes across the northwestern edge of a much larger gravity high. The northeast end of the profile shows a southwest tilt that indicates a small regional was not removed, and this tilt is modeled as the result of a deep crustal feature.

## 5.6 Observations and Results

The residual Bouguer anomaly map (Figure 5.5) and the models shown in Figures 5.11, 5.13, and 5.15 display evidence for a variety of interesting upper-crustal features. Here we address our interpretation of their significance. We examined correlations between mapped regional geologic features and gravity and magnetic anomalies. This

example is from the area of the southwest end of Local Profile B and shows that some of the surface features within the Ucayali basin are clearly correlated with deep structures. In this case, the correlation is between a northwest trending geologic feature and a Bouguer anomaly high that occurs south of the profile (Figure 5.13). The fact that there is only a line of gravity measurements crossing this geologic feature suggests that the coincident gravity high would follow the geologic feature if a good distribution of gravity readings were available.

Analysis of spatial correlations yield three features that are also constrained, at least in part, by seismic data. On Local Profile A, we interpret the Cushabatay uplift (Figures 5.11 and 5.12) as being due to two Paleozoic horst blocks. Gravity and magnetic anomaly that occur at the extreme northeast corner of the Local Profile B, is interpreted as the structurally distinct Contaya uplift, which is due to a combination of thinning of Cretaceous and younger strata and a large horst block (Figures 5.13 and 5.14). On Local Profile C, we interpret the Shira Mountain high to be due to a combination of thinning of Cretaceous and younger strata and a broad horst block (Figures 5.15 and 5.16). We interpret this as being due to inverted Paleozoic grabens. We certainly believe that the horst blocks discussed above could have experienced inversion due to Andean and even late Paleozoic tectonism. In addition, the thick Paleozoic sections in all three models of the local profiles could be due in part to structural thickening on faults that in most cases do not significantly offset the basement. However as discussed below, we favor the idea that these thick sections are due to the development of a passive margin sedimentary sequence.

## 5.7 Conclusions

The integration approach of this project has helped to define the structural geometry of the Ucayali basin and its regional setting. With the help of the residual gravity map and regional gravity models, we have characterized the major structural features and regional architecture that dominates this area.

Horizontal gradient magnitude and the horizontal derivative of the tile derivative of the TMI suggest two trends of lineaments. Northwest-southeast trending lineaments, which are indicative of Precambrian structures, are sub-parallel to the late Paleozoic fold are thrust belt that resulted from the shortening associated with early formation of the Andes. These fold and thrust belt are following the old zones of weaknesses that exist within in the Precambrian basement. The east east-northeast lineaments are located beneath the Fitzcarrald Arch that has been interpreted to lie above the buoyant Nazca ridge. We interpret this lineament as part of the Ene Pisco – Abancay Fitzcarrald tectonic lineament, which is one of the five tectonic domains of the subandean region, and it is oriented east-northeast.

The depth-to-basement map suggests the depth to the shallowest magnetic sources. The depth to the shallowest Precambrian basement map in Figure 5.9 suggests a Precambrian depth that deepens northwesterly lies beneath the Ucayali basin. A large proportion of this basin (southeastern) has an estimated depth that is less than ~ 5 km. Beneath the Marañon basin, the Precambrian basement is much deeper (~ >10 km). In some cases, our depth from the gravity model correlates with the basement depth estimates from Euler deconvolution, while in other cases it does not.

All the integrated models derived for the local profiles display features with two dominant wavelengths. We interpret the longer wavelengths to be due to relief on the Precambrian basement that probably dates from the rifting that broke-up the Neoproterozoic Rodinian supercontinent and produced a passive margin that remained largely undisturbed until at least the late Paleozoic. This interdomipretation is based on two other areas where we have done considerable research. The first is in Poland where we studied the Paleozoic margin of Baltica as part of a large international effort called POLONAISE' 97 (Figures 5.17 – 5.19). Here our work showed the surprising result that the Permian salt basin of central and northern Poland is underlain by a thick sequence of low velocity material that is almost certainly sedimentary in nature. The thickness and geometry of this material (Figure 5.21) suggests that it represents a passive margin sequence that was not destroyed by the late Paleozoic Variscan orogeny, and thus, this orogeny is due to a "soft" collision between Baltica and the Bohemian massif (Figure 5.19). The second area is the Ouachita margin that rims the Gulf of Mexico (Figure 5.20). As along the margin of Baltica, the seismic and gravity model across the southern margin of cratonal North America (Laurentia) shows that the Paleozoic passive margin is largely in tact and that the Ouachita orogeny in this region is also due to a soft collision between the Sabine uplift and North America. Figure 5.21 shows the models of these two margins at the same scale. Regional tectonic interpretations of both of these margins suggest that they experienced considerable strike-slip motion as they formed, so they are narrow. We suggest that the western margin of Southern America of the Peru region experienced a similar long period of passive margin development that is largely preserved today.

The shorter-wavelength features in the models appear to be largely due to basement-involved uplifts that have some similarity to Laramide foreland structures in Wyoming. Some of these structures may have an element of inheritance from the older structures related to the rifted margin of the northern South American craton. In any case, our interpretations indicate that thick sections of probable passive margin strata are present and that the deep structure is probably not too complex.

## 5.8 Acknowledgments

We like to thanks Hess Corporation for their financial support of the author for one-year, and the seismic and potential field dataset via GETECH

## 5.9 References


Barbosa, V. C. F., J.B.C. Silva, and W.E. Medeiros, 1999, Stability analysis and improvement of structural index estimation in Euler deconvolution: Geophysics, **64**, 48-60.

Blakely, R. J., 1996, Potential theory in gravity and magnetic applications: Cambridge University Press.

Chung, J. F., 1999, Geological and geophysical study of Peru's Andean foothills and adjacent basins: M.S, University of South Carolina.

Espurt, N., P. Baby, S. Brusset, M. Roddaz, W. Hermoza, V. Regard, P.O. Antoine, R. Salas-Gismondi, and R.Bolaños, 2007, How does the Nazca Ridge subduction influence the modern Amazonian foreland basin: Geological Society of America, **35**, 515-518.

Espurt, N., S. Brusset, P. Baby, W. Hermoza, R.Bolaños, D. Uyen, and J. Déramond, 2008, Paleozoic structural controls on shortening transfer in the Sub-Andean foreland thrust system, Ene and southern Ucayali basins, Peru: Tectonics, **27**, TC3009.

Gansser, A., 1973, Facts and theories on the Andes: Journal of the Geological Society of London, **129**, 93-131.

Gerbault, M., and G. Hérail, 2005, Andean geodynamics: Main Issues and contributions from the 5th ISAG, Toulouse: Tectonophysics, **399**, 1-13.

Grauch, V. J. S., and L. Cordell, 1987, Limitation of determining density or magnetic boundaries from the horizontal gradient of gravity or pseudogravity data: Geophysics, **52**, 118-121.

Henderson, R. G., and I. Zietz, 1949, The upward continuation of anomalies in total magnetic intensity fields: Geophysics, **14**, 517-534.

Jacobsen, B. H., 1987, A Case for upward continuation as a standard separation filter for potential-field maps: Geophysics, **52**, 1138-1987.

Jacques, J. M., 2003a, A tectonostratigraphic synthesis of the Sub-Andean basins: implications for the geotectonic segmentation of the Andean Belt: Journal of the Geological Society of London, **160**, 687-701.

Jaillard, E., G. Hérail, T. Monfret, E. Díaz-Martínez, P. Baby, A. Lavenu, and J.F. Dumont, 2000, Tectonic evolution of the Andes of Ecuador, Peru, Bolivia and northernmost Chile, *in* U. G. Cordani, E.J. Milani, A. Thomaz Filho, and D.A. Campos, ed., Tectonic Evolution of South America, 481-559.

Jordan, T. E., B. L. Isacks, R.W. Allmendinger, J.A. Brewer, V.A. Ramos, and C.J. Ando, 1983, Andean tectonics related to geometry of the subducted Nazca plate: Geological Society of America Bulletin, **94**, 341-361.

Kis, K. I., 1990, Transfer properties of the reduction of magnetic anomalies to the pole and to the equator: Geophysics, **55**, 1141-1147.

Kley, J., C.R. Monaldi, and J.A. Salfity, 1999, Along-strike segmentation of the Andean foreland: causes and consequences: Tectonophysics, **301**, 75-94.

Kley, J., C.R. Monaldi, and J.A. Salfity, 1999, Along-strike segmentation of the Andean foreland: causes and consequences: Tectonophysics, **301**, 75-94.

Lamb, S. and P. Davis, 2003, Cenozoic climate change as a possible cause for the rise of the Andes: Nature, 425, 792-797.

Litherland, M. J. A. A., and R.A. Jemielita, 1994, The metamorphic belt of Ecuador: Overseas Memoir, **11**, 147.

Mamani, M., A. Tassara, and G. Wörner, 2008, Composition and structural control of crustal domains in the central Andes: Geochemistry Geophysics Geosystems, **9**, 1-13.

Mathalone, J. M. P., and R.M. Montoya, 1995, Petroleum geology of the sub-Andean Basins of Peru, *in* A. J. Tankard, R. Suárez Soruco, and H.J. Welsink, ed., Petroleum Basins of South America, 62, 423-458.

Mégard, F., 1984, The Andean orogenic period and its major structures in central and northern Peru: Journal of the Geological Society of London, **141**, 893-900.

Miller, H. G., and V. Singh, 1994, Potential field tilt - a new concept for location of potential field sources: Journal of Applied Geophysics, **32**, 213-217.

PARSEP, 2002, The hydrocarbon potential of NE Peru, Huallaga, Santiago and Marañon Basin study: Projecto de Asistencia para La Reglamentacion del Sector Energetico del Peru.

Phillips, J. D., 2007, Geosoft executables (GX's) developed by the U.S. Geological Survey, version 2.0 with notes on GX development from Fortran code: U.S. Department of Interior, U.S. Geological Survey.

Ramos, V. A., 1999, Plate tectonic setting of the Andean Cordillera: Episodes, **22**, 183-190.

Ramos, V. A., and A. Aleman, 2000, Tectonic evolution of the Andes, *in* U. G. Cordani, E.J. Milani, A. Thomaz Filho, and D.A. Campos, ed., Tectonic Evolution of South America, 635-685.

Reid, A. B., J.M. Allsop, H. Granser, A.J. Millett, and I.W. Somerton, 1990, Magnetic interpretation in three dimensions using Euler deconvolution: Geophysics, **55**, 80-91.

Robinson, E. S., 1970, The upward continuation of anomalies in total magnetic intensity fields: Geophysics, **35**, 920-926.

Roest, W. R., J. Verhoef, and M. Pilkington, 1992, Magnetic interpretation using 3-D analytical signal: Geophysics, **57**, 116-125.

Sobolev, S. V., and A.Y. Babeyko, 2005, What drives orogeny in the Andes?: Geology, **33**, 617-620.

Suárez, G., P. Molnar, and B.C. Burchfield, 1983, Seismicity, fault plane solutions, depth of faulting, and active tectonics of the Andes of Peru, Ecuador and southern Colombia: Journal of Geophysical Research, **88**, 10403-10428.

Tassara, A., 2005, Interaction between the Nazca and South America plates and formation of the Altiplano-Puna plateau: Review of flexural analysis along the Andean margin ($15^{o}$-$34^{o}$S): Tectonophysics, **399**, 39-57.

Tassara, A., H. Götze, S. Schmidt, and R. Hackney, 2006, Three-dimensional density model of the Nazca plate model and the Andean continental margin: Journal of Geophysical Research, **111**, 1-26.

Thompson, D. T., 1982, EULDPH: A new technique for making computer-assisted depth estimates from magnetic data: Geophysics, **47**, 31-37.

Verduzco, B., D. J. Fairhead., C. M. Green, and C. MacKenzie, 2004, The meter reader - New insight into magnetic derivatives for structural mapping: The Leading Edge, **23**, 116-119.

Wortel, M. J. R., 1984, Spatial and temporal variation in the Andean subduction zone: Journal of the Geological Society of London, **141**, 783-791.

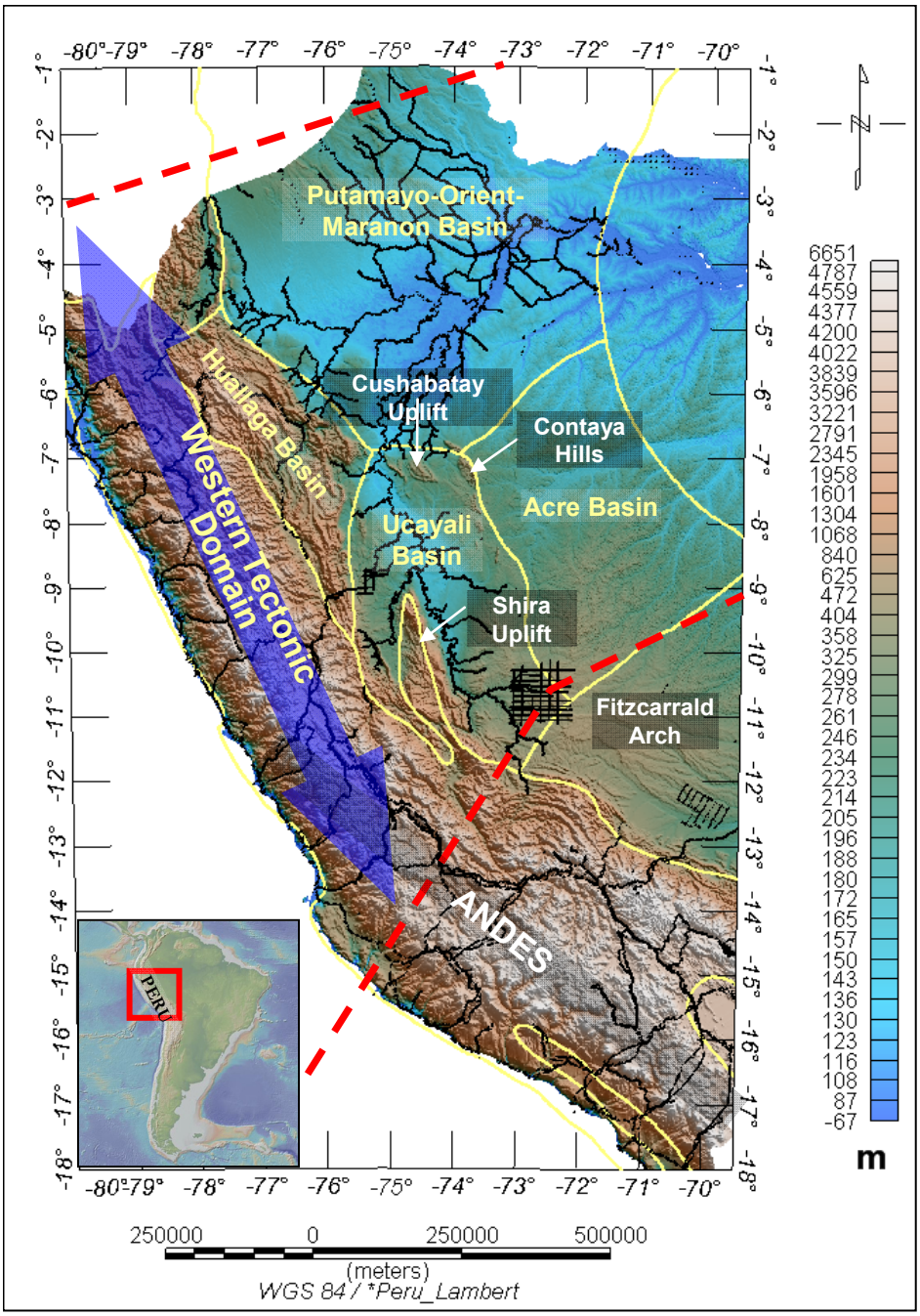


Figure 5.1. Digital elevation map of the Andes with major geologic features, structural uplift, subandean basins, and the transverse tectonic lineaments shown. Black-dot lines indicate the distribution of the gravity point used in this study. Red dashed lines are two of the five structural lineaments that divide the Andean belt into five tectonic domains(boundaries extracted from Jacques, 2003).

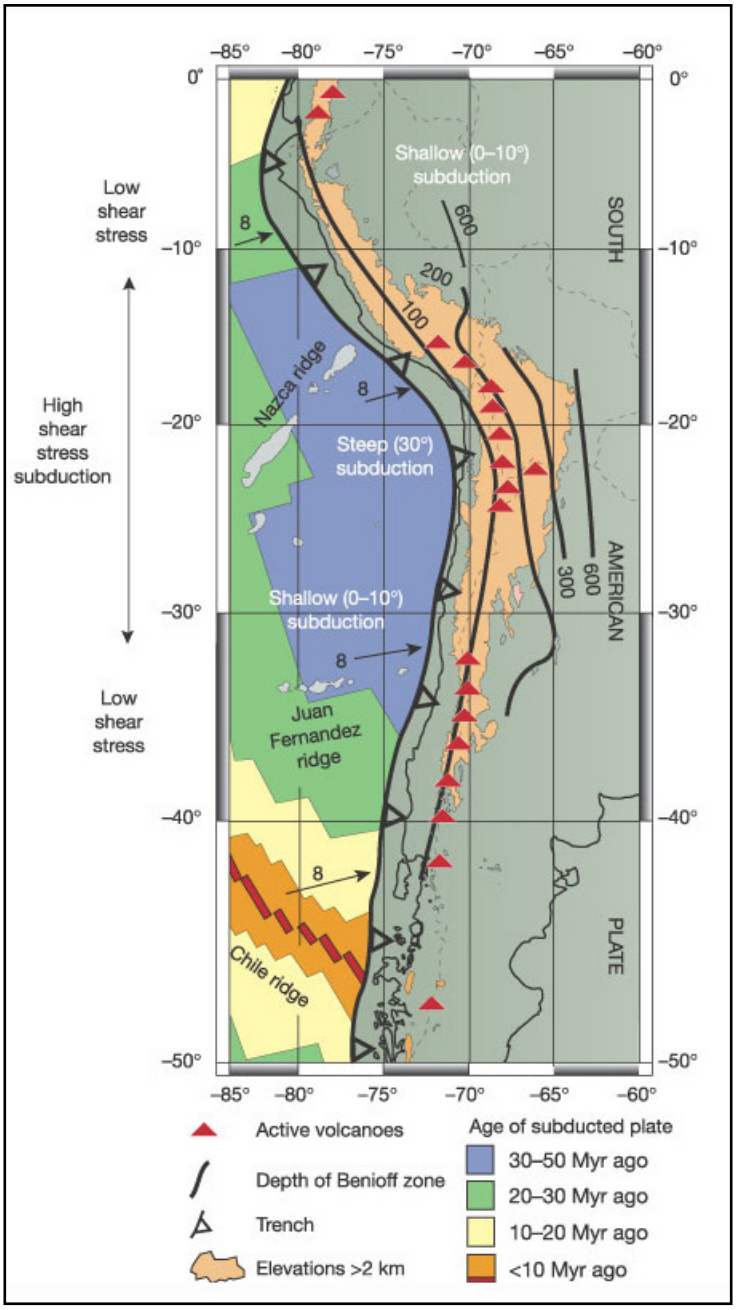


Figure 5.2.The tectonic map of the Andean plate margin showing the age and plate geometry of the subducting Nazca plate and volcanic arc locations. (Map from Lamp and Davis, 2003.

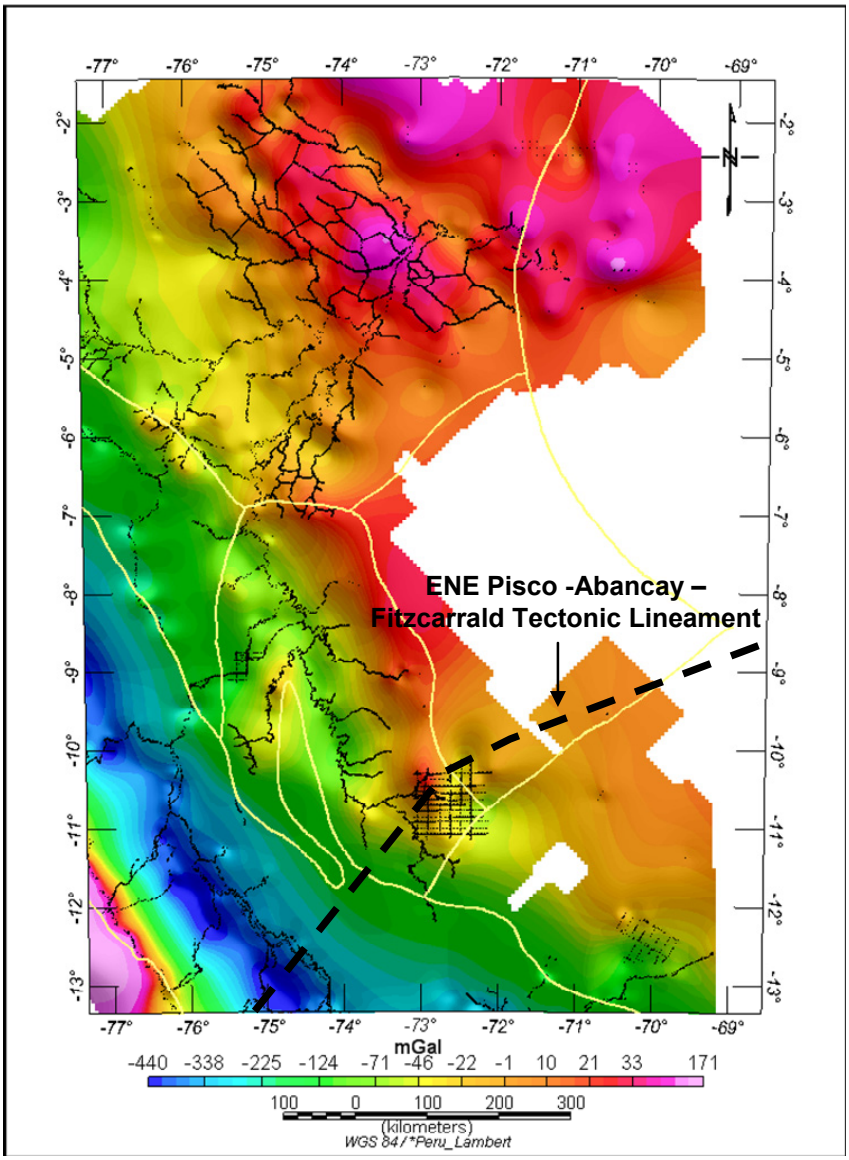


Figure 5.3. Complete Bouguer anomaly map showing the distribution of the onshore gravity data points (black dots) and the tectonic lineaments surrounding the Peruvian Sub-Andean basins

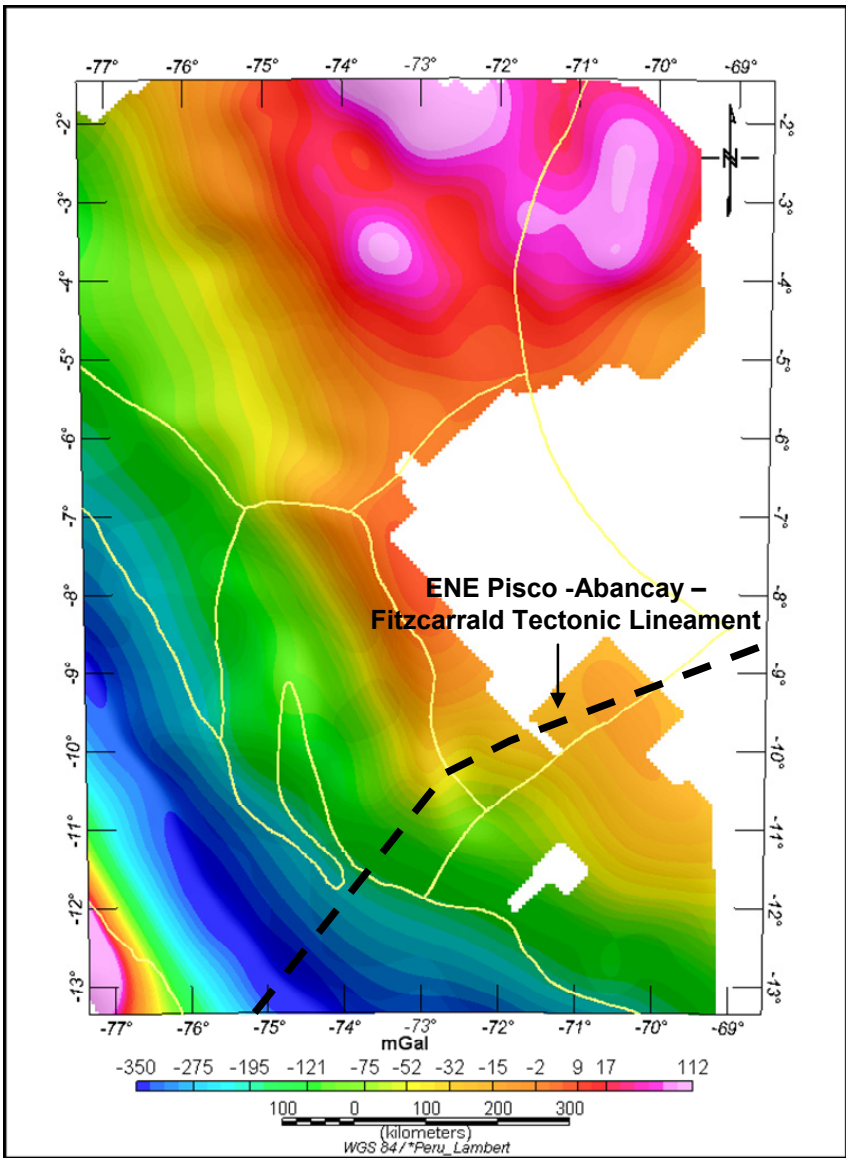


Figure 5.4. Upward continuation map generated from the upward continuation height of 30 km. The large negative and positive anomaly is associated with the Andeans and Brazilian cratonic shield

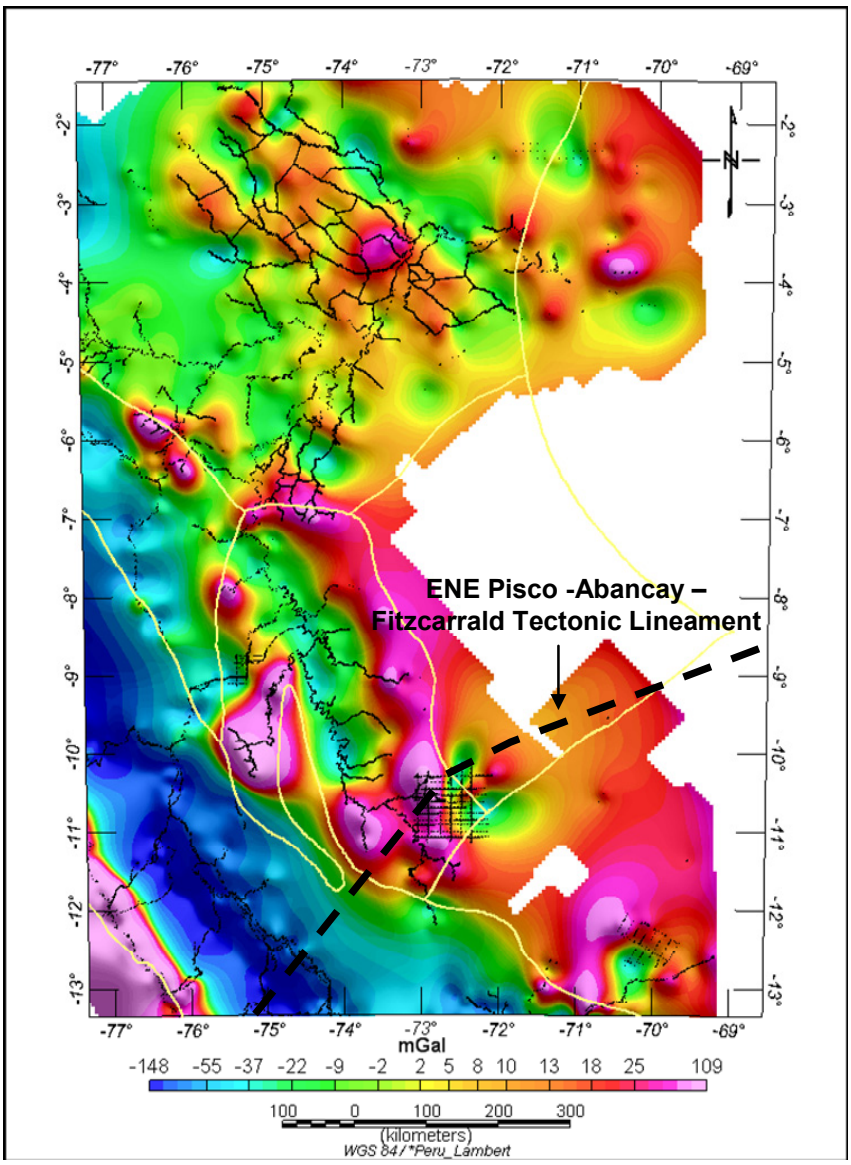


Figure 5.5. Residual Bouguer gravity anomaly map generated by subtracting a 30 km upward continuation grid from the complete Bouguer grid. The ENE Pisco-Abancay-Fitzcarrald tectonic lineament is one of the transverse tectonic lineaments as suite of deep crustal discontinuities.

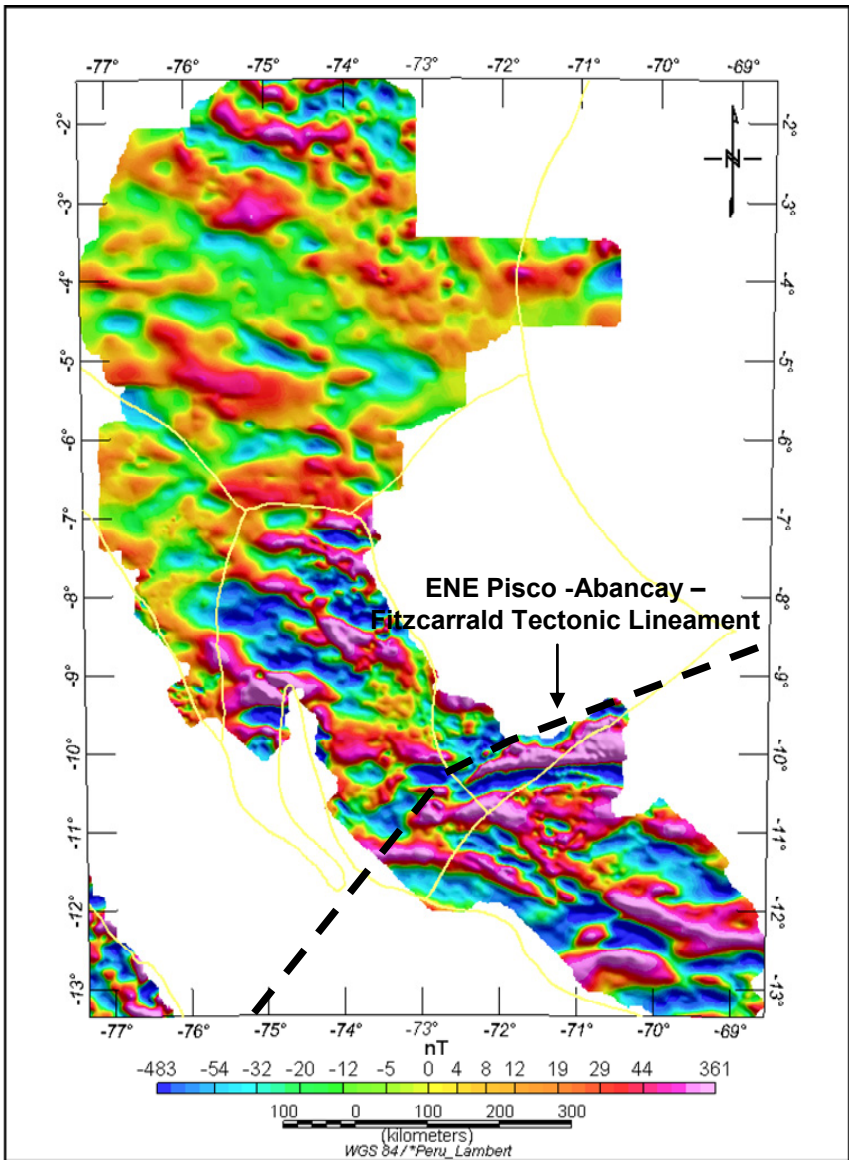


Figure 5.6. Reduced-to-the-equator (RTE) residual total magnetic intensity anomaly map.

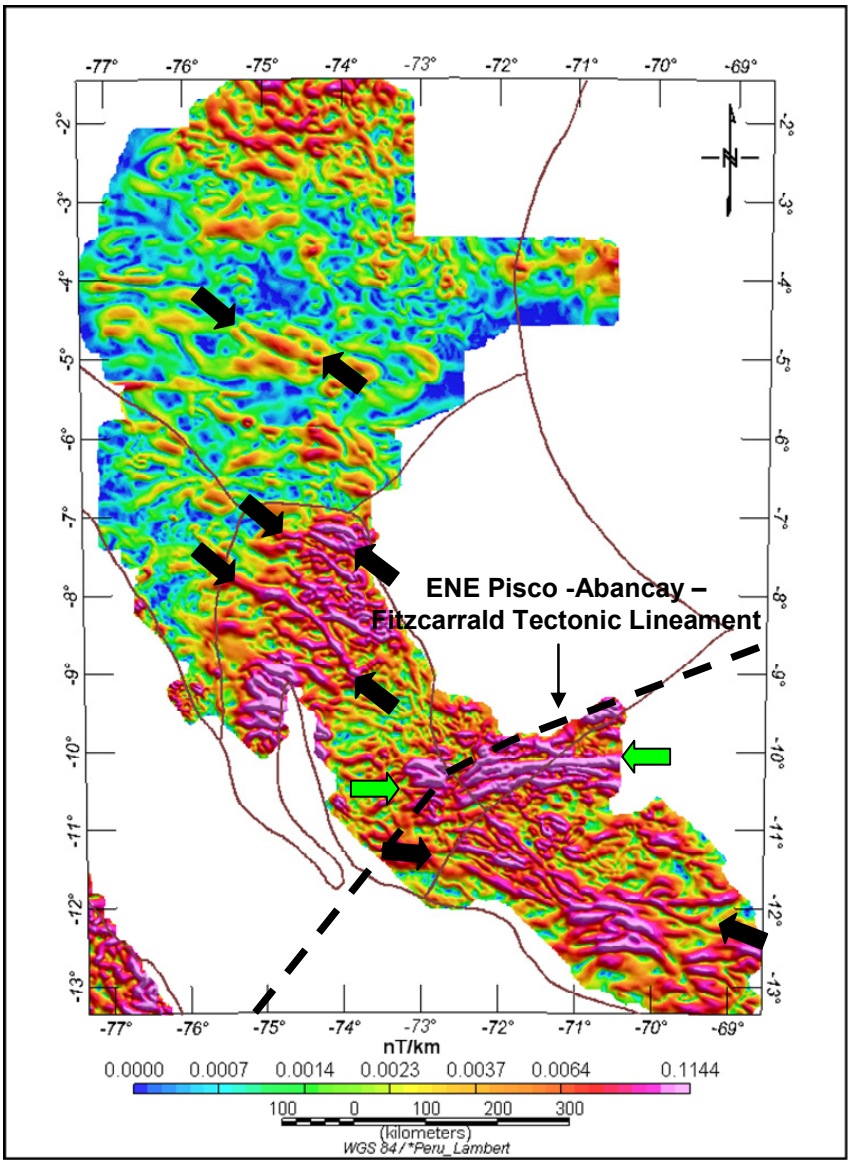


Figure 5.7. Horizontal gradient magnitude of the total magnetic intensity map shows lineament in the basement rocks of Peru. The maxima are the location of magnetic source edges, which could be a fault.

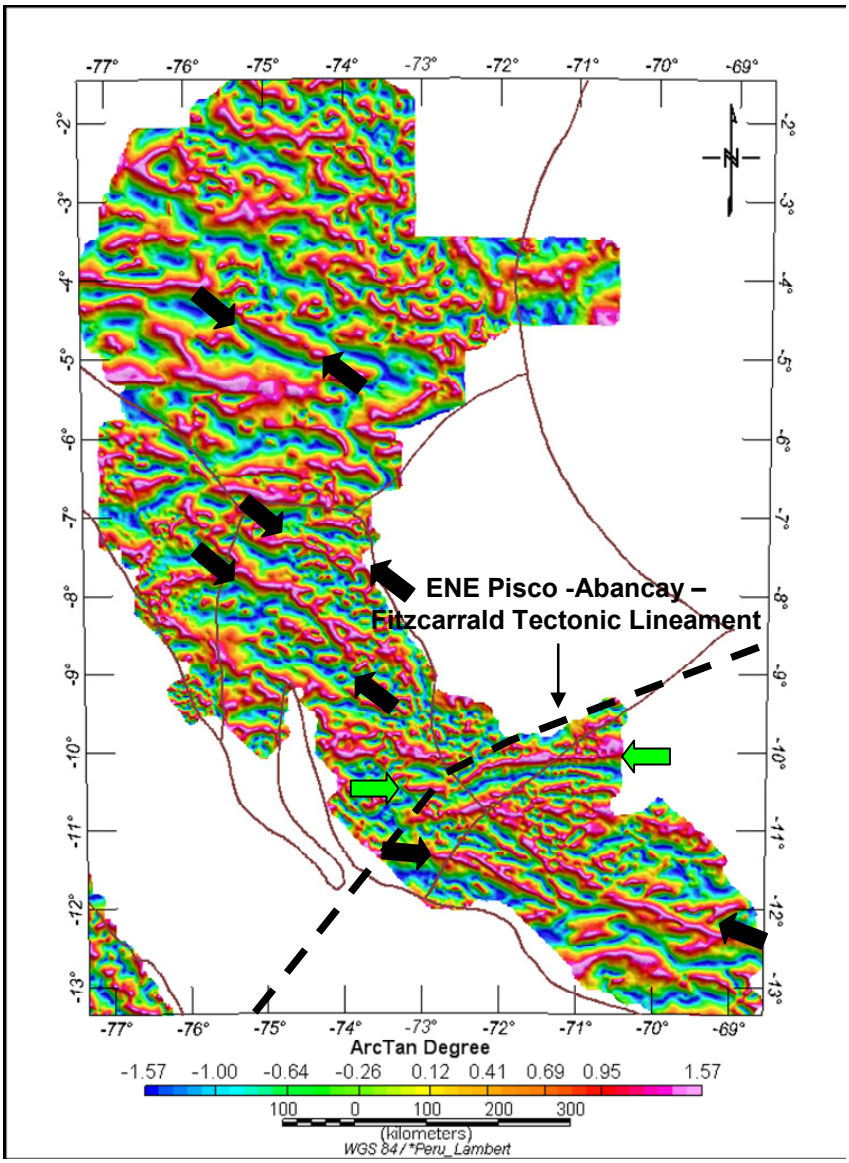


Figure 5.8. Tilt derivative of the total magnetic intensity anomaly map shows magnetic source edge continuity and subtle Precambrian basement features.

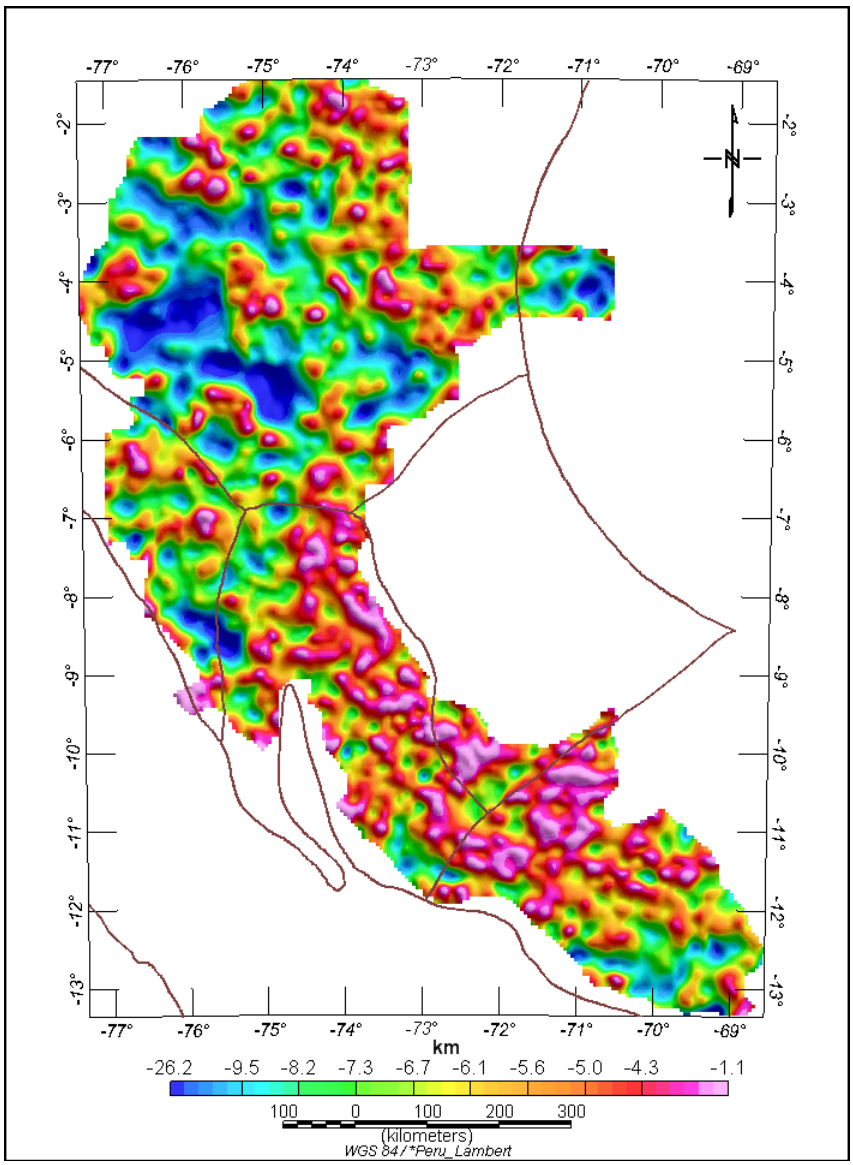


Figure 5.9 Euler depth estimates indicating the depth to the shallowest magnetic sources.

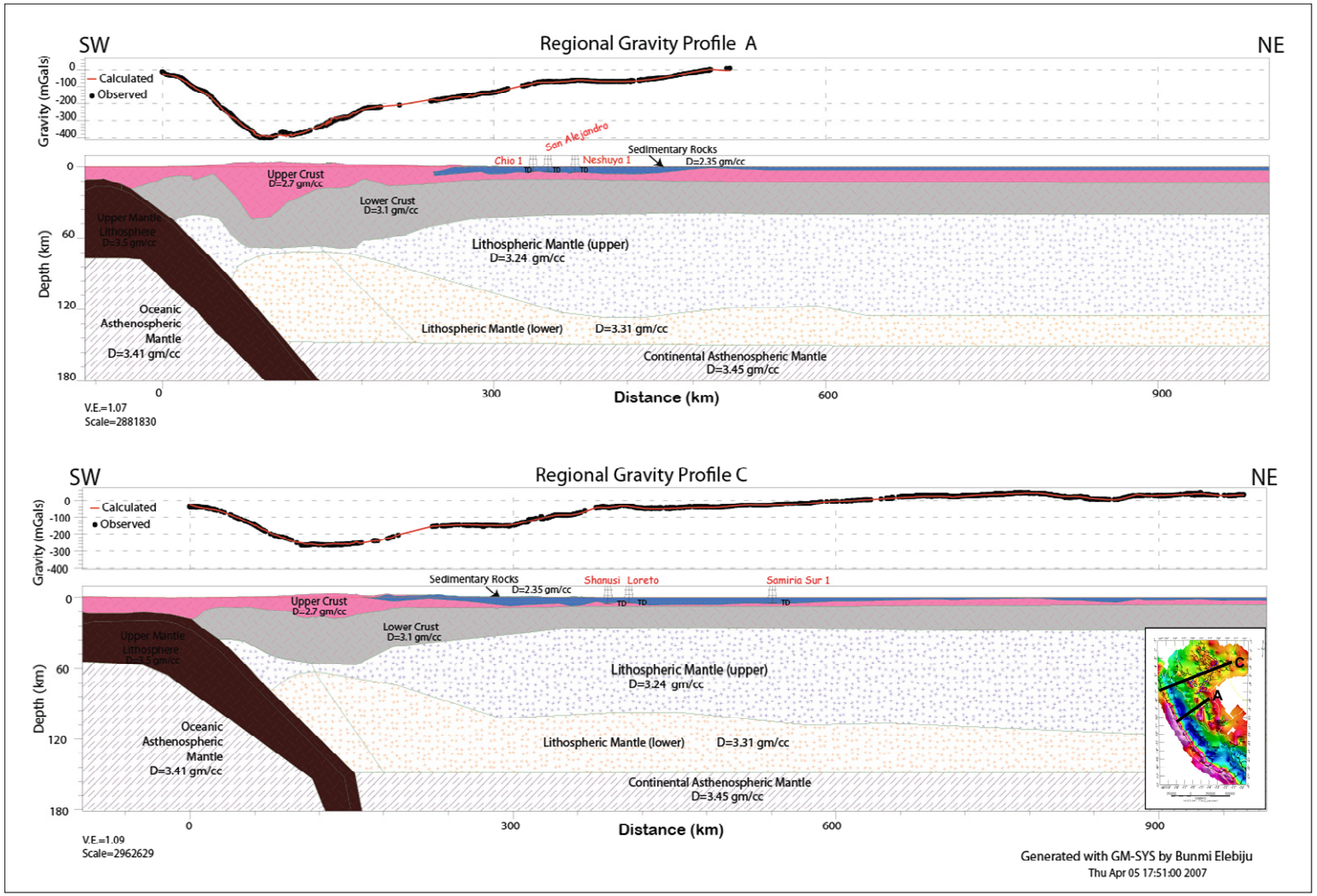


Figure 5.10. Two northeast trending regional gravity profiles across the Peruvian sub-Andes. Crust thickness increase from the north part of the Ucayali basin to the south. Inset map shows the location of these profile lines. (Initial density from models adapted from Tassara et al., 2006).

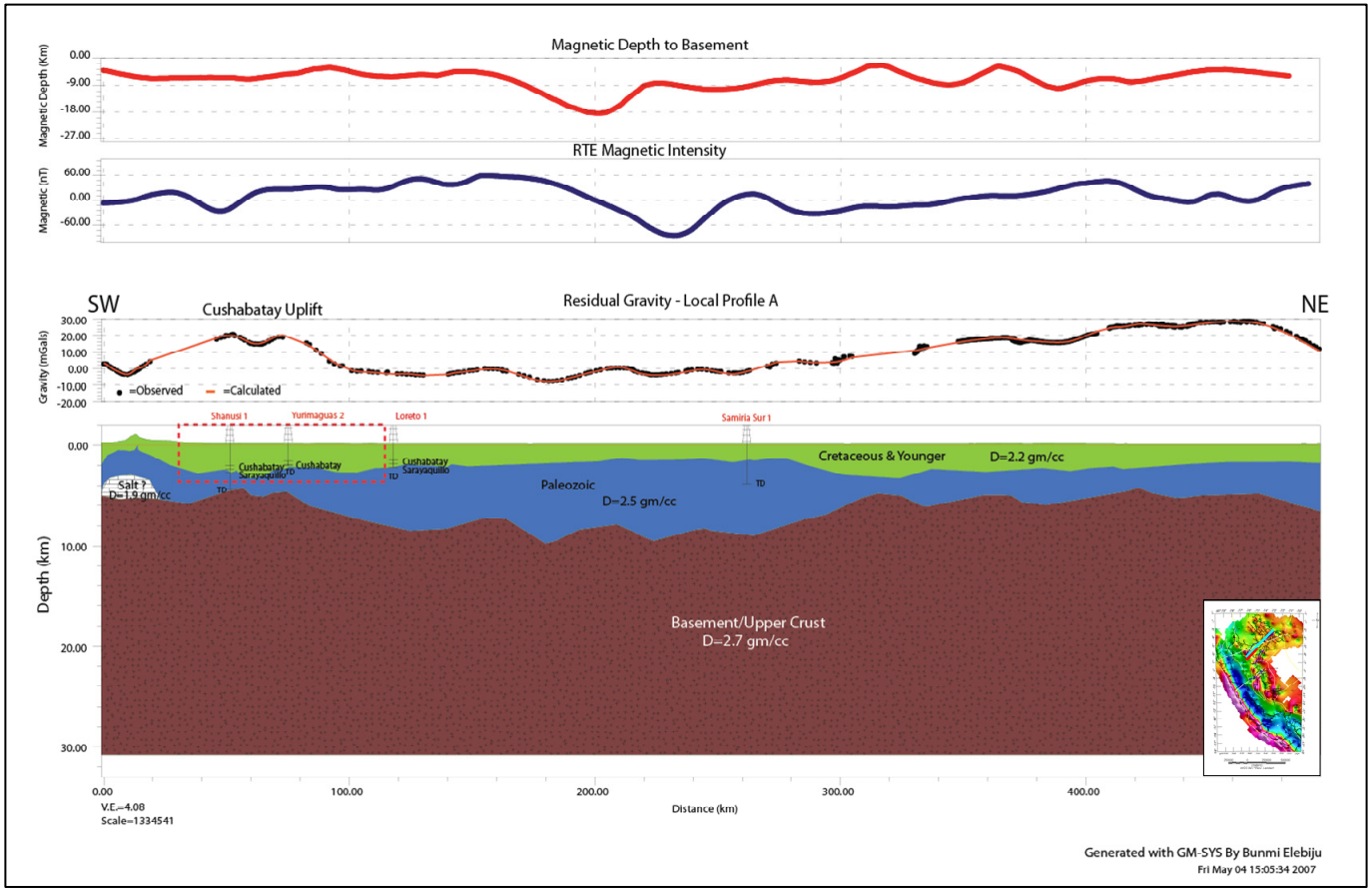


Figure 5.11. Local northeast trending gravity profile line A across the Ucayali basin, Peru. Red-dashed rectangle is the location of seismic section in Figure 5.12 used to constrain the gravity. Inset map shows the location of the profile line (Cyan line is the gravity and red line is the seismic line).

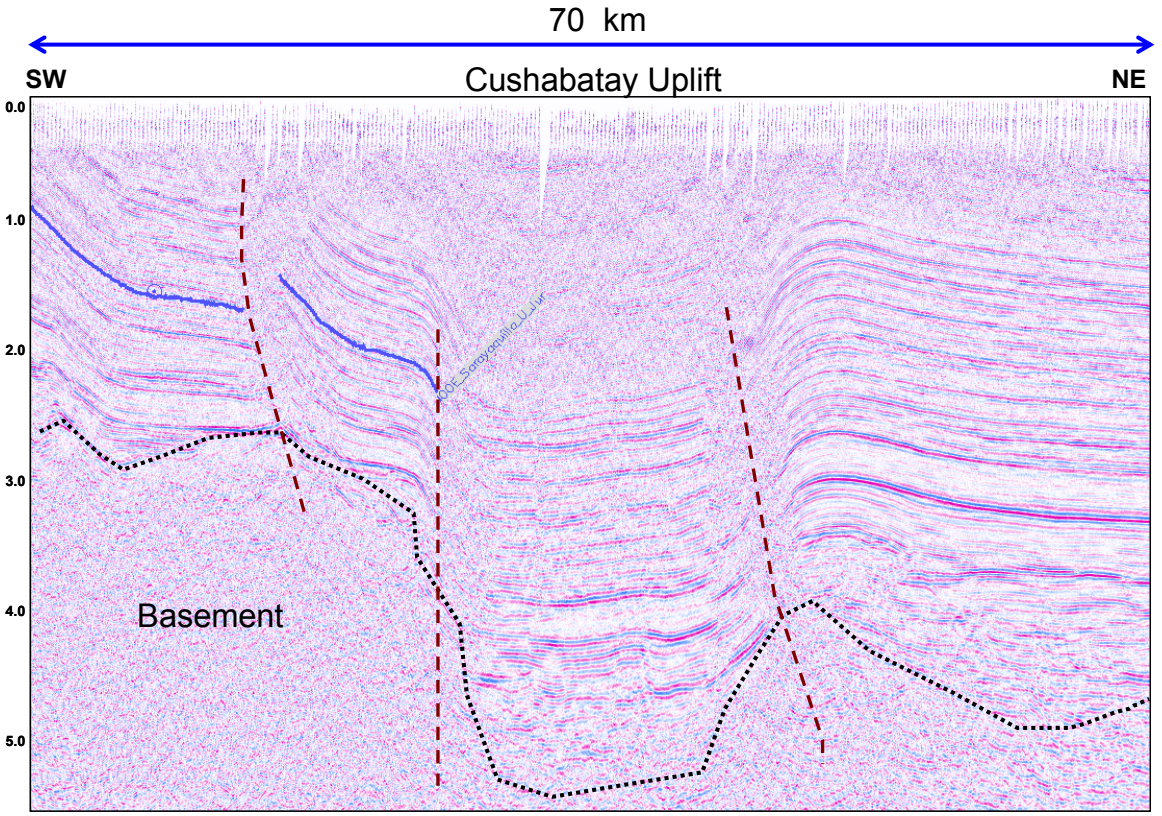


Figure 5.12. Seismic section used as a constraint for the gravity model in Figure 11. Black-dotted line and the brown-dashed line are the interpreted top of basement and faults respectively. Cushabatay Uplift is a half graben that is filled with sediments (PARSEP, 2002).

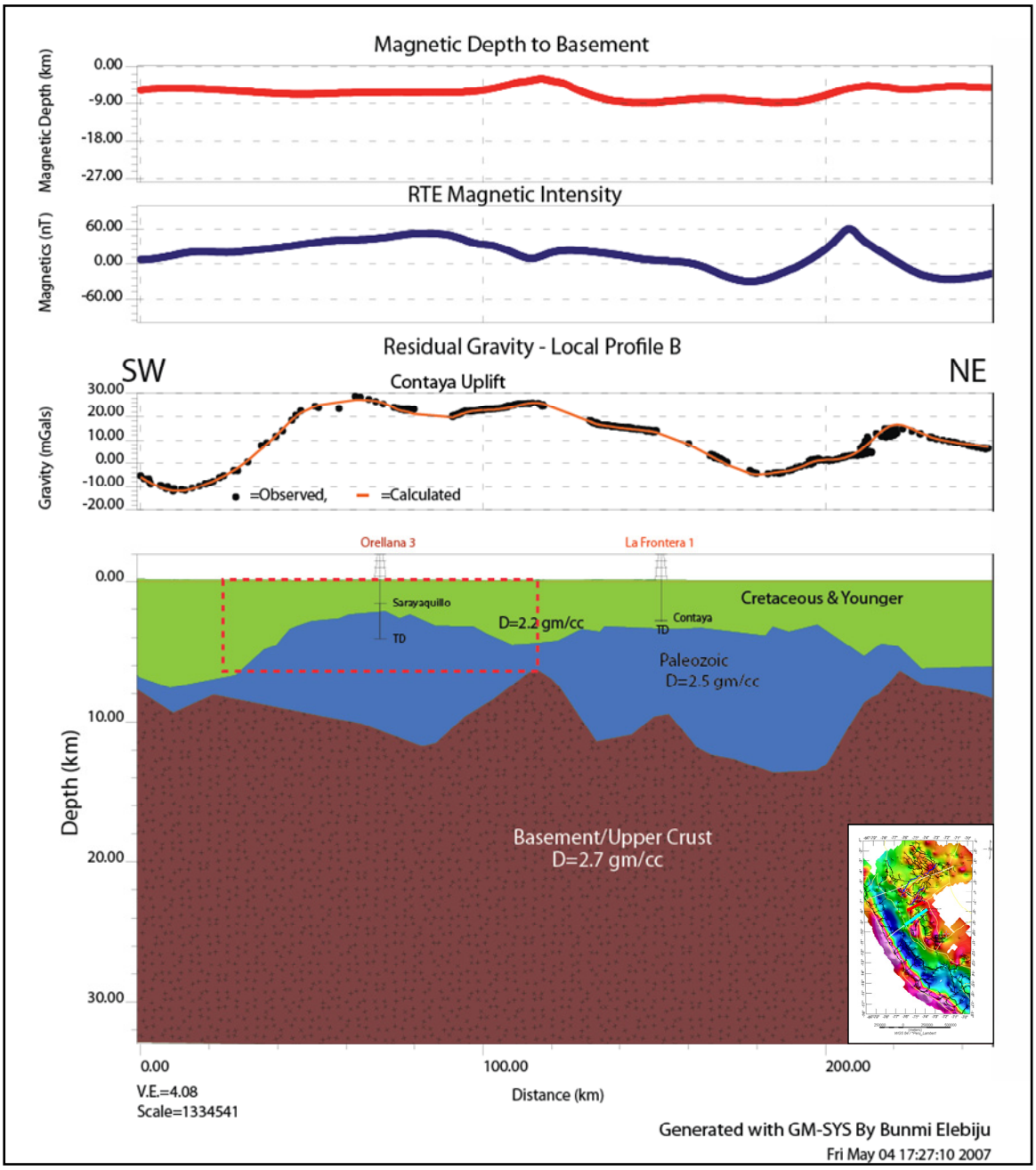


Figure 5.13. Local northeast trending gravity profile line B across the Ucayali basin, Peru. Red-dashed rectangle is the location of seismic section in Figure 5.14 used to constrain the gravity. Inset map shows the location of the profile line (Cyan line is the gravity and red line is the seismic line).

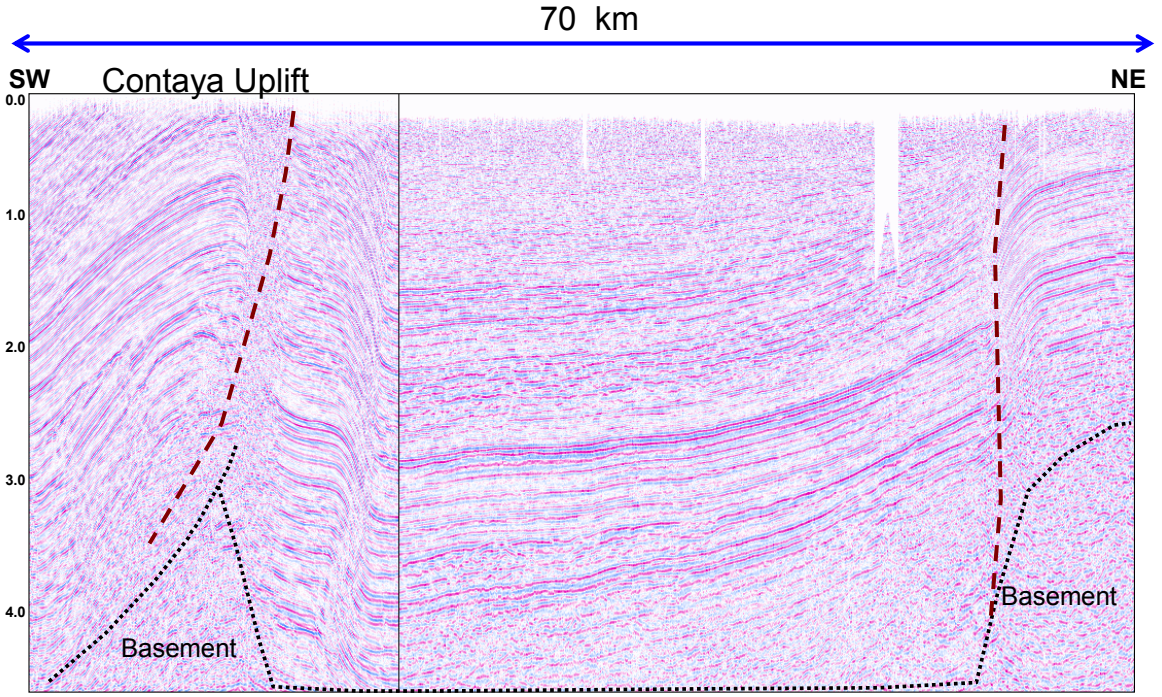


Figure 5.14. . Seismic section used as a constraint for the gravity model in Figure 5.13. Black-dotted line and the brown-dashed line are the interpreted top of basement and faults respectively. Contaya Uplift is an ancestral horst structure (PARSEP, 2002).

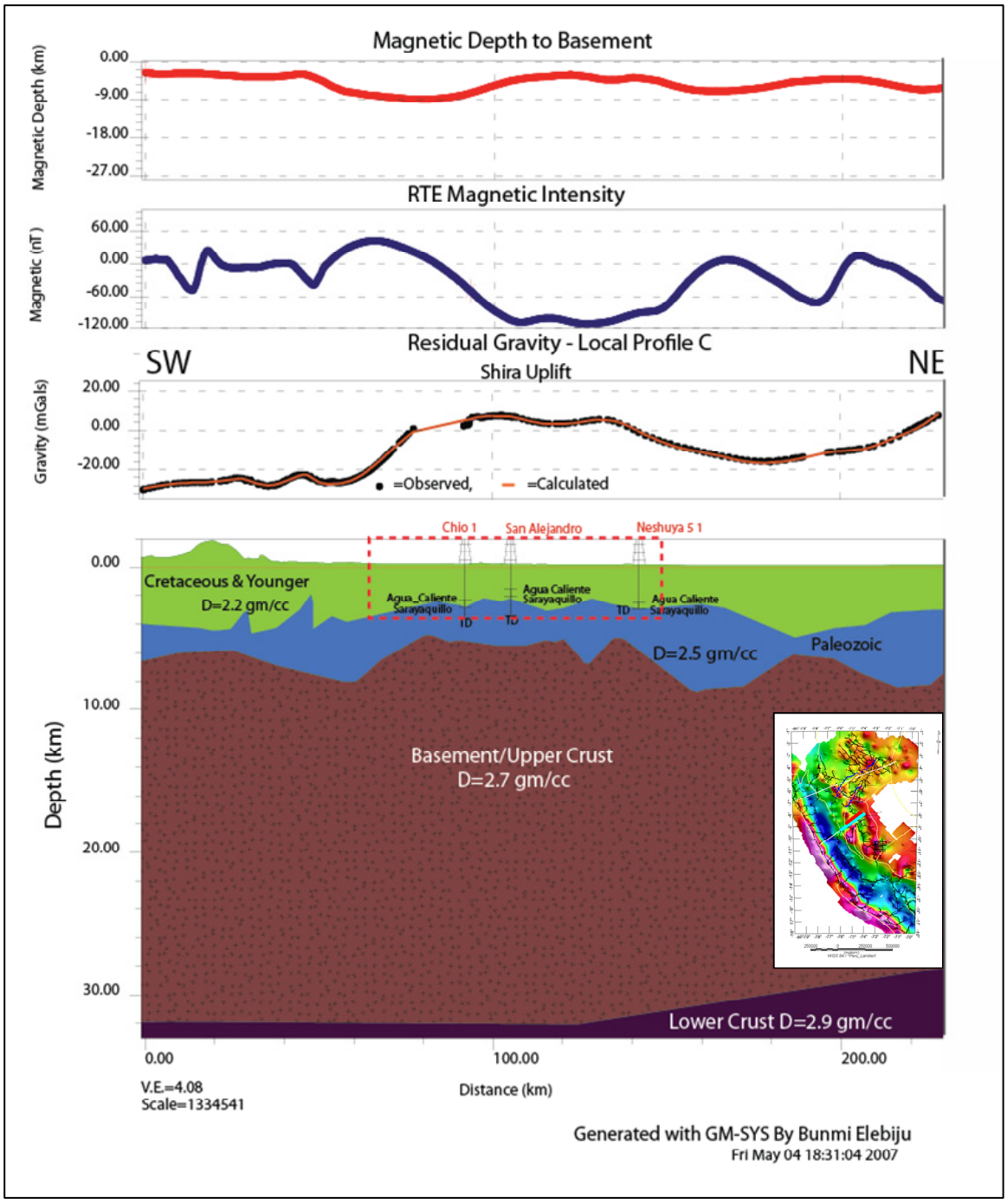


Figure 5.15. Local northeast trending gravity profile line C across the Ucayali basin, Peru. Red-dashed rectangle is the location of seismic section in Figure 5.16 used to constrain the gravity. Inset map shows the location of the profile line (Cyan line is the gravity and red line is the seismic line).

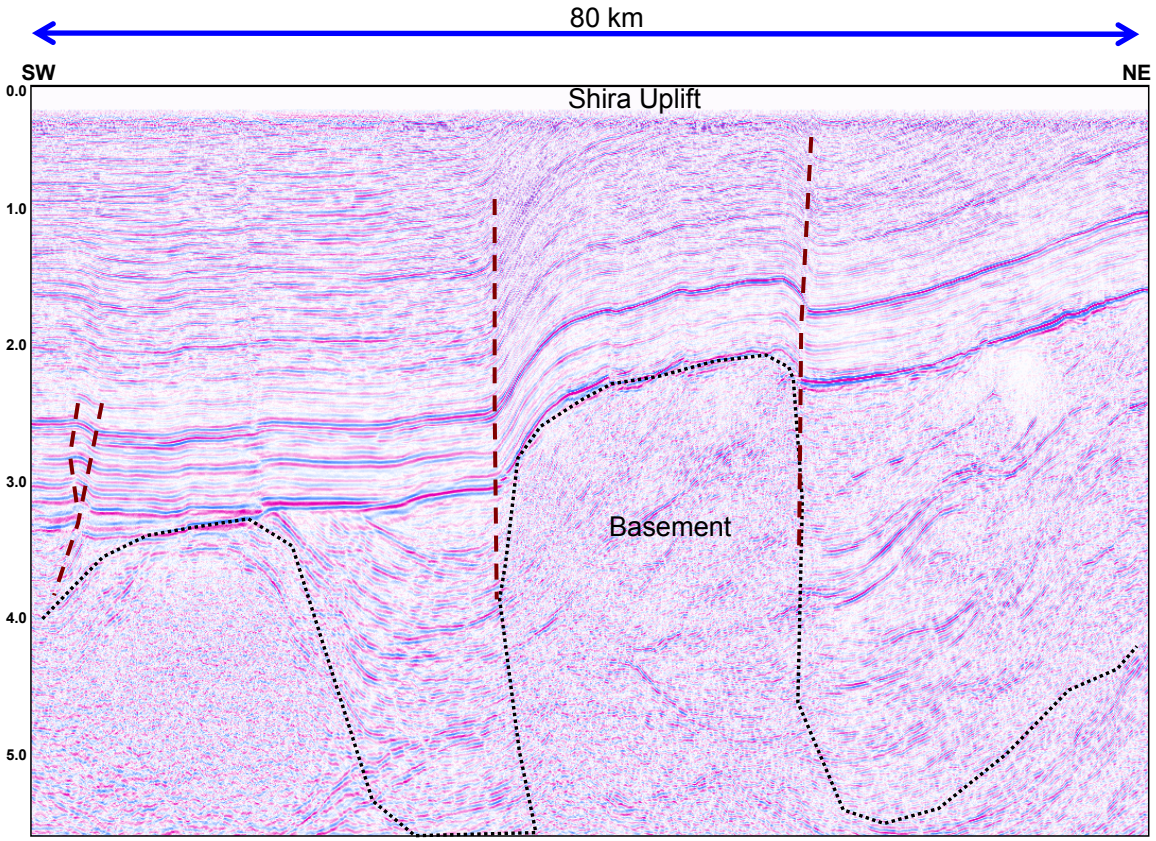


Figure 5.16. Seismic section used as a constraint for the gravity model in Figure 5.15. Black-dotted line and the brown-dashed line are the interpreted top of basement and faults respectively. Shira uplift is an ancestral horst block (PARSEP, 2002).

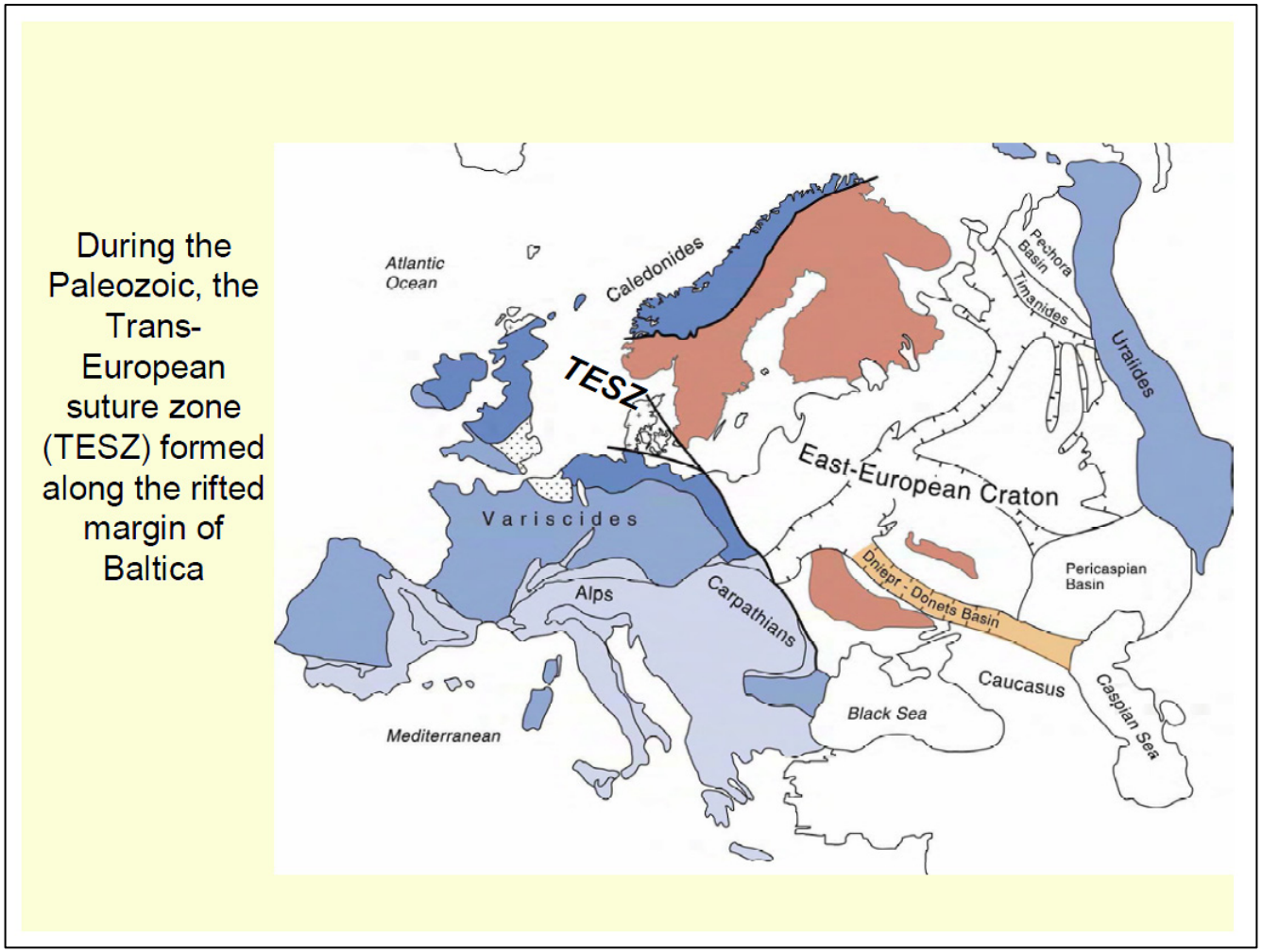


Figure 5.17. Tectonic index map of Europe.

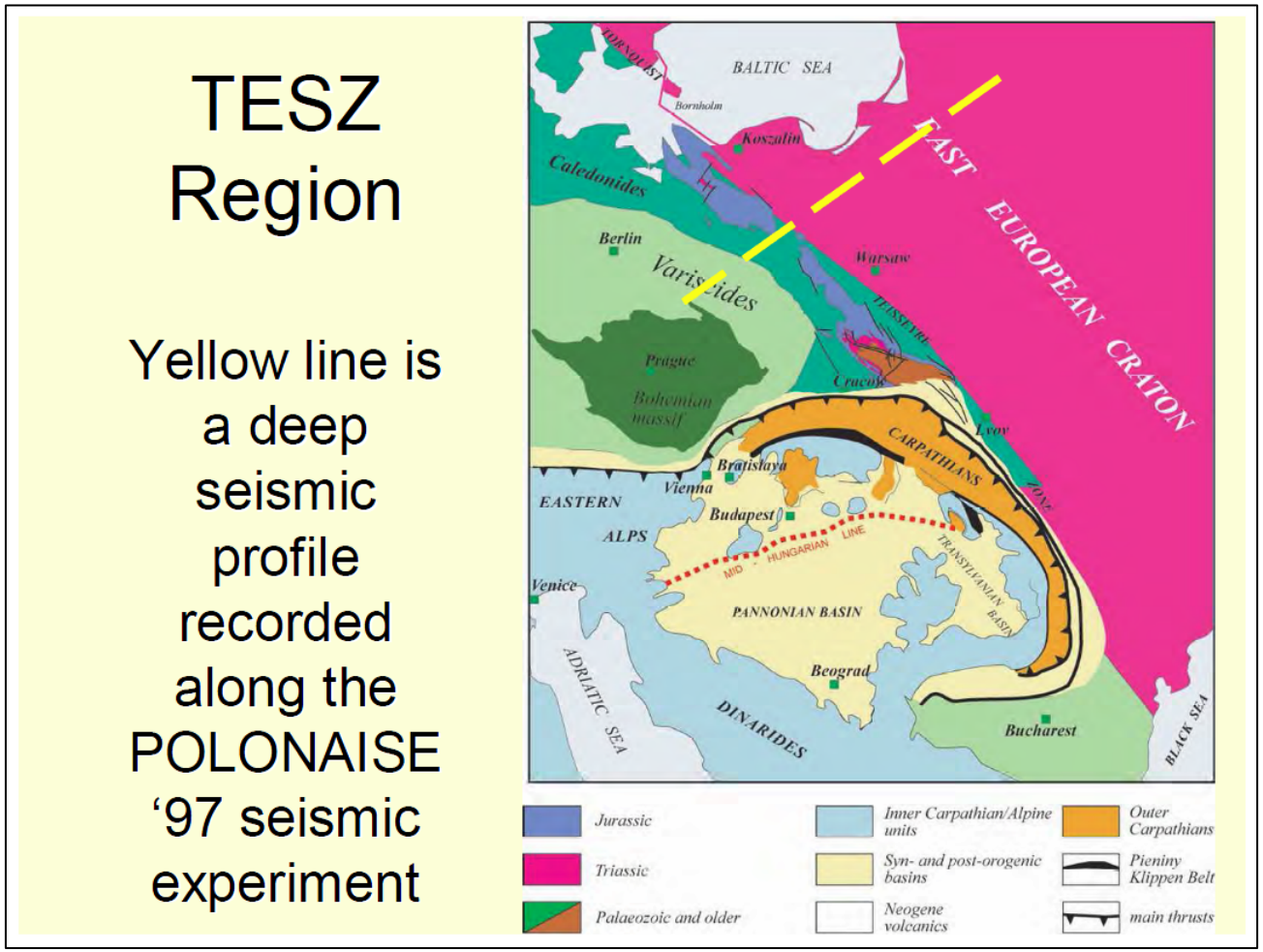


Figure 5.18. Tectonic index map showing the P4 seismic profile that extend across Poland.

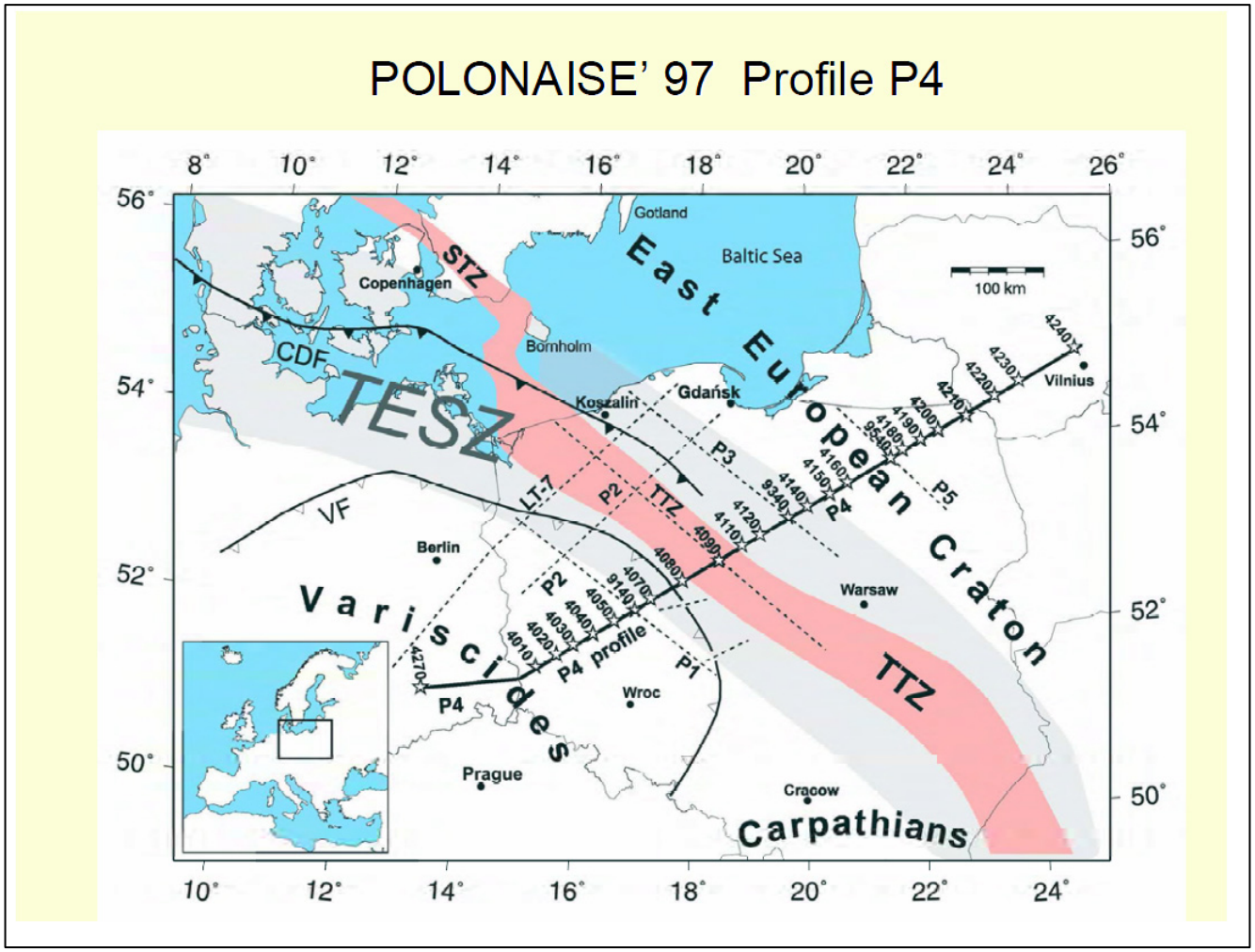


Figure 5.19. Map showing the location and shotpoint along profile P4 of the POILONAISE'97 experiment.

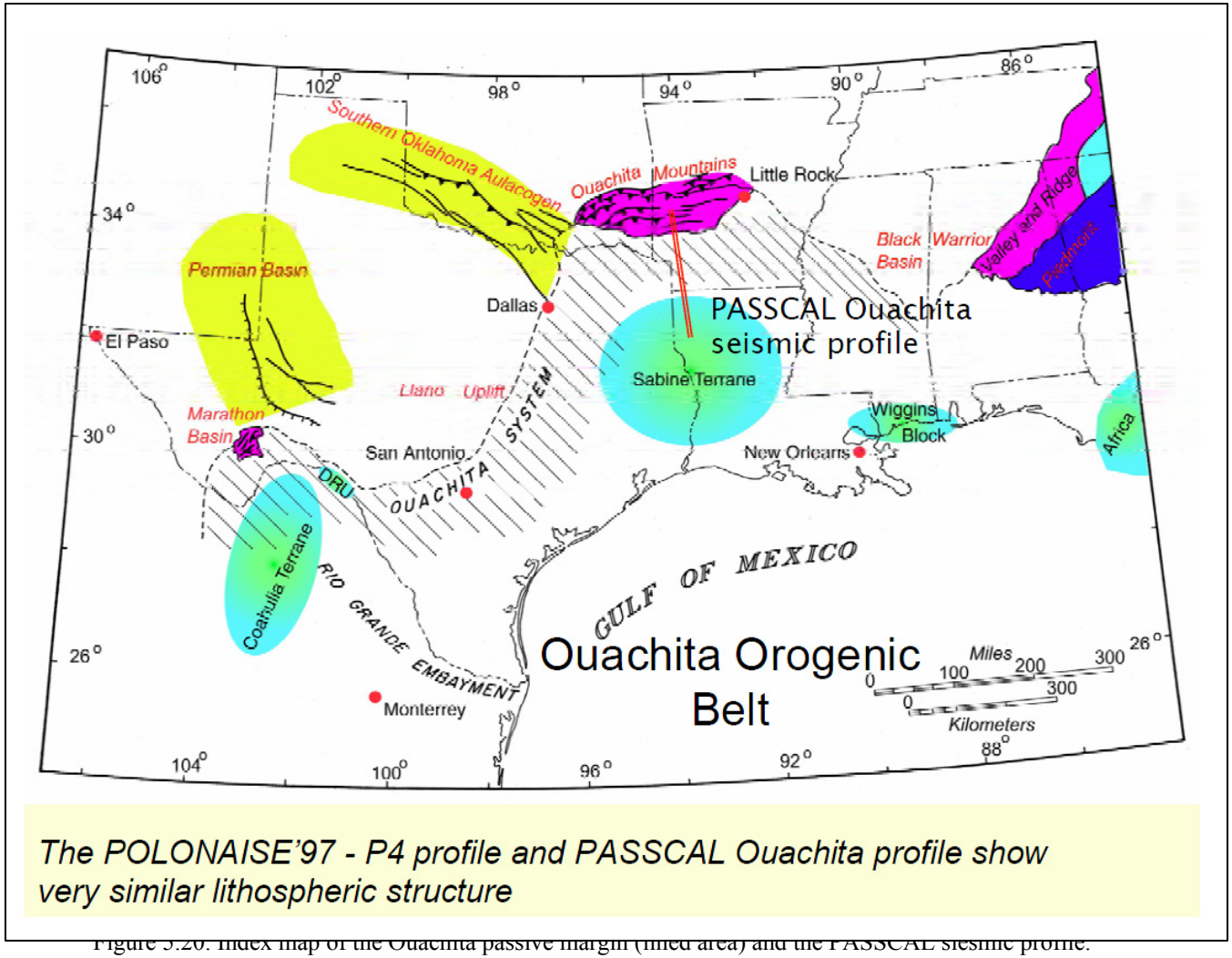


Figure 3.20: Index map of the Ouachita passive margin (filled area) and the PASSCAL seismic profile.

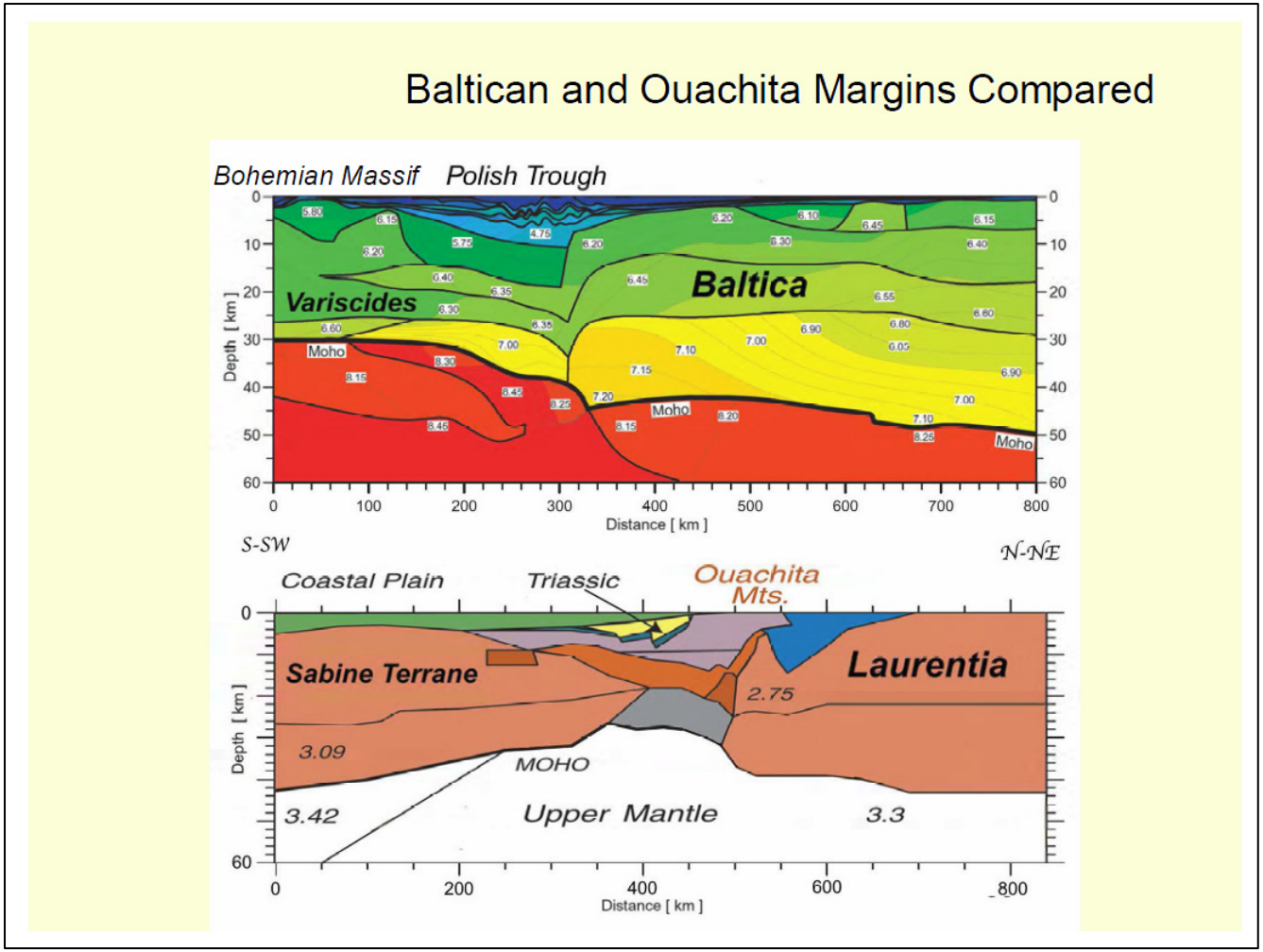


Figure 5.21. Seismic velocity model for profile P4 and the integrated (seismic/gravity) model for the Ouachitas.

Table 5.1. Table of wells used in constraining the gravity models

| UWI | Well Name | Surface X (m) | Surface Y (m) | KB (m) | Bottom Depth (m) | Working Datum (m) |
|---|---|---|---|---|---|---|
| 100000281349 | Chio 1 | 474751.895 | 9024124.745 | 0 | 3825.2 | 0 |
| | Loreto 1 | 435205.879 | 9345590.315 | 242.621 | 4156.56 | 242.621 |
| 100000061649 | Neshuya 1 | 513158.382 | 9055279.335 | 264 | 3230.9 | 264 |
| 100000243902 | Orellana 3 | 479925.177 | 9240630.054 | 156 | 4207.46 | 156 |
| | Orellana 3X | 479700.458 | 9240246.71 | 149.352 | 4207.46 | 149.352 |
| | Palmera 1 | 606303.543 | 9336318.8 | 153.314 | 3931.31 | 153.314 |
| 100000061687 | Platanal 01 | 640595.44 | 9001284.291 | 0 | 3510.8 | |
| 100000116093 | Rio Caco 1 | 592938.272 | 8975785.562 | 192.01 | 2865 | 192.01 |
| | Samiria Sur 1 | 516085.153 | 9397822.395 | 154.534 | 3953.87 | 154.534 |
| 100000277446 | San Alejandro 1 | 488564.569 | 9025784.95 | 271 | 3581.7 | 271 |
| 100000116094 | Sanuya 1 | 608729.698 | 8983519.367 | 185 | 3435.1 | 185 |
| | Shanusi 1 | 375153.08 | 9328952.41 | 181.966 | 4487.6 | 181.966 |
| | Tamanco 1 | 569891.14 | 9354796.722 | 140.818 | 4208.07 | 140.818 |
| 100000116095 | Tiruntan 1 | 515155.463 | 9124912.218 | 163.068 | 4349.8 | 163.068 |
| | Yurimaguas 2 1 | 373730.305 | 9353971.638 | 274.93 | 2313.74 | 274.93 |

# Chapter 6: Implications of This Study

Three integrated geophysical studies that investigated the linkage between Precambrian studies and sedimentary structures show that structures we see within the sedimentary section have links with Precambrian structures. These sedimentary structures follow zones of weakness that exist in the Precambrian basement, which can be mapped with potential field data. Most of the Precambrian basement structures do not have a surface expression, and during basement lineament reactivation, stress released within these structures is propagated upward into the sedimentary section and expressed as structures such as faults. Information about where potential breaks can occur within the sedimentary section can also be determined from observation of weakness zones within the Precambrian basement.

We have also demonstrated that potential field data, especially the high-resolution aeromagnetic (HRAM) data is effective in mapping basement structures at the scale of seismic reflection surveys. Therefore, in untested area or geological complex areas (e.g., subsalt exploration) where seismic data is either unavailable or limited, aeromagnetic data, which are relatively cheap and readily available than can be used to predict the kind of structures to expect within a sedimentary section. The extent of structures such as faults whose locations are known locally via seismic data can be determined through the help of aeromagnetic data. Thus, this kind of information can help in choosing a location for additional seismic surveying or what existing seismic data to purchase.